Development and Characterization of Conducting Polymer Actuators

by

Priam Vasudevan Pillai

B.S., University of California, Berkeley in Mechanical Engineering
(2004)
B.S., University of California, Berkeley in Material Science and
Engineering (2004)
S.M., Massachusetts Institute of Technology (2007)

Submitted to the Department of Mechanical Engineering
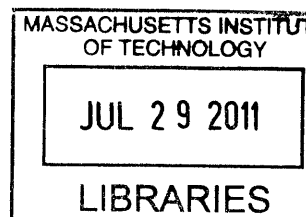in partial fulfillment of the requirements for the degree of

Doctor of Philosophy in Mechanical Engineering

at the

MASSACHUSETTS INSTITUTE OF TECHNOLOGY

June 2011

Author . . . .
Department of Mechanical Engineering
May 2, 2011
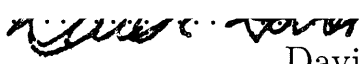
Certified by. . . . .
Ian W. Hunter
Hatsapolous Professor of Mechanical Engineering
Thesis Supervisor

Accepted by . . . .
David Hardt
Chairman, Department Committee on Graduate Theses

Development and Characterization of Conducting Polymer Actuators

by

Priam Vasudevan Pillai

Submitted to the Department of Mechanical Engineering
on May 2, 2011, in partial fulfillment of the
requirements for the degree of
Doctor of Philosophy in Mechanical Engineering

Abstract

Conducting polymers such as polypyrrole, polythiophene and polyaniline are currently studied as novel biologically inspired actuators. The actuation mechanism of these materials depends upon the motion of ions in and out of the polymer film during electrochemical cycling. The diffusion of ions into the bulk of the film causes the dynamic mechanical and electrical properties of the material to change during oxidation and reduction. The mechanism of this change is not fully understood, as it can depend on many different factors such as oxidation state, solvation of the film and the level of counter ion swelling. In-situ measurement of the dynamic mechanical compliance and electrical impedance of polypyrrole as a function of charge is difficult, since the compliance depends upon the excitation frequency as well as the electrochemical stimulus. Here, we have developed novel experimental techniques that use stochastic input waveforms to dynamically measure the compliance and impedance response of conducting polymers as a function of frequency and an electrochemical stimulus. A stochastic stress input signal with a bandwidth of 30 Hz is used, which allows us to compute the mechanical compliance transfer function of polypyrrole as function of the electrochemistry. The low frequency compliance changes between 50-80%, as charge is injected into polypyrrole in neat 1-butyl-3-methylimidazolium hexafluorophosphate. The compliance changes reversibly as ions diffuse in and out of the film, which indicates that the compliance depends upon the level of counter ion swelling. The effect of cationic and anionic charging on the polypyrrole compliance is demonstrated in multiple ionic/solvent combinations. The stochastic signals are also used to the characterize the isometric and isotonic responses of conducting polymer actuators. This technique is used to demonstrate the effect of temperature and solution conductivity on actuation and to develop methods that can be used to improve polymer actuator performance. Efficient techniques to incorporate functionalized carbon nanotubes into conducting polymers using layer by layer deposition and drop casting methods have been explored. These new composite materials and techniques significantly reduce creep, improve conductivity and increase stiffness of the polymer actuators.

3

Thesis Supervisor: Ian W. Hunter
Title: Hatsapolous Professor of Mechanical Engineering

Acknowledgments

As a student at MIT, I have interacted with amazingly brilliant, motivated and inspiring people. They have motivated and challenged me throughout my time at MIT and have contributed to an exceptional experience during the past 6 years. First of all I would like to thank my adviser Prof Ian Hunter who has guided me through this work and has allowed me to have the amazing opportunity to work in the Bioinstrumentation lab. His kindness and patience have allowed me to feel my way into the fascinating world of conducting polymers, system identification, robotics and has made my experience here truly exceptional. Some of my most inspirational research moments have come from speaking to Nate Vandesteeg, Rachel Pytel, Tim Fofonoff, Jean Chang, Ellen Chen and Eli Paster. All have brought different expertise and experiences that have been invaluable for me in the process of doing my own research. It has also been a great opportunity to work with my colleagues in the Bioinstumentation Lab Dr. Andrew Taberner, Dr. Cathy Hogan, Nate Ball, Bryan Ruddy, Nate Wiedenman, Brian Hemond, Jan Schnorr, Adam Wahab, Kerri Keng and Miguel Saez, all of whom have very different skills and have enriched my experience at the lab. I would like to thank Angela Chen who made the lab seem less intimidating when I first joined by her sense of humor. A lot of this work is possible due the wonderful work some of my UROPs. Lauren Montemayor, Juan Lozada, Emmanual Hernandez, Juan Diaz, Sonia Buckley who have been amazing UROPs. I would also like to send a shout out to all the wonderful folks who I have gotten to know through Wednesday night dinner and my friends at MIT. They have shown me that there is more to life than just research and classes and have put up with my eccentricities over the last two years. Life in Boston would not be very interesting without these guys. And of course, I would like to thank my family. Mama and Dada without whom I would never have been what I am today. Their encouragement, patience and support have been more than any child should ask for and definitely more than I sometimes deserved. My brother Baba and sister Minerva who both have shared in my ups and downs over the last few years and have always laughed at me and made me laugh at

myself during both the ups and downs. I would also like to thank Mabel Chan for reading my thesis and standing by me during the times when research takes a front seat to spending time with her. I would also like to thank Professor Derek Rowell and Professor Tim Swager who have provided guidance during the course of this work.

Contents

List of Figures

9

10

11

12

13

15

List of Tables

Symbols

α Strain to charge ratio

Φ Cross Spectral Density

σ Stress

ϵ strain

s Laplace Variable

Acronyms

ACN Acetonitrile

AIC Akaike information criteria

AICc modified Akaike information criteria

ALS adapted least squares

BF$_4$ tetrafluoroborate ion

BMIM$^+$ 1-butyl-3-methylimidazolium ion

BMIMBF$_4$ 1-butyl-3-methylimidazolium tetrafluoroborate

BMIMPF$_6$ 1-butyl-3-methylimidazolium hexafluorophosphate

Cl chloride ion

CNT carbon nanotube

CP conducting polymer

DBSA dodecyl benzene sulfonate ion

DCM dichloromethane

DEHS dioctyl-sulfosuccinate ion

DEM Diffusive Elastic Model

E error signals

EDMA Electrochemical Dynamic Mechanical Analyser

EDOT 3,4-ethylenedioxythiophene

FIR finite impulse response

G modulus

J compliance

LiTFSI lithium trifluorosulfonamide

LMS least mean squares

LTI lnear time invariant

MSE mean squared error

NaDEHS sodium dioctyl sulfosuccinate

NaPF$_6$ sodium hexafluorophosphate

PA polyaniline

PA-CNT polyaniline-carbon nanotube composite

PEDOT-CNT Poly(3,4-ethylenedioxythiophene)-carbon nanotube composite

PC propylene carbonate

PDF probability density function

PEDOT poly(3,4-ethylenedioxythiophene)

PF$_6^-$ hexafluorophosphate ion

PID proportional, integral and derivative.

PPy polypyrrole

PPy-CNT polypyrrole-carbon nanotube composite

PPy-DEHS polypyrrole doped with dioctylsulfosuccinate ion

PPy-PF$_6$ polypyrrole doped with hexafluorophosphate ion

RLS recursive least squares

SEDMA stochastic electrochemical dynamic mechanical analyzer

SEM scanning electron microscopy

SSE sum of squared errors

SSID stochastic system identification

sCNT carbon nanotube covalently functionalized with sulfonate groups

fCNT functionalized carbon nanotubes

TBAP tetrabutylammonium hexafluorophosphate

TEAP tetraethylammonium hexafluorophosphate

TGA thermogravimetric analysis

TMAP tetramethylammonium hexafluorophosphate

TFSI trifluorosulfonamide

VAF variance accounted for

Chapter 1

Introduction

Engineers seek to develop machines that mimic systems that are widely seen in nature. These systems display a diverse set of adaptations, which have evolved over millions of years of evolution that allow them to thrive in many different environments. Using these as inspiration, numerous technologies exist that are deemed to be bio-inspired. In the case of developing "muscle like" actuators, there is a significant lack of actuator technologies that behave as real muscle. Mammalian skeletal muscle is capable of generating large work densities (20-70 kJ/kg), large deflections (20%) at high strain rates (50% per second) for millions of cycles [16, 66]. They are capable of highly efficient energy conversion rates and well as capable of regenerating themselves when damaged. They are also truly integrated systems that combine energy storage, control elements and sensing. No other man made actuator is capable of matching the performance of mammalian muscle. Traditional engines and electrical motors are efficient, but are large, inflexible and cannot be easily incorporated in systems that require small, flexible actuators. For instance, small robotic flying insects or fishes would require development of an actuator that would be flexible and lightweight. Actuators that complement or enhance the natural abilities of soldiers, emergency first responders or people with disabilities would have to be light and be easily incorporated into their clothing. To accomplish this new actuator technologies have to be developed that are lightweight, quiet and easily incorporable into many different configurations.

There are a number of artificial muscle technologies that are have been developed that respond to electrical, chemical or thermal stimuli. Madden et al [86, 88] review the technologies available to designers developing applications that require new novel actuators. These include dielectric elastomers, ferroelectric polymers, liquid crystal elastomers, shape memory alloys, ionic polymer metal composites (IPMC), electroactive ceramics, carbon nanotubes and electroactive polymers. None of these technologies can completely reproduce the performance of mammalian skeletal muscle. For example, dielectric elastomers, ferroelectric polymers and liquid crystal elastomers have speeds greater than 50%/s [88] but require large voltages (greater than 5 kV) to operate. This can make them impractical for many biological applications. Actuators based on IPMCs, carbon nanotubes shape and memory alloys can generate large forces at low voltages but have limited strains (less than 1%). conducting polymers (CPs) are another class of actuator materials that can generate strains of typically up to 10 % at low potentials (less than 10 V). CPs have a number of attractive properties such as being lightweight, inexpensive and are easy to mold and shape into any conceivable form. These materials can also be nanostructured [105] and be configured to produce large stresses [89]. The performance of these materials can be hampered by small strain rates where response times can last for several seconds with excessive levels of creep. This thesis seeks to further develop the use of conducting polymer actuators by developing novel experimental techniques using stochastic system identification (SSID). Using these techniques additional insight can be gained into the mechanisms that underlie the actuation behavior in these materials and thereby improve the overall actuator performance.

1.1 Conducting Polymers

The first conducting polymer synthesized was polyacetylene [30] in 1977, which resulted in a Nobel prize for Shirakawa, MacDiarmid and Heeger in 2000. Polyacetylene is the simplest conducting polymer structure where the electrical conductivity is determined by placing alternating carbon-carbon double bonds on the backbone of the
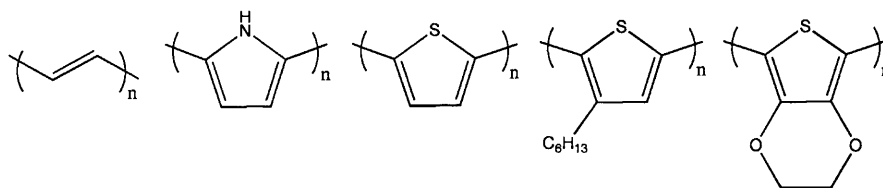
Figure 1-1: Conducting polymers listed in order: polyacetylene, polypyrrole, polythiophene, poly(3-hexylthiophene), poly(3,4-ethylenedioxythiophene)

polymer [146]. In bulk form the intrinsic conductivity of these polymers are not realized since the polymer chains are entwined within one another. In this case, the polymers need to be doped with ions, effectively making them semiconductors [113]. The conductivity of polyacetylene is unstable in air and it cannot be used for traditional actuators. Subsequently, a large number of conducting polymer materials have been synthesized over the past 30 years. These can be fabricated in a number of different forms making the especially suited to development. Figure 1-1 shows some of the more common conducting polymers. Researchers have developed numerous applications for CPs. These include electrical components (passive electronic elements, transistors) [125], memory elements [22, 120], sensors [3, 55, 64, 145, 148], super capacitors [9, 96, 114] and actuators [16, 43, 84, 128]. The versatility of these materials therefore makes them ideal candidates to create the building blocks of multi functional artificial biological systems. When the same material platform is used to develop many different components the lines between the components can be blurred. For example, a conducting polymer actuator can also serve as a strain sensor, a resistor or a capacitor as part of an electrical circuit [99]. They can serve as structural members of a microfluidic device, with a tunable stiffness and impedance that can be adjusted as desired. CPs have also been shown to have applications for battery electrodes [74, 92], neural probes [35, 54], coatings to prevent corrosion [126], membranes to separate gasses [6], and even antennas [31, 102]. Developing applications that combine multiple functionalities of conducting polymers will require new experimental techniques to decouple the effects that can influence polymer performance.

23

1.2 System Identification

It is important for scientists to be able to infer models of a system using observations about the system. System identification deals with the study of generating efficient and informative mathematical models of a system by using these observations [80]. These techniques describe methods to calculate parameters of linear and non-linear system models given a set of data. Linear and non-linear variants of these techniques have been used to study mechanical properties of skin [29], muscle [53, 76, 94] and lung tissue [151]. They have also been extensively adapted to study non-linear physiological systems such as human joints [70], eye position (vestibular ocular reflex) [50] and auditory systems [25]. These systems can be described using a single impulse response or non-linear model structures such as Wiener or Hammerstein systems that have cascaded linear and non-linear components. Hunter et al [65] developed techniques using Volterra kernels that are used to characterized non-linear cascaded systems.

lnear time invariant (LTI) systems can be described as a linear combination of inputs and output. Many systems display LTI type behavior. For example, DC motors can be modeled as LTI systems when they are used with high bandwidth current amplifiers and the effects of friction are negligible. In a number of cases, systems can be characterized as LTI under small perturbations. A purely linear system can be completely characterized using its impulse response function. The impulse response function is the response of a system to a instantaneous burst of an input. It is well known that for an LTI system with an impulse response h, the output y is given by a convolution.

$$y(kT) = \int_{\tau=0}^{\infty} h(\tau)u(kT - \tau)\, d\tau \qquad (1.1)$$

where, T is the sampling interval, u is the input and $k = 1, 2, 3....$ For LTI systems, system identification involves simply identifying the parameters of the impulse response function. This can be accomplished using multiple methods. The simplest method would be to input a delta function input and measure the corresponding output, which would be the impulse response. However, generating a perfect delta

function input is nearly impossible. The impulse response can also be estimated using step or sinusoidal inputs. However, to use these the experiment would have to be repeated multiple times to eliminate the effects of noise and transients.

A better method to obtain the impulse response would be to use a stochastic input signal, which has all the components of the desired frequencies. These tests can be easily split apart and averaged, which increases the sensitivity of the measurement. A stochastic input that contains all frequencies at equal probabilities is considered white. These signals are uncorrelated with themselves with an autocorrelation of zero except for at a lag of zero. These are also uncorrelated with any additive noise disturbance that can influence the response. From a practical standpoint the frequency content of an input signal cannot be completely white since it will be limited by the bandwidth of the input source. Generally, input signals are filtered using a low pass filter so that high frequency noise sources are not stimulated and to prevent aliasing. The other parameter that can be used to shape the stochastic input is its probability density function (PDF). Gaussian signals are the most commonly used type of signals, but random binary, uniform and pseudo random binary sequences can also be used. These signals fulfill the requirements of persistent excitation and have crest factors close to 1. In addition, the physical limitations of the system input must also be considered. For example, the input signal must not break or saturate the system being tested nor must it reach the limits of the sensors being used.

Once an input waveform is chosen, there are many methods that can be used to estimate an impulse response. The next step is to choose a suitable model structure. In many cases a finite impulse response (FIR) model structure is suitable to fit the data. A FIR model only depends on lagged input and approaches zero after a finite number of lags. A FIR model is simple to model and easy to understand. In addition, it is generally easier to relate the parameters of an FIR model to variables that have useful physical interpretations. These models can be calculated in multiple methods using data in both time domain and frequency domain. The two most commonly used techniques in this thesis are

- Spectral analysis which involves dividing a appropriately windowed cross power

25

spectral density of the input and output by the auto power spectral density of the input. This results in an empirical transfer function estimate that can be used to further characterize the system. The transfer function can be estimated using

$$\hat{H}(e^{i\omega}) = \frac{\Phi_{yu}(\omega)}{\Phi_{uu}(\omega)} \qquad (1.2)$$

where $\hat{H}$ is the estimated transfer function, Φ_{yu} is the input output cross spectral density, Φ_{uu} is the input auto spectral density and ω is the frequency. The impulse response is obtained using the inverse Fourier transform of this estimate.

- Correlation analysis can also be used to estimate the impulse response function directly. These involve time domain techniques such as least mean squares (LMS), recursive least squares (RLS) and adapted least squares (ALS). LMS can be used to conduct off-line identification while RLS and ALS can be used for real time identification of the impulse response. Consider a single input single output system (SISO), where y is the output and u is an input. The output has additive noise (e), which can be related by the impulse response function (h) by the equation,

$$y(kT) = \sum_{l=1}^{N} h(l)u_{k-l} + e_k \qquad (1.3)$$

Assuming that the noise is gaussian white and uncorellated with the input one can develop the relationship

$$h(k) = \frac{1}{T}\left[R^{-1}\phi_{yu}(k)\right] \quad where \; k = 1 \cdots N \qquad (1.4)$$

where

$$\phi_{yu}(k) = \frac{1}{N}\sum_{l=1}^{N} y(l)u(l+k-1) \qquad (1.5)$$

$$\phi_{uu}(k) = \frac{1}{N}\sum_{l=1}^{N} u(l)u(l+k-1) \qquad (1.6)$$

26

$$
R = \begin{pmatrix} \phi_{uu}(1) & \phi_{uu}(2) & . & . & \phi_{uu}(N) \\ \phi_{uu}(2) & \phi_{uu}(1) & . & . & \phi_{uu}(N-1) \\ . & . & . & . & . \\ . & . & . & . & . \\ \phi_{uu}(N) & \phi_{uu}(N-1) & . & . & \phi_{uu}(1) \end{pmatrix} \qquad (1.7)
$$

Here, R is a Toeplitz matrix generated using the autocorrelation function (ϕ_{uu}) of the input and ϕ_{yu} is the input output cross correlation function. Calculating the impulse response involves inverting the Toeplitz matrix, which can be done using a efficiently singular value decomposition. This data can also be averaged and windowed to give a precise of the impulse response.

The details of the data analysis, filtering and types of models chosen depends on the specific system been considered. These are given in Chapters 3, 4 and 5.

1.3 Conducting Polymer Actuators

In order to be used as an actuator, conducting polymers need to be able to stand freely as a bulk material and be mechanically stable enough to be tested in a dynamic mechanical analyzer (DMA). When such free standing films are created we can measure mechanical deformations in the polymer when an electrochemical stimulus is applied to the polymer. Thus input electrical work is converted into mechanical work, which is performed against a known force. In the case of conducting polymers, actuation is driven by the diffusion of ions entering and exiting the polymer (Fig. 1-2). This mechanism has been observed in many different types of conducting polymer actuator systems including polypyrrole [7, 18, 87, 100], various polythiophenes [7, 28, 49, 142, 150], poly(3,4-ethylenedioxythiophene) [146] and polyanilines [133, 137, 142]. Since these materials are driven electrochemically there are a number of variables that need to be controlled. The physical properties of the polymer such as electrical conductivity, modulus, dopant ion and porosity have significant influence on the overall strain and strain rate that can be achieved. The chemical environment

27

such as the ion type and concentration, electrolyte and temperature can influence the strains and lifetimes of the actuator. There are significant drawbacks that limit the use of these polymer actuators in practical applications. During actuation there is a permanent deformation that is caused by irreversible diffusion within the polymer that permanently increases the gaps between polymer chains. In addition, since actuation depends on diffusion of ions through the polymer film, these actuators have inherently slow speeds.
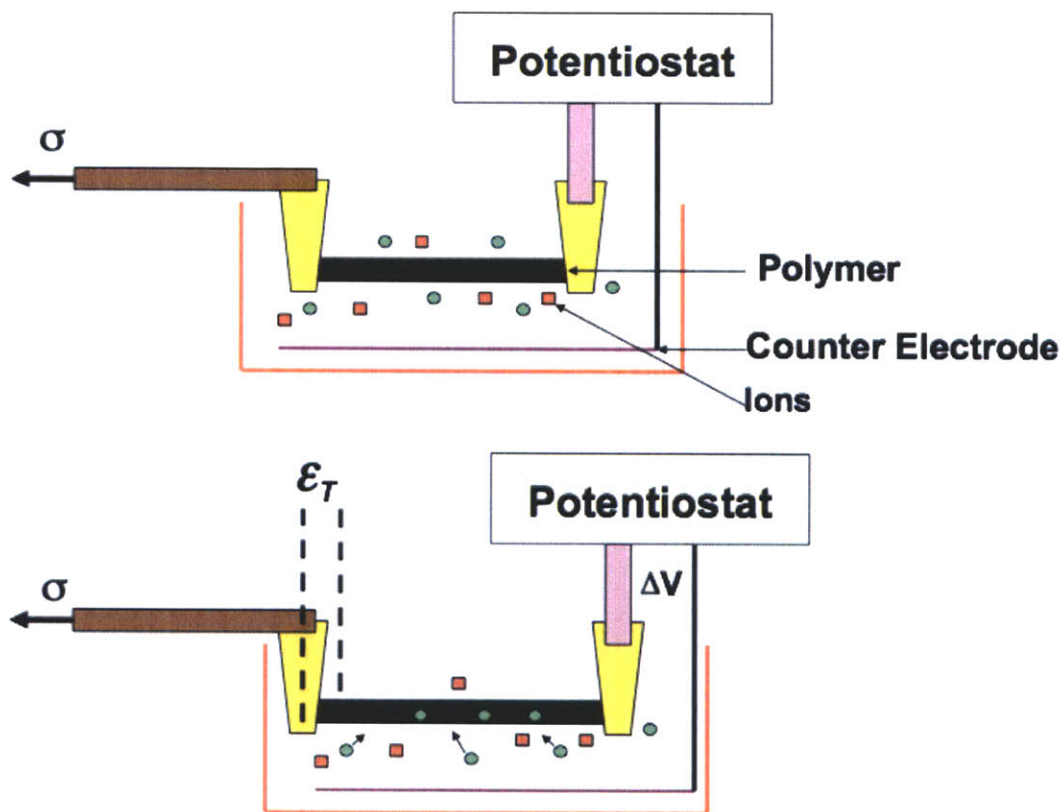
Figure 1-2: Schematic of conducting polymer actuation mechanism. Top: Conducting polymer in its unactuated state. The polymer is submerged in an electrolyte in the presence of ions. Bottom: A potential is applied to the polymer that drives ions into the film which cause the volumetric expansion.

Even with its limited performance as an actuator, many groups have attempted to use conducting polymers in a variety of applications. From underwater autonomous vehicles [15, 27, 37] to being active elements in microfuidic/MEMS devices [17, 129, 131, 132] .

1.3.1 Synthesis

Conducting polymers can be synthesis using both chemical and electrochemical methods. With the exception of polythiophenes [146] the preferred method to synthesize CPs is to use electrochemical deposition. These give rise to films that are mechanically stable, with high conductivities (10,000 S/m). The monomer is generally placed in an electrochemical 3 electrode cell mixed with a suitable solvent such as propylene carbonate or acetonitrile. The CP films grow on the working electrode of the cell when a constant potential or current is applied. For example, 005 M pyrrole can be grown on the surface of a glassy carbon electrode in the presence of 0.05M tetraethylammonium hexafluorophosphate (TEAP) in propylene carbonate (PC). The deposition is carried out at a constant current of 1.5 A/m^2 for 10 hours at -40 °C. A black, free standing film of polypyrrole (PPy) with a thickness of 20 μm results after this process is complete. This material is polypyrrole doped with hexafluorophosphate and is termed polypyrrole doped with hexafluorophosphate ion (PPy-PF$_6$). This is the most common type of material that is used as a conducting polymer actuator and is used in most parts of this thesis.

1.4 Chapter Descriptions

Chapter 2   Development of a Dynamic Mechanical Analyzer is presented that can perform stochastic system identification measurements. The details of design and signal processing are presented. The various sample configurations that can be used with this system is discussed.

Chapter 3   A stochastic technique is developed to measure the compliance of a conducting polymer. The compliance is measured as a function of counter ion swelling, solvent and the type of cation or anion dominating the actuation process.

Chapter 4   The electrical impedance of the polymer is characterized using stochastic signals. The application of a simultaneous actuator and strain sensor is demon-

strated.

Chapter 5   This chapter describes the stochastic signals that are used to characterize the isometric and isotonic responses of conducting polymer actuators. This technique is used to demonstrate the effect of temperature and solution conductivity on actuation and to develop methods that can be used to improve polymer actuator performance.

Chapter 6   Efficient techniques to incorporate functionalized carbon nanotubes into conducting polymers using layer-by-layer deposition and drop casting methods have been explored. These materials significantly reduce creep, improve conductivity and increase stiffness of the polymer actuators.

Chapter 7   Conclusions drawn from this thesis and their implications to polymer actuators are discussed. Possible areas of future work are also discussed.

Chapter 2

Electrochemical Dynamic Mechanical Analyzer

Any good instrument that can be used to measure artificial muscle actuator properties must measure active strain, active stress, work per cycle, and modulus as a function of frequency, oxidation state and efficiency. In addition, the instrument should be able to adapt to multiple sample configurations that can include thin rectangular films (less than 100 μm in thickness), fibers, and sheets for measurements in the film thickness direction. It must have the ability to measure actuators of varying lengths, widths and thicknesses. The components must also be made from materials that can tolerate multiple chemical and electrochemical environments while being exposed to relatively large potentials and currents. In addition, clamps that attach to the polymer samples must be conductive enough to make sufficient electrical contact with the polymer, but also minimize leakage currents. Artificial muscle materials can generate a variety of strains and deflections (ranging from 100 nm up to a few millimeters), forces (between 1 mV to 10 N) at potentials between 0-10 V. The instrument must be able to adapt to these requirements and is called an Electrochemical Dynamic Mechanical Analyser (EDMA)

2.1 Prior Instruments

Developing an instrument to measure the stress or force (isometric actuation) at constant strain is relatively simple. The polymer must be clamped in tension with one end attached to a force sensor. A potential can then be applied to a polymer and the force measured using a force sensor. Isotonic actuation (constant force) is a bit more complicated to implement. Various authors use different approaches to conduct isotonic measurements. Many custom instruments have been built for this purpose [24, 87, 112, 146]. These have a linear actuator that can move to keep the tension on the polymer a constant. This involves a feedback loop around some form of force sensor that controls the linear actuator. These are the most versatile instruments, since they can be adapted to measure conducting polymer actuators in multiple configurations and are capable of using arbitrary signals for stress and strain. Other instruments are commercially available lever arm systems [119]. These instruments are used to test muscle materials that have been adapted for conducting polymers [47, 124]. These are convenient to use but can be limited and expensive to adapt for different configurations. The other method for an isotonic actuation test is to use a weight (pre-load) hanging from an actuating polymer in a vertical configuration or suspended over a pulley. The position of the weight is measured using a laser displacement measurement system [58]. This method is again limited, since it cannot impose an arbitrary stress or strain.

2.2 Design of EDMA

The Electrochemical Dynamic Mechanical Analyser (EDMA) used in this work is adapted from the instrument developed by Nathan Vandersteeg [146] in 2006. A schematic of the polymer actuation mechanism and the device is shown in Fig. 1-2. A CP must be submerged in an electrolyte with counter-ions to actuate. It is attached to a mechanical stage that can apply any arbitrary stress (σ) signal. The strain (ϵ) can be measured using encoders present on the stage. The potential is controlled

using a potentiostat that can apply a voltage relative to a counter electrode in a three-electrode electrochemical cell. When a potential is applied, ions diffuse into the polymer and causes a volumetric expansion [16, 98]. Equ. 2.1 shows the total strain the polymer can generate due to ion diffusion [87].

$$\epsilon_T(s) = J(Q, s)\sigma(s) + \alpha Q(s) \tag{2.1}$$

Here, J is the compliance, Q is the charge density and s is the Laplace variable. The EDMA must be designed to measure each one of these components. A position sensor can be used to measure the strain, a force sensor can be used to measure the stress, the potential and current can be measured using a potentiostat that drives the polymer actuator. The charge can be obtained by simply integrating the current signal. Note that this is just an approximation since part of the current goes into charging a double layer and does not contribute to the strain. However, the double layer charging can be considered to be small at large time scales.

This thesis has developed instrumentation that can independently measure all the parameters relevant to polymer actuators. The setup consists of a linear brushless servomotor (ALS 130, Aerotech, Pittsburg, PA) that includes an inbuilt non-contact linear encoder with a resolution of 0.1 μm. This was used to control the displacement (strain) of the polymer. The stage is driven and controlled using a digital servo amplifier (NL Drive HL, Aerotech, Pittsburg, PA) with an inbuilt proportional, integral and derivative. (PID) controller and a D/A converter that converts the encoder signal to an analog signal. These signals can be adjusted so that different lengths and strains can be measured using the apparatus. This can then be adapted to measure strains in fibers, thin films as well as make thickness direction measurements where a resolution of 100 nm is needed.
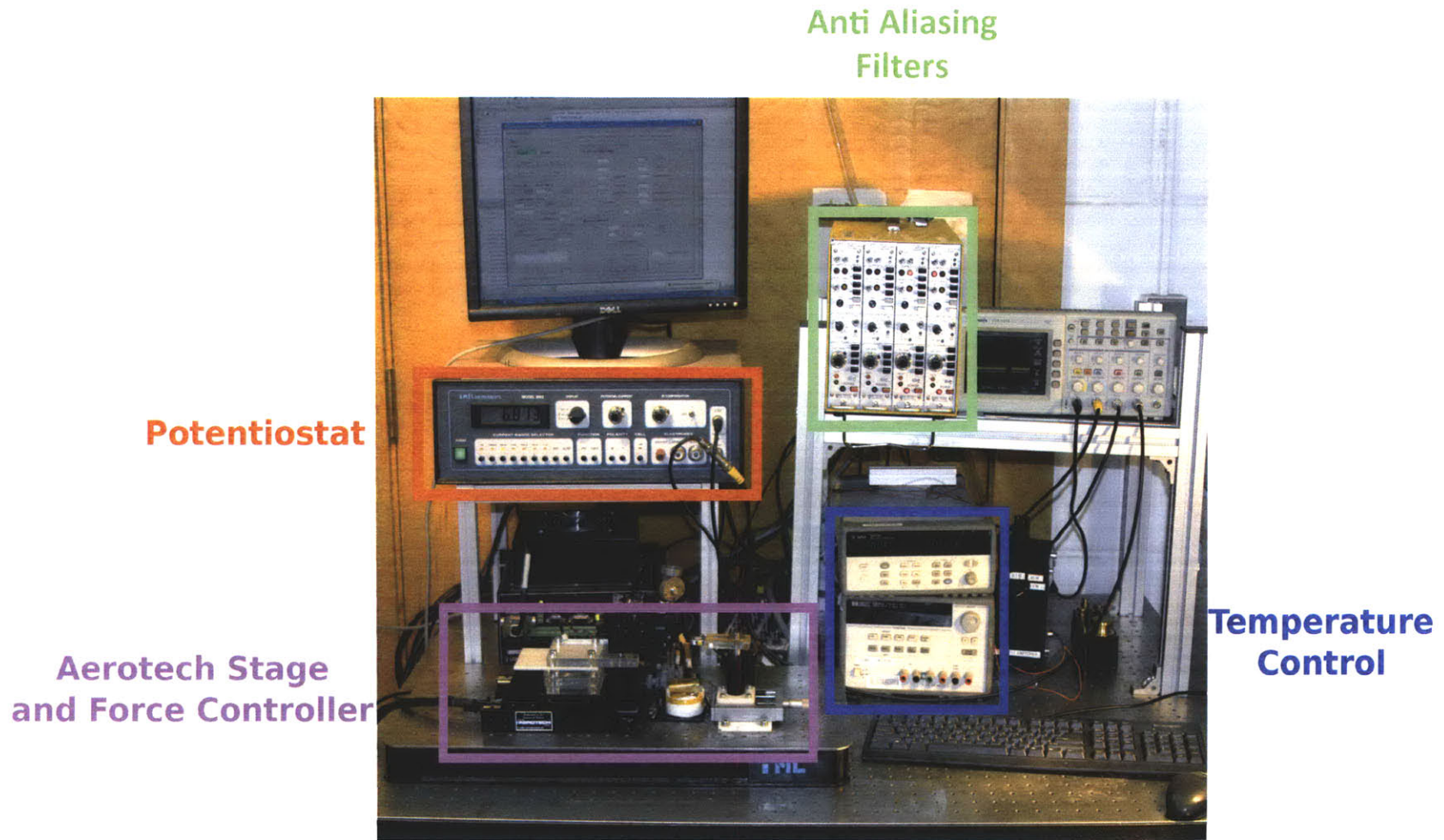
Figure 2-1: Picture of the entire EDMA showing all the components: the Aerotech stage and force sensor, the potentiostat, signal conditioning and anti aliasing filters and the temperature control module.

A S-beam load sensor (LSB 200, Futek, Irvine, CA, max load 1 N) is used to measure the load (i.e. stress); and these are interchangeable in order to measure maximum loads as low as 0.1 N and up to 45 N. This can be used to measure a wide range of polymeric materials and geometries. The load and displacement signals are amplified using signal-conditioning amplifiers (Model 2311, Vishay Electronics), which also filter the signals at 100 Hz using a second order Butterworth filter. This provides anti-aliasing as well as corrects for temperature drift and improves noise rejection. A potentiostat (Model 2053, AMEL Instruments) drives a three-electrode cell that incorporates the polymer as the working electrode. The loads, displacement, potential and current are all sampled with 16 bits of precision using a PCI card (PCI 6052E, National Instruments Corp. Austin, TX) with software written in Visual Basic. This instrument will henceforth be called the stochastic electrochemical dynamic mechanical analyzer (EDMA) (Fig. 2-1).
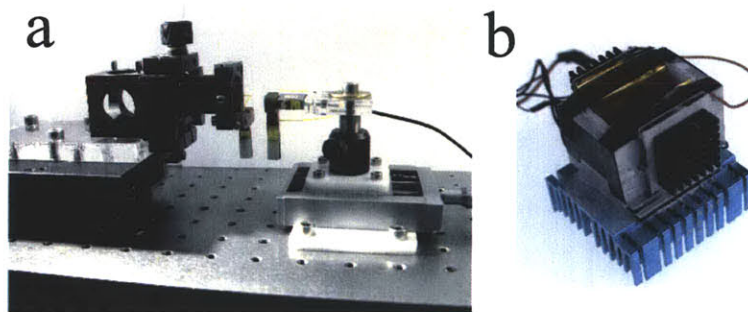
Figure 2-2: (a) Photograph of the SEDMA. The Aerotech linear stage is attached to the left clamp using a manual micro-positioning system. The other clamp is attached to the Futek force sensor. The micro-positioning system allows us to align the polymer so that it is in line with the force sensor. (b) The electrochemical bath that the sample is immersed. Peltier heaters allow heating and cooling of the electrolyte and ensure a constant temperature during tests.

The samples are placed between the custom built clamps (see Fig. 2-2a) which then can be submerged in a bath (Fig. 2-2b) filled with electrolyte. The electrochemical bath is made of either nylon or Teflon and resistant to most solvents. The clamps are laser machined from Delrin infused with Teflon (McMaster-Carr, Aurora, OH) and are inert to the chemical environments being used (specifically to PC, $BMIMPF_6$, ACN and dichloromethane (DCM)). Electrical contact to the polymer

is made inside the clamp using gold foil. This prevents leakage currents from parts of the contacts that are exposed to the electrolyte. The clamps are mounted on a precision optical positioner that can ensure that the samples are aligned. The temperature of the bath containing the electrolyte is also controlled using a Peltier heater and a PID controller (Fig. 2-2b). The temperature of the bath and the electrolyte can range from 20 °C to 80 °C. The polymer is the working electrode and part of a three-electrode electrochemical cell. The electrolyte bath consists of stainless steel counter electrode with a surface area at least 200 times larger than the surface area of the polymer to ensure that the reactions at the working electrode are not surface area limited by the counter electrode. A silver wire electrode was placed near the polymer and was used as a reference electrode. For the electrolytes and potential ranges tested in this thesis, the silver wire electrode is stable and does not contribute to a drift in potential.

2.3 EDMA Configurations

The clamps for the EDMA are extremely adaptable and can be used to make actuation measurements on many different sample configurations. They are modular and can be easily replaced with different clamps that are suited for making measurements on long thin films, fibers, and non-free standing films. Fig. 2-3 shows the different possible configurations of the EDMA. The rapid sample replacement clamps are the most commonly used, and their functionality is described elsewhere [105, 110, 146]. The sections below describe the design and typical results obtained from each configuration.

System ID Clamps
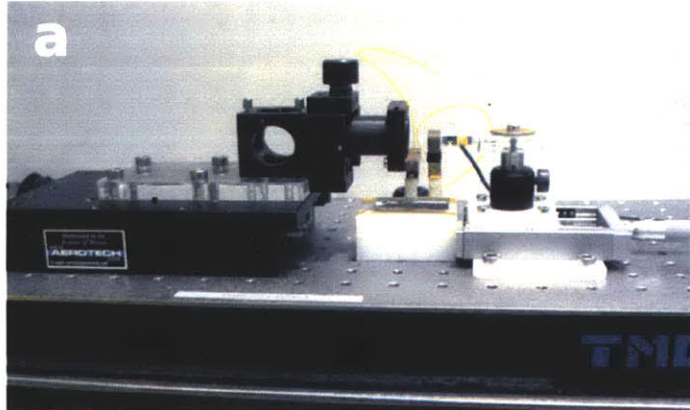
Rapid Sample Replacement
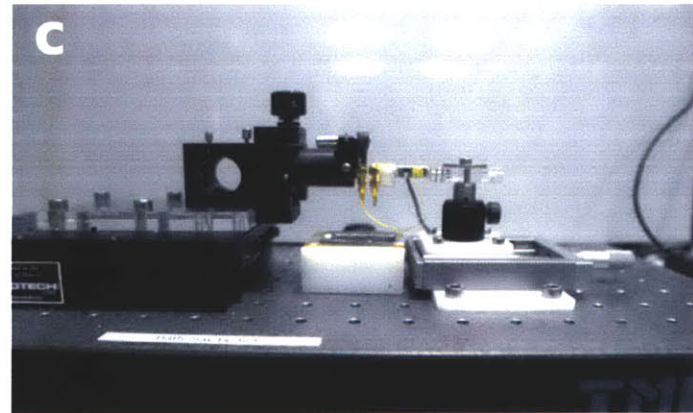
Micro-Wire Clamps
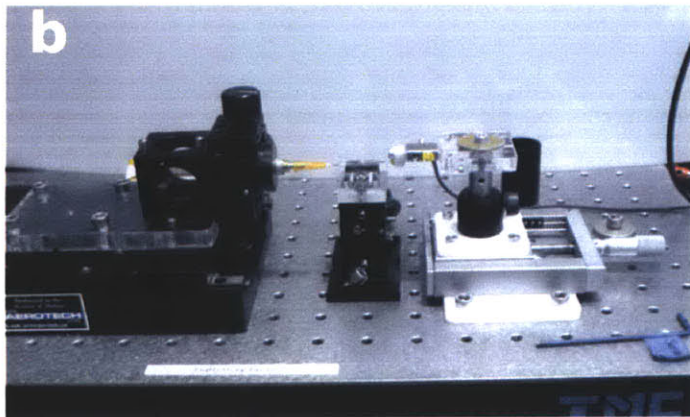
In-situ Actuation Setup
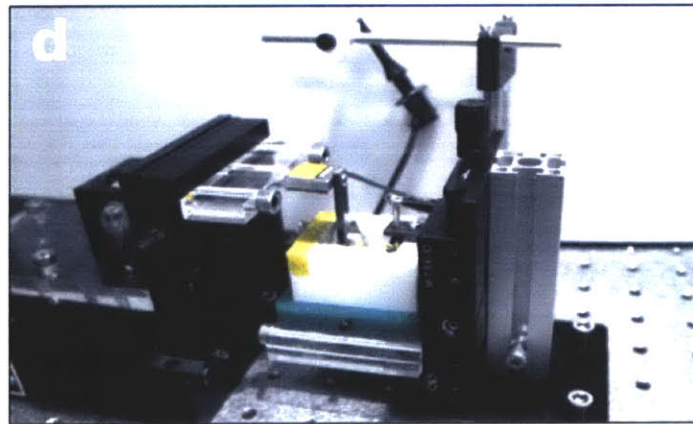
Figure 2-3: The different clamps configurations of the EDMA. a) The clamps used to conduct system ID experiments with the Delrin clamps and the internal gold foil. b) Clamps to conduct tests on micro-wires. The wires are clamped in the syringes using a crimp. c) Gold plated alligator clips are used when multiple samples need to be loaded and unloaded into the instrument. d) Setup to conduct measurement of non-free standing films.

2.3.1 Actuation of Polymer Fibers

Numerous techniques exist to create conducting polymer fibers and have been summarized in [115, 116]. These fibers can have potential applications in textiles [33, 75], neural wires and probes [11, 81], antennas [102], and a variety of sensors [118, 83, 95, 75]. However, mechanical testing on these fibers can be difficult, since they cannot be easily clamped onto any traditional DMA and be actuated at the same time. The stochastic electrochemical dynamic mechanical analyzer (SEDMA) was modified and tested with the help of Miguel Saez. The Delrin clamps were replaced with needle clamps described in [115]. The 20 μm square cross-section wires are crimped into needles and screwed on to the Aerotech stage and the load cell. The load cell used had a 0.1 N maximum force rating which was necessary to keep the forces on the wire above the noise level of the sensor. The electrochemical bath was created using a wire electrical discharge machining process. The channel created was 2 mm in width, and the electrolyte was held in place using surface tension (See Fig. 2-4: Left). A

(b) Isotonic strain response
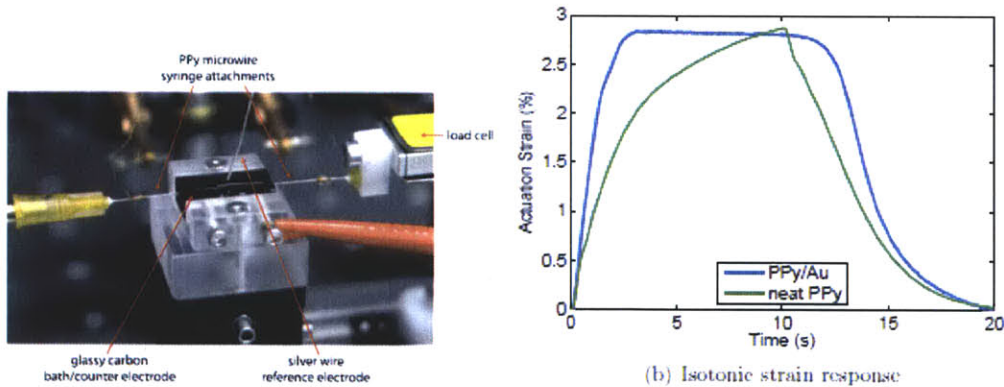
Figure 2-4: Left: Setup for actuating polypyrrole fibers. Right: Typical isotonic data from a polypyrrole fiber at an 1 MPa preload. (Adapted from [115, 116])

typical result that can be obtained from this setup is shown in Fig. 2-4. PPy films, one coated with gold and one without, were actuated in neat $BMIMPF_6$. The typical strains obtained from fibers were larger than the strains obtained from thin films generated from the same material. In addition, the gold-coated PPy-Au films were significantly faster than the plain PPy films.

38

2.3.2   In-Situ Characterization of Polymers

Current actuation verification techniques in the development of CPs require that the electrodeposited thin films have robust material properties. They have to be robust enough so that they can be removed from the deposition surface (free-standing), which severely limits the different types of films that can be tested. However, a few researchers have developed techniques to measure actuation in the thickness direction in thin films [67, 109, 130]. These techniques can be complex and difficult to implement and interpret. However, the EDMA can be easily adapted as a screening tool to characterize new CP films, which cannot be peeled off a substrate. This allows for the in-situ measurement of actuation in thin films of CPs. This instrument measures actuation in the thickness direction of conducting polymer thin films in the deposition environment. (This work was done with the help of Lauren Montemayor).
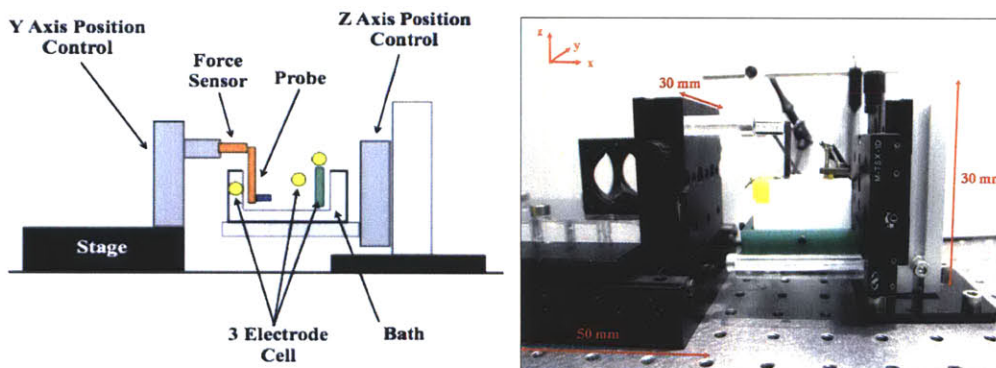
Figure 2-5: Left: Schematic of instrument for electrochemical cycling tests. Right: Picture of fabricated instrument. (Adapted from [93])

A schematic of the set-up is shown in Fig. 2-5. The stage allows for movement up to 50 mm in the x-direction. The vertical (z-direction) and horizontal (y-direction) position controllers allow for a total of up to 30 mm of movement. The interaction of these two position controllers allows for the probe to measure a variety of points on the film. The ability of the instrument to survey various points on the conducting polymer allows us to observe the effects of film thickness on polymer actuation without removing the sample. This is a useful characteristic due to the thickness

39

gradient of vertically deposited CP thin films. The PPy film is grown in a deposition bath constructed of Teflon and is capable of holding a glassy carbon electrode (deposition surface) and approximately 20 mL of electrolyte. The deposition bath fits directly into the testing set-up, allowing the deposition environment to double as the actuation environment. The glassy carbon is covered with Kapton tape exposing only the film area, which is approximately 15 mm × 15 mm. A thin sheet of stainless steel, with an area of approximately 1300 mm^2, functions as the counter electrode and is placed opposite the working electrode in the deposition environment. The reference electrode (silver wire) is placed close to the working electrode in the electrolyte. To measure the actuation of the PPy films in the thickness direction, a force sensor and probe are attached to the stage via the horizontal (y-direction) position controller. A 0.1 N force sensor (Futek, LSB 200), capable of force detection with an accuracy of 0.1 mN, is attached to a small Delrin beam with a nylon screw at the end. The beam and screw are submerged in the electrolyte. Delrin and nylon were chosen as the materials to transfer actuation forces because they do not deteriorate in the presence of propylene carbonate, which is used as the solvent. The actuation force generated by the film is transferred from the tip of the nylon screw (which makes contact with the film) through the Delrin beam, and is measured at the force sensor. Fig. 2-5 (right) shows the fabricated set-up. The performance of the
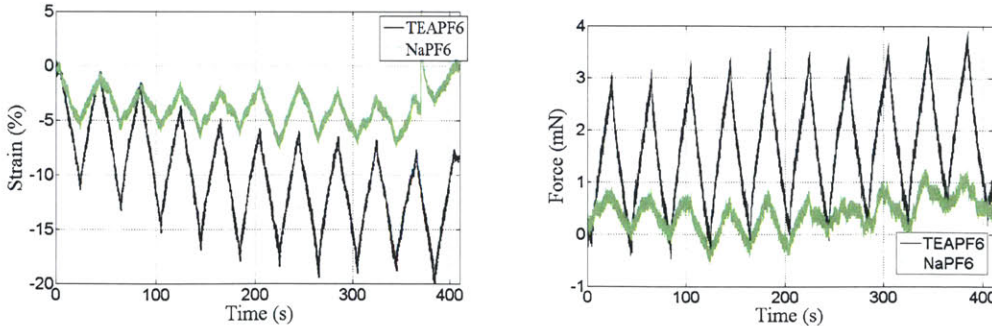
Figure 2-6: Left: Isometric response at preload = -5 mN, Right: Isotonic response at target load = -5 mN, for TEAP and NaPF$_6$ doped polypyrrole films in 0.05 M solution of the respective electrolytes.

instrument was characterized in Montemayor et al [93]. As shown in Fig. 2-6 right,

tetramethylammonium hexafluorophosphate (TMAP) doped PPy films produced the largest strains of approximately 25% while, $NaPF_6$ doped films produced the smaller strains at approximately 3%, which are comparable to previous results [130]. As seen in Figure 3, the percent strain magnitude over a cycle is approximately constant, while the change in absolute position varies due to the creep in the films. This shows that the instrument is capable of detecting and measuring changes in force and position of various non free standing conducting polymers in the presence of electrochemical cycling.

2.3.3 Clamps for System ID measurements

The clamps used to conduct the system identification experiments were described briefly in Sec 2.2. The clamps need to provide a large clamping force within a chemical environment so that the polymer does not slip during actuation or when a stochastic stress input is applied to the material. To do this, the films were screwed into a clamp with two M2.5 screws. There is a gold foil between the clamping plates through which a potential is applied to the polymer. The gold foil needs to be shielded from the chemical environment, since all the current must flow through the polymer and not the foil. This minimizes the parasitic currents that can degrade polymer performance and complicate the identification procedure [105, 124]. The clamps are manufactured from Teflon infused with Delrin, which is harder than pure Teflon and can be laser machined. This allows for a large and even clamping force. It also retains the properties of the Teflon since it is inert to many different solvents. However, over multiple experiments the Teflon infused with Delrin do show signs of fatigue and must be replaced periodically.

2.4 Conclusions

The development of an EDMA is described in this chapter. This instrument is capable of measuring forces and displacements in electrochemical environments for multiple polymer configurations. The modular design allows for us to easily change compo-
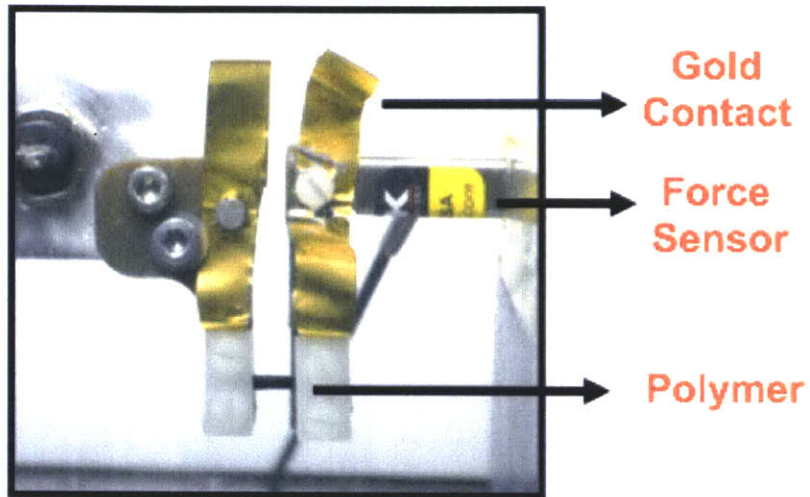
Figure 2-7: Clamps used for system identification experiments.

nents for a number of different configurations. In addition having temperature control allows us to actuate the polymer at high temperatures. In subsequent chapters, the EDMA has been used to conduct tests using stochastic waveforms for force, potentials and currents. These have been used to gain additional insight into the performance of conducting polymer actuators and have been used to improve their properties. The EDMA described in this chapter can be adapted for multiple polymer configurations and provides a versatile tool that is used to characterize conducting polymer actuators.

Chapter 3

Mechanical Characterization

The compliance of many conducting polymer materials are strong functions of their input stimuli and hence are also studied as materials with tunable stiffnesss [21, 26, 44, 109, 124]. The implications that a significant change in elastic modulus has on actuation have been discussed widely in [18, 133, 135, 136]. There are a few techniques that are used to measure the moduli, but these techniques cannot measure them as a function of the changing stimulus. In this chapter, a technique is used to dynamically measure the modulus or compliance as a function of frequency and excitation state of conducting polymers. These films undergo dimensional changes based on diffusion of ions in and out of the polymer films coupled with a change of dynamic stiffness or compliance of the material. If the conducting polymer is held in tension, then this changing compliance contributes to the overall strain. Understanding this phenomenon can help improve actuator performance by increasing the overall strain as well as increase its bandwidth. A variety of experimental techniques have led to a number of discrepancies in the literature associated with how the compliance changes during electrochemical cycling [109]. Pytel et al [109] superimposed a sinusoidal stress perturbation while applying a square wave potential. Others [12, 98, 135] held the polymer at a desired potential, and the modulus was tested at a constant strain rate. These techniques are only capable of measuring the dynamic compliance at single frequencies and at discrete oxidation states. Shao et al. [124] measured the storage and loss modulus of polypyrrole as a function of oxidation state, load and frequency for a

43

single electrolyte-solvent combination. Their technique used a constant or ramp loads superimposed on a higher frequency sinusoidal stress perturbation. This technique is limited since it can only measure the modulus at a given load, oxidation state and a single frequency at a time. In order to fully characterize the response, we would have to measure the compliance at all relevant frequencies at numerous oxidation states which would be time consuming and inefficient.

A more efficient technique would be to compute the compliance impulse response as a function of a slowly changing potential input. The impulse response function can be convolved with any input stress waveform to predict the strain waveform. The impulse response function can also be used to calculate the frequency response function of the compliance. This approach involves applying a stochastic stress waveform and measuring the resulting strain while simultaneously applying a potential waveform. We can then use SSID techniques [69, 80] to estimate the compliance impulse response function of the polymer.

3.1 Theoretical Considerations

The total polymer strain ϵ_T is composed of two components, one from the changing dynamic compliance (J) and another from a volumetric expansion caused during charge injection [85]. This is given by

$$\epsilon_T(s) = J(Q, s)\sigma + \alpha Q(s) \tag{3.1}$$

where α is the strain to charge ratio and Q is the volumetric charge injected into the polymer. Here, s represents the Laplace variable and $J(Q, s)$ is the compliance transfer function of the polymer. A block diagram illustrating the experimental setup and Equ. 3.1 and described in Sec. 2.2 is shown in Fig. 3-1. The measured quantities of stress (σ_m) and strain (ϵ_m) can be used to calculate the compliance. These differ from the true values due to random measurement errors (E_1, E_2). The errors are assumed to be time independent, white signals with a Gaussian probability distribution with zero mean and constant variance. The mechanical dynamics of the stage

44
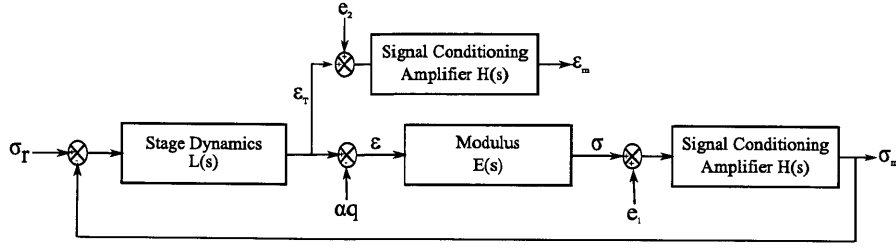
Figure 3-1: Simplified block diagram of the instrument developed. Both the strain and stress signals were measured and sent through signal conditioning amplifiers and anti-aliasing filters with transfer function H(s).

is represented by the transfer function $L(s)$. The stage controller uses an internal feedback loop that targets the desired stress input (σ_r). This enables us to get a higher bandwidth input and allows us better control over the input signal but also can complicate the SSID procedure.

To understand the effects of the feedback on the SSID procedure, we can construct the following equations based on the block diagram in Fig. 3-1.

$$\sigma_m = \frac{H}{HGL+1}E_2 - \frac{HG\alpha}{HGL+1}Q + \frac{HGL}{HGL+1}\sigma_r$$

$$\epsilon_m = HE_1 + \left(\frac{H^2L}{HGL+1}E_2 + \frac{H^2LG\alpha}{HGL+1}Q + \frac{HL}{HGL+1}\sigma_r \right) \tag{3.2}$$

Note that all expressions are in the Laplace domain. Using these, we can calculate expressions for the auto ($\Phi_{\sigma_m \sigma_m}$) and cross-spectral density functions[69] ($\Phi_{\epsilon_m \sigma_m}$) to derive

$$G \times \Phi_{\epsilon_m \sigma_m} - \Phi_{\sigma_m \sigma_m} = -\frac{HH^* \left(GQG^*Q^*\alpha^2 + E_2 E_2^* \right)}{H^*G^*L^* + 1} \tag{3.3}$$

This assumes that the noise signals (E_1, E_2) and the inputs (Q, σ_r) are all uncorrelated with each other. The modulus G and α are the parameters to be identified. Using dimensional analysis, we can show that the second term on the right hand side of Equ. 3.3 can be assumed to be small relative to the other terms. If there is no electrochemical input (Q=0), the compliance (J) is obtained by dividing the input

45

output cross-spectral density by the input auto-spectral density [69].

$$J = \frac{\Phi_{\epsilon_m \sigma_m}}{\Phi_{\sigma_m \sigma_m}} \qquad (3.4)$$

An equivalent expression can be obtained in the time domain, where the compliance impulse response function can be calculated by deconvolving the input auto-correlation function from the input output cross-correlation function using a Toeplitz matrix inversion [103, 104]. If there is an electrochemical input, the volumetric strain can simply be subtracted from the total strain data. The compliance is then calculated using the residual strains and the stress input. The quality of the system identification procedure can be assessed using the coherence squared (γ^2), given by Equ. 3.5. If there is any significant sensor noise or nonlinearities within the system, the coherence squared will be less than one[69].

$$\gamma^2 = \frac{\overline{\Phi}_{\epsilon_m \sigma_m} \overline{\Phi}^{*}_{\epsilon_m \sigma_m}}{\overline{\Phi}_{\epsilon_m \epsilon_m} \overline{\Phi}_{\sigma_m \sigma_m}} \qquad (3.5)$$

3.2 Input Design

The beginning of any systematic exercise in system identification starts with the choice of inputs and outputs. In the case of measuring compliance, the natural choice is to consider stress as an input and strain as an output. Next the form of the input signal must be specified. Conducting linear system identification using signals with a Gaussian probability density function (PDF) is ubiquitous. When a signal with a Gaussian PDF is input into a linear system the output will also have a Gaussian PDF. For a purely linear system, a small range of inputs can be sufficient to fully characterize the system. Gaussian white signals also satisfy the conditions of persistent excitation, have a large crest factor and are informative [80]. In addition there are physical limitations to the input when considering the range of stresses that can be applied to a polymer. The input waveform σ_r is a stochastic waveform with a Gaussian PDF centered on the linear viscoelastic region of the polymer (See Fig. 3-2).

46
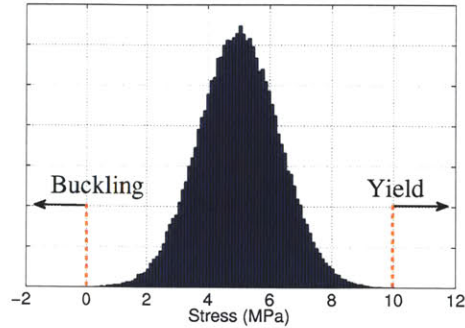
Figure 3-2: Typical PDF of stress waveform applied to the polymer. The PDF is centered between the zero stress state and the yield point.

This was determined using a uniaxial tensile test to measure the loads at which the polymer yields and breaks. These give the range of stress that can be applied to the polymer without causing yielding or buckling which would appear as nonlinearities in the response. During normal polymer actuator performance, it should never be in a buckled state because the polymer cannot sustain any compressive loads. In addition, applying large loads to the conducting polymer material will cause it to yield. Again in any practical application, any plastic deformation of the polymer should be avoided; hence, this region of the stress-strain curve must also be avoided. Fig. 3-3 shows the effect of the stochastic stress input on three different common polymers. The more compliant (Latex and PDMS) show both the buckling and yield that appear as nonlinearities in the system ID procedure.

There is no obvious criteria that can provide an optimal bandwidth of the input. Ideally the input is limited so that it does not excite higher noise modes that can become aliased. Additionally, the frequency of the input should have large power at desirable frequencies (i.e. frequency that can influence the bode plot the most). In this case, the actuator used limits the bandwidth of the stress input, and the Aerotech stage can generate an input bandwidth up to 30 Hz. Since CP based actuators rarely actuate past 2 Hz, characterizing the compliance past 30 Hz is not necessary. Due to the presence of the anti-aliasing filters and a sampling rate of 1000 Hz, aliasing was not a problem. However, for actuators with larger bandwidths, higher frequencies can be achieved by using a piezoelectric actuator with a smaller stroke and an interferometer

47

to measure the displacement [140].

Polypyrrole

Latex

PDMS
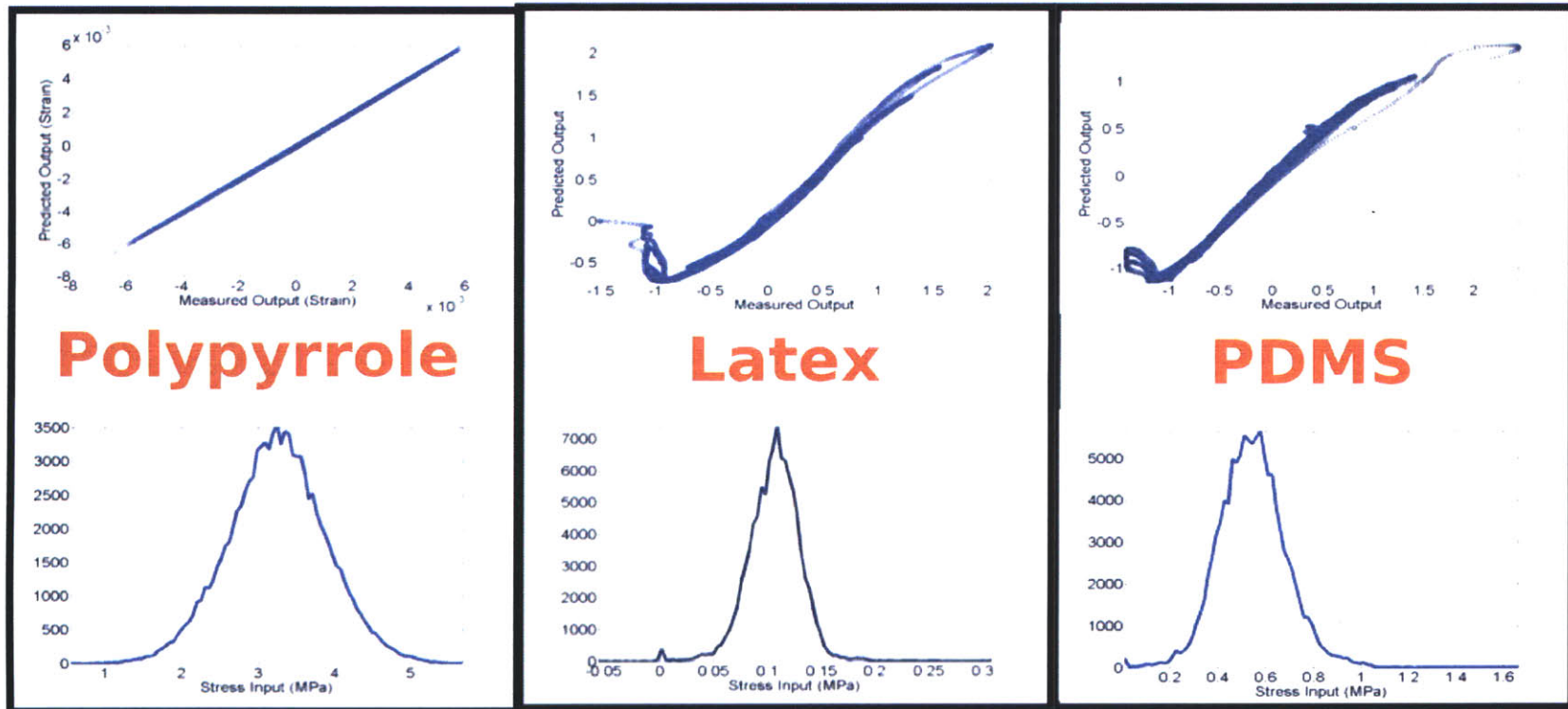
Figure 3-3: Result of SSID procedures on three different polymers of varying compliances. Left: PPy-PF$_6$ excited using the stress input described in Sec 3.2. The response shows no nonlinearities since the predicted output (strain) and the true output are the same. Middle: Stochastic stress input applied on latex showing both buckling (small strains) and yield (large strains). Right: Stochastic stress input applied on PDMS showing both buckling (small strains) and yield (large strains).

3.3 Mechanical Characterization

The conducting polymer PPy was used to validate the instrument's performance. Polypyrrole was chosen due to robust mechanical properties and its ubiquitous use as a polymer actuator [85, 84]. The pyrrole monomer (Aldrich 99%, St. Louis, MO) was vacuum distilled before use. Polypyrrole was electrodeposited on a glassy carbon substrate at $-40\,^{\circ}C$ at a constant current density of 1.0 A/m^2. The deposition solution used was 0.05 M pyrrole in 0.05 M TEAP in propylene carbonate. The resulting polypyrrole films were peeled from the surface of the electrode and cut in 2 mm $\times$ 10 mm strips. The thickness of the films were between 10 and 20 μm.

Before testing, the sample was preconditioned by applying the input stochastic stress signal for 100 s before the data was collected. A subsequent test was conducted to measure the dynamic compliance using the stochastic stress input without any electrochemical excitation. The samples were clamped in the apparatus and immersed in BMIMPF$_6$. The PPy samples were excited using the stress input described in Sec. 3.2, and strain data were measured using the encoders on the stage. The dynamic compliance transfer function was calculated using Equ. 3.4. In order to compare the response obtained using the stochastic signals, applying a sinusoidal stress waveform at discrete frequencies and measuring the corresponding strain calculated the compliance. The compliance at each frequency is then the ratio of the strain amplitude with respect to the stress amplitude. The coherence squared was also calculated from the same stochastic stress-strain data.

The calculated compliance impulse response function of polypyrrole is shown in Fig. 3-4a. The impulse response function rises to 200 GPa^{-1} and falls to zero within 20 lags or 0.02 s. Therefore, a 40 point impulse response function will be used to model the data. Additionally, a third order model with three independent time constants can be fitted to the impulse response (Fig. 3-4a). The predicted strain, is compared with the measured strain and the variance accounted is calculated. Using the nonparametric estimate, the variance accounted for is 99%; it is 96% using the third order parametric model. This implies that the system behaves linearly within the
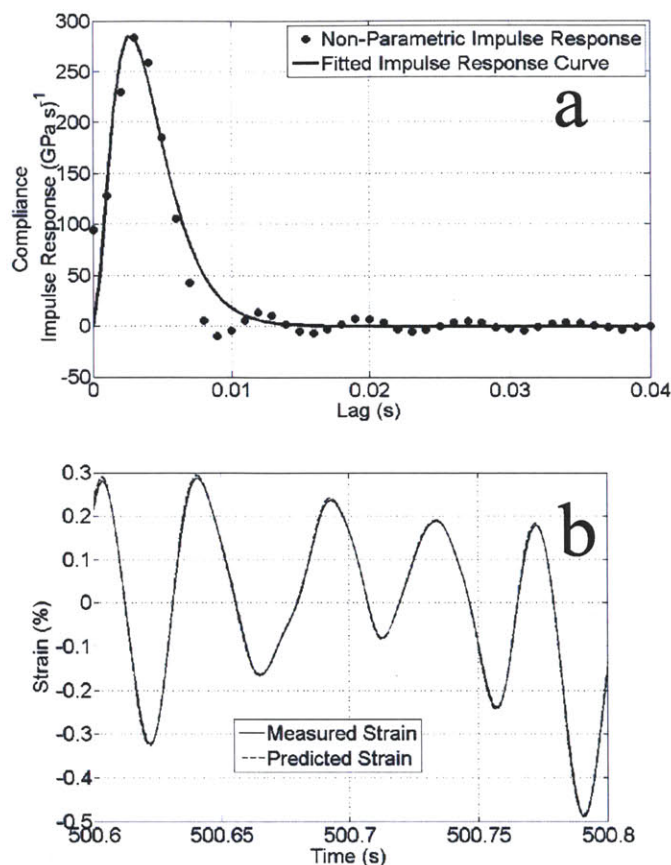
Figure 3-4: The calculated compliance response of polypyrrole without any electro-chemical input. (a) The impulse response representation of the transfer function. A three time constant expression that is fitted to the non-parametric impulse response is also shown. (b) A section of the predicted strain calculated using the non-parametric impulse response compared with the measured strain (From. [106])

amplitude range tested, and we observed no load dependence of the compliance in the $BMIMPF_6$ system. Different data sets were collected from the same material, and the parameters of the impulse response function changes by 2-3%.

The frequency domain representation of the compliance transfer function is shown in Fig. 3-5. The low frequency compliance was 2 GPa^{-1}, which corresponds to an elastic modulus of 500 ± 10 MPa. This matches with prior studies conducted on the same material [109, 124] implying that this compliance is physically meaningful. There was a gradual reduction in the compliance until 100 Hz, after which there was a large drop in the compliance. This is due to the signal conditioning amplifiers,

which filter the signal at 100 Hz. The compliance was also calculated using the discrete sinusoidal stress input, which matches the gain and phase calculated from the stochastic stress input. However, the coherence squared (Fig. 3-5c) estimate was close to one only until 100 Hz, after which there was a large drop. This would indicate that the compliance response shown in Fig. 3-5a was only valid up to 100 Hz. Since the length of the test was about 100 s, the coherence starts to fall below one for frequencies less than 0.01 Hz. If longer tests are conducted, the coherence remains high at lower frequencies. The compliance calculated by the discrete sinusoidal input follows the compliance calculated from the stochastic stress input up to 100 Hz, after which it begins to deviate; which confirms the observations from the coherence plot. Since the bandwidth of these polymer actuators is typically less than 2 Hz, characterizing the compliance at higher frequencies is unnecessary. Our input stress is within a range of 2 to 10 MPa, and it should be noted that the response calculated is accurate within that stress range. At higher stresses, the polymer would yield and the response would become nonlinear.

3.4 Influence of Electrochemistry on Compliance

To characterize the effect of the oxidation and reduction on PPy compliance, an ionic liquid $BMIMPF_6$ was used. $BMIMPF_6$ at moderate voltages drives only the cation ($BMIM^+$) in and out of the polymer film [71, 82, 109]. This work was done with the assistance of Emmanual Hernandez. This also avoids incorporation of solvent into the polymer that can influence the polymer compliance response [124]. The samples were clamped into the SEDMA and preconditioned by applying a stochastic stress input signal for 100 s, after which we applied a triangular wave potential input without the stress waveform until the electrochemical response is stabilized. This preconditioning is necessary to remove initial transients that occur during electrochemical cycling. In the subsequent test, two separate inputs are used to excite the polymer, an electrochemical potential between 0.8 V to -0.8 V and the stochastic stress. Tests were conducted at rates ranging from 500 mV/s to 1 mV/s, and the compliance re-
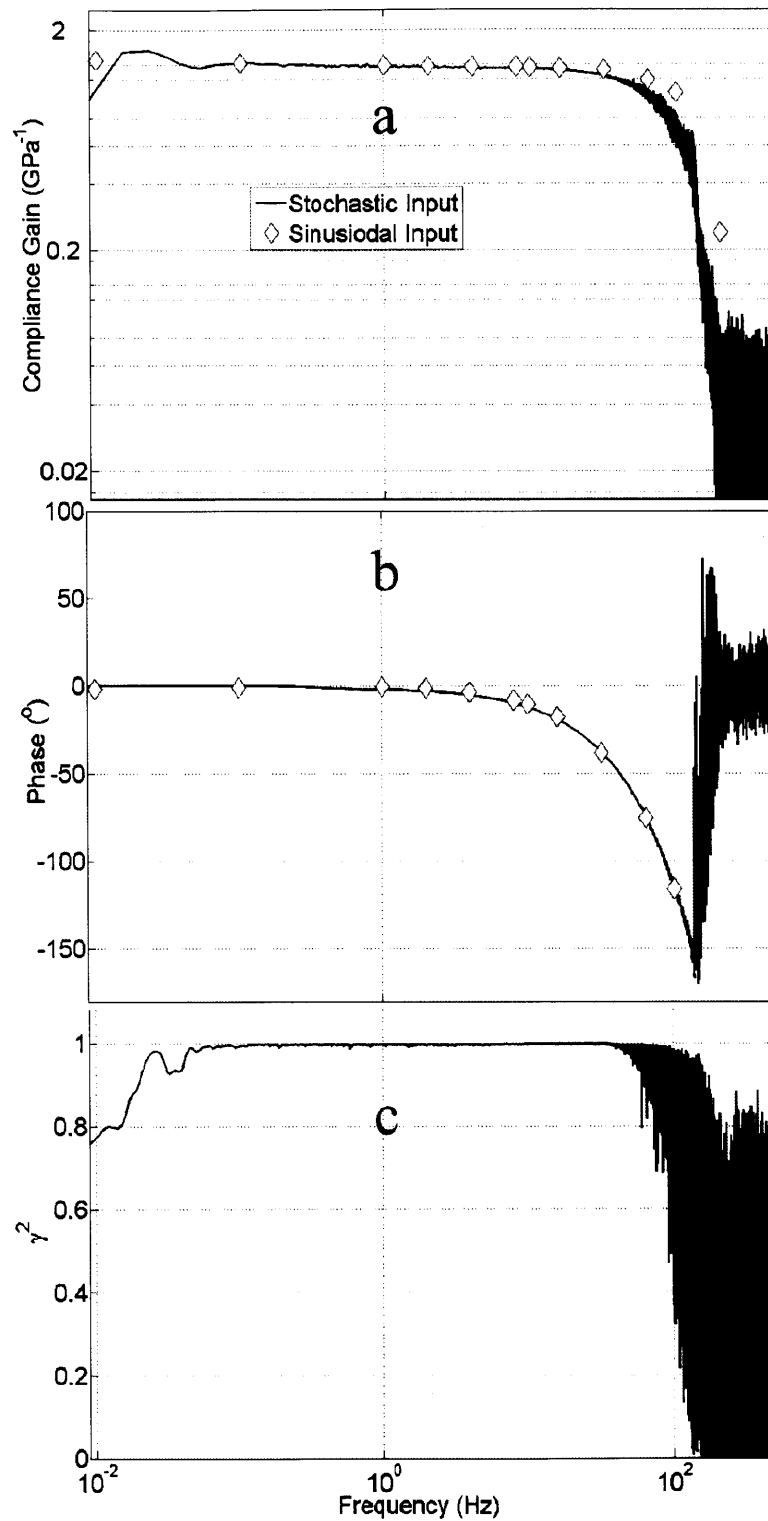
Figure 3-5: (a,b) Frequency domain representation of the compliance transfer function of polypyrrole (PPy). The function was calculated using both a stochastic input as well as a sinusoidal input. c: Coherence squared calculated using Equ. 3.5. This implies that the response is either nonlinear or has significant noise after 100 Hz (From. [106]).

53

sponse stabilized at rates below 5 mV/s. Fig. 3-6 shows the maximum value of the cross correlation between the low frequency compliance gain (DC compliance) and the charge. Here, the cross-correlation term stabilized below 10 mV/s, indicating that this is enough time for the compliance to reach a steady state value. If charge is driven at faster rates, the compliance does not have enough time to stabilize, and the measurement of the compliance is meaningless. The stress input was the same as described in Sec. 3.2, and all tests were conducted at 27 °C. The resulting strain was a high frequency strain superimposed on a low frequency strain (See Fig. 3-7).
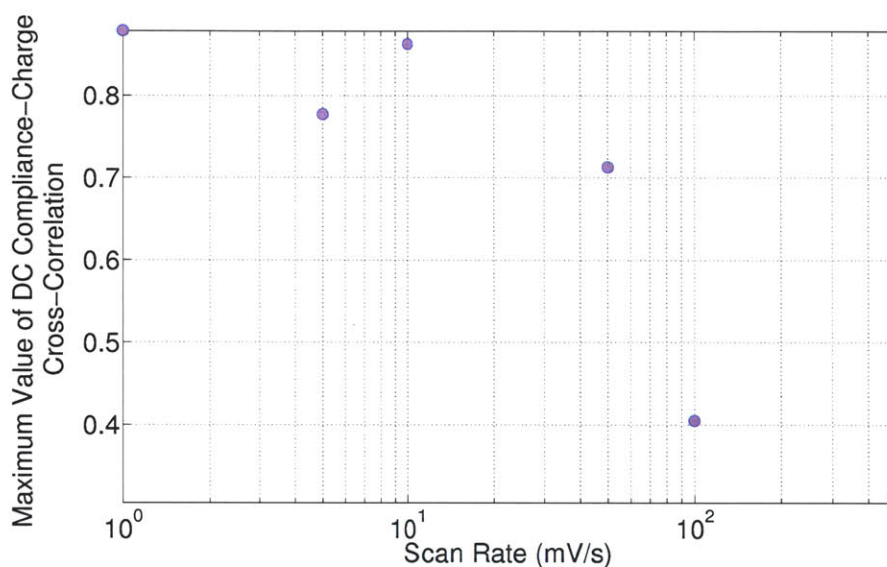
Figure 3-6: DC Compliance-Charge cross-correlation showing the response stabilizes below 10 mV/s.
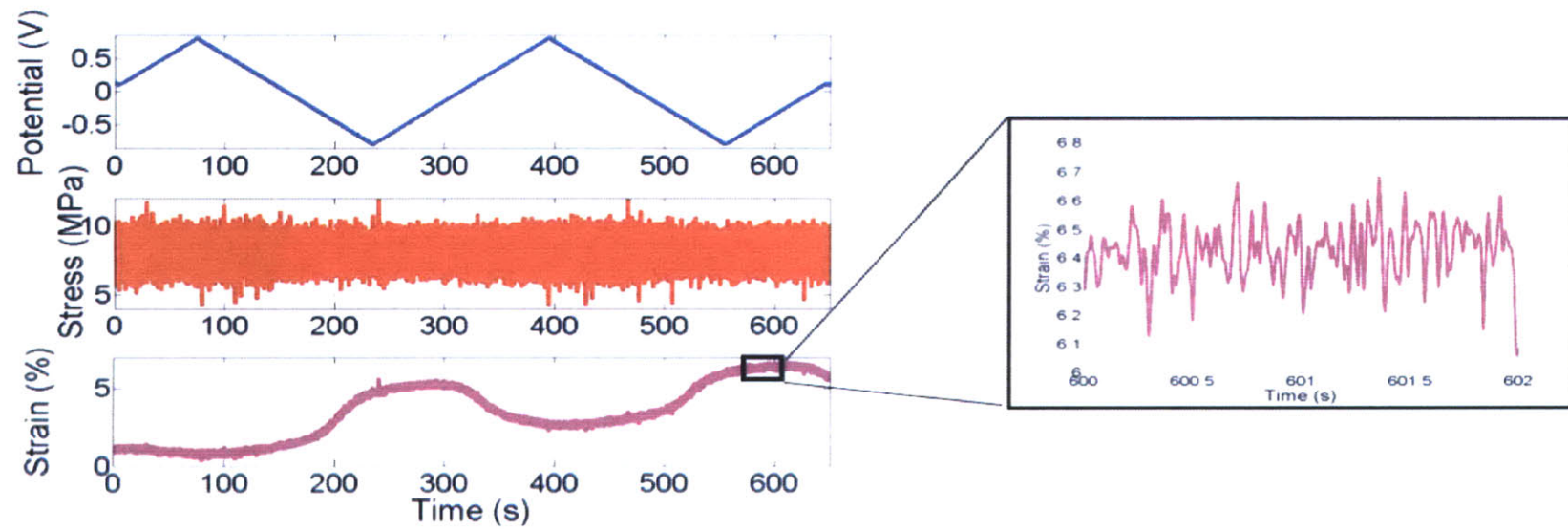
Figure 3-7: Polypyrrole being excited using a triangle wave voltage input that varies at 10mV/sec and the stochastic stress input. The output strain has a low frequency volumetric component proportional to the charge superimposed on a high frequency strain (From [103]).
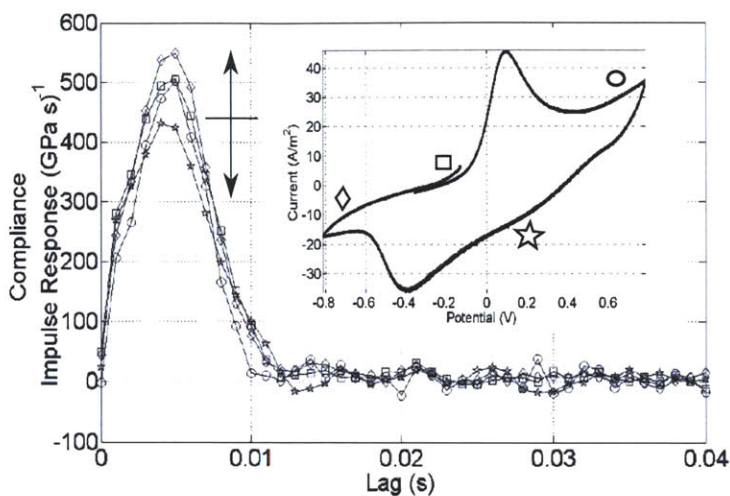
Figure 3-8: The compliance impulse response function calculated at multiple parts of the cyclic voltamogram: the impulse response sweeps up and down as the potential is swept back and forth. Insert: The cyclic voltamogram obtained at 5 mV/s. The symbols represent the regions where the impulse responses in the figure are calculated (From [106]).

The resulting strain was composed of a low frequency strain proportional to the charge injected into the polymer and a high frequency strain due to input stress. The resulting stress and strain data were sectioned into sequences of 10 seconds, and the data were detrended. The impulse response and frequency response functions for each of the sections were calculated. Since the frequency of the applied potential is 5 mV/s, there was little change to the compliance due to charge injection during the 10 s interval. The compliance impulse response functions are strongly correlated with the charge injected into the polymer and changes by 40-50% during electrochemical cycling. This exceeds the variation of the impulse response coming from the noise within the system. The changing compliance impulse response function is shown in Fig. 3-8. Each function is measured at different regions of the cyclic voltamogram (shown in the insert). The low frequency gain (gain at 0.2 Hz) of the compliance is the area under the curve of the impulse response function and shows the most significant change. The changing low frequency compliance due to charge injection is shown in Fig.3-10. As the BMIM$^+$ ions diffuse into the polypyrrole, the low frequency compliance changes significantly during each cycle. The BMIM$^+$ ions only change the

56

low frequency component of the compliance transfer function they do not affect the natural frequency or the damping of the compliance. There are parasitic reactions not due to polymer charging that cause the slow drift in charge (Fig. 3-10) and do not directly influence the compliance [123].
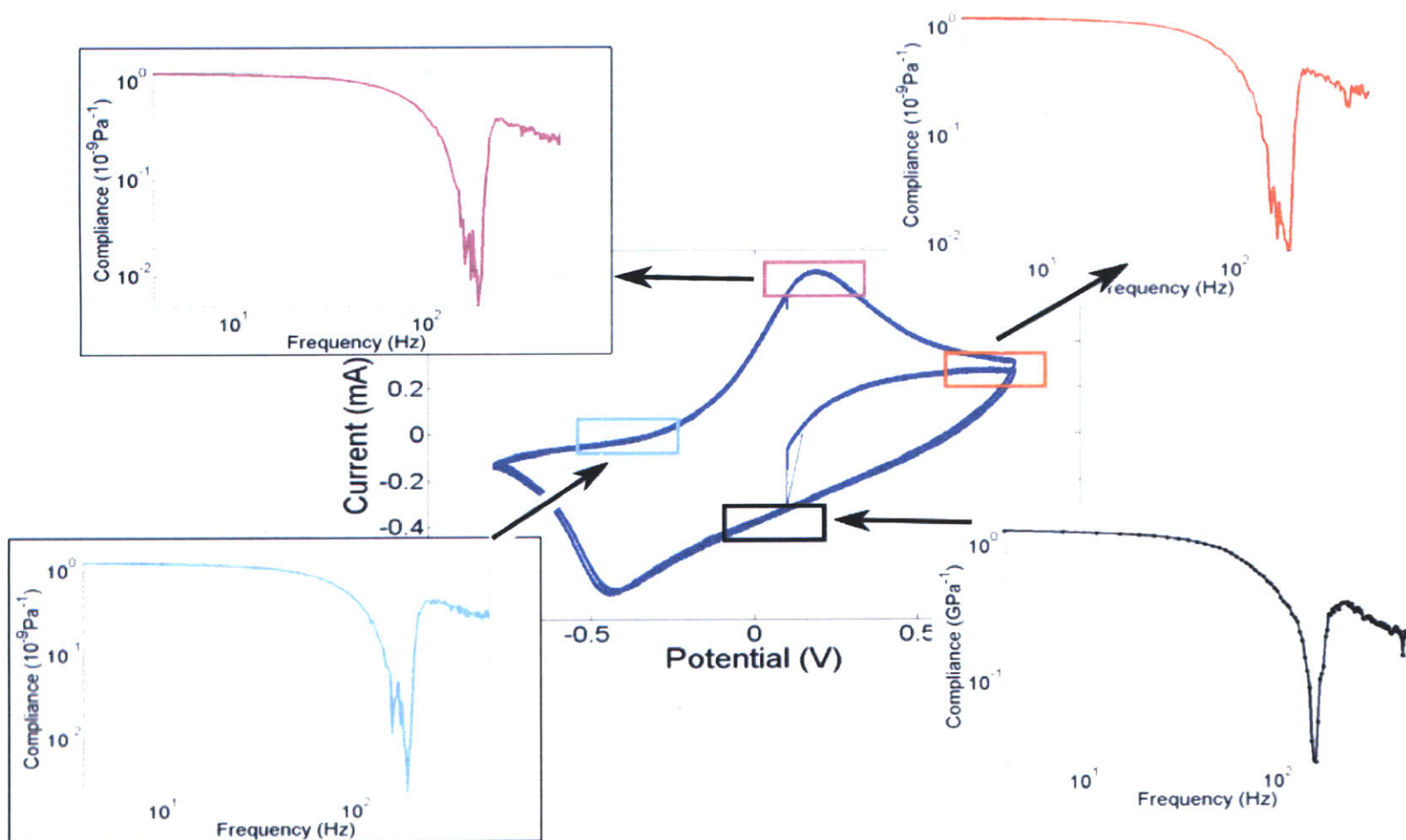
Figure 3-9: Evolving compliance frequency response functions around the cyclic voltamogram. The low frequency value of the compliance shifts up and down as the polymer is oxidized and reduced.
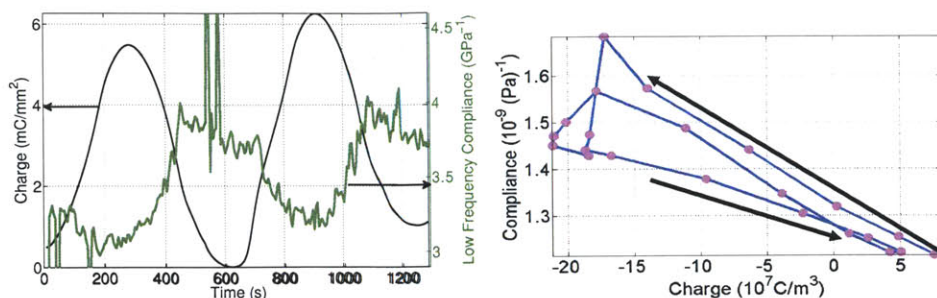
Figure 3-10: Charge injected into the polymer and the corresponding and low frequency gain of the dynamic compliance. The PPy strip is driven by a 5 mV/s triangle wave potential waveform (From [106, 103]).

There is a change of approximately 30-80% in compliance when actuating neat $BMIMPF_6$, which corroborates results obtained by Pytel et al. [109]. The 30% increase in compliance corresponds with ions diffusing into the polymer matrix and seems to be independent of the oxidation state. The compliance can then be cycled back and forth as the film expands and contracts with some drift due to parasitic charging effects.

To further validate the effectiveness of these techniques, further experiments were carried out in solutions of 0.05 M $BMIMPF_6$ in PC and 0.05 M TEAP in PC. These systems were chosen to understand the influence of solvent and the effect of anions such as PF_6^-. The potential window can be controlled so that only one ion motion can occur [110, 143]. It was observed that relative to neat $BMIMPF_6$ system, both the 0.05 M $BMIMPF_6$ in PC and the 0.05 M TEAP in PC have larger changes in compliance (See Fig. 3-11). Regardless of the actuation system, the compliance always decreases as ions enter the film (i.e. on reduction when $BMIM^+$ diffuse into the polymer and oxidation when PF_6^- moves into the film). This confirms the observations made by Pytel et al.in [110] that counterion swelling produces a large change in polymer compliance. They also reported a change of modulus of around three times in similar systems, which have not been reproduced here. This can be due to averaging that is done during the identification procedure. To further understand the influence on the compliance, a survey was conducted by actuation PPy-PF_6 in multiple solvent-ion combinations. Various authors have shown large strains and strain rates in various

59
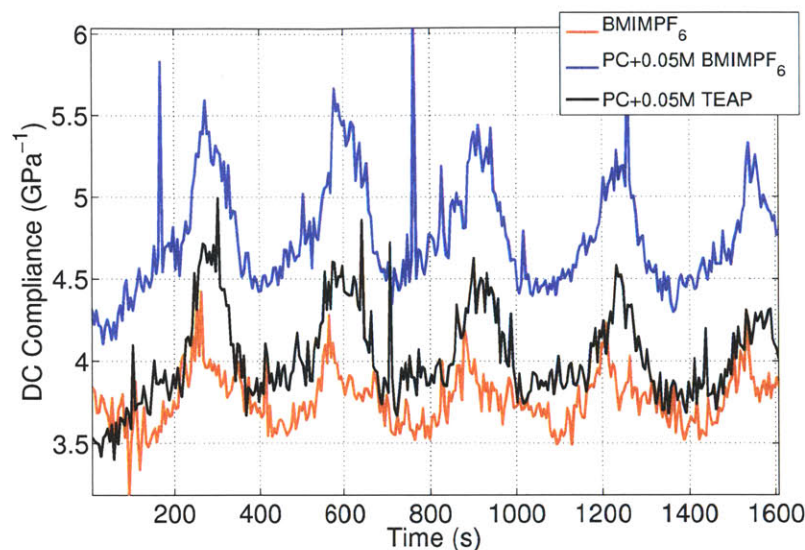
Figure 3-11: Evolution of the compliance of PPy-PF$_6$ actuated in neat BMIMPF$_6$, 0.05 M BMIMPF$_6$ in PC and 0.05 M TEAP in PC. The films were actuated between 0.8 V and -0.8 V at 10 mV/s, and the impulse response and the DC compliance was calculated as described in Sec 3.4 .

ionic systems such as aq NaPF$_6$ [57, 97, 123] and 0.05 M lithium trifluorosulfonamide (LiTFSI) in PC [59, 60]. However, the influence of actuation on the compliance was not fully characterized in these studies. Fig. 3-12 shows the changing DC compliance of PPy-PF$_6$ as the film undergoes electrochemical cycling. As the films are actuated, most of the change in compliance is seen while the film is reduced during the influx of cations into the polymer film. From Fig. 3.1, the influx of cations in the systems containing BMIMPF$_6$, NaPF$_6$ and 1-butyl-3-methylimidazolium tetrafluoroborate (BMIMBF$_4$) cause the polymer to become more compliant. Additionally, the motion of the smaller sodium causes the largest changes in compliance. However, as further cycling is conducted, this compliance change decreases. This is probably due to the large potentials applied in an aqueous system that is known to cause degradation in the polymer [123]. Motion of larger BMIM$^+$ cation causes a smaller but more reproducible change in compliance, with the type of anion (hexafluorophosphate ion (PF$_6^-$) or tetrafluoroborate ion (BF$_4^-$)) making little difference.

Table 3.1 shows a summary of the maximum compliance change in all the systems
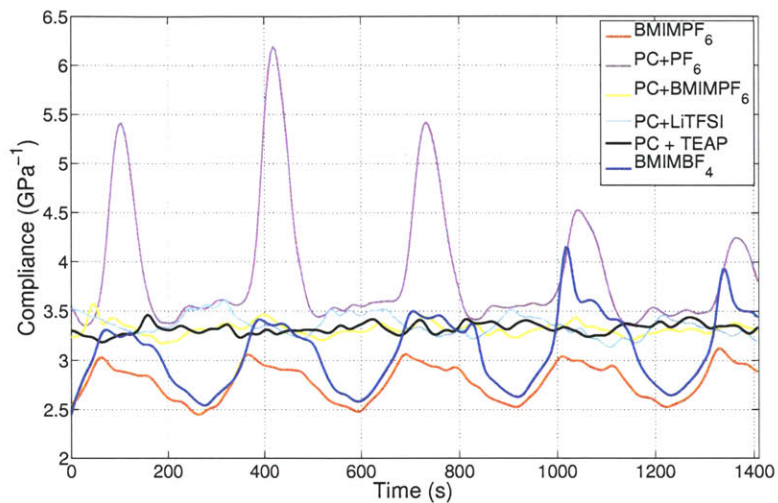
Figure 3-12: Influence of ion diffusion on the compliance of PPy-PF$_6$. The films were excited using a 10 mV/s triangle wave between 0.8V to -0.8V for 5 cycles. The compliance was calculated using techniques described in Sec. 3.2.

Table 3.1: Maximum percent changes in compliance observed in PPy-PF$_6$ actuated in numerous electrolyte combinations. All were tested with the input described in Sec. 3.2

Actuation System	Percent Change in Compliance
BMIMPF$_6$	80%
0.05 M BMIMPF$_6$ in PC	57%
0.05 M LiTFSI in PC	40%
0.05 M NaPF$_6$ aq	115%
0.05 M TEAP in PC	50%

tested. As stated earlier, the compliance change is greatest in systems that are cation dominated. These systems are also closely associated with having larger actuation strains [82, 123]. This shows that optimizing these effects can lead to larger strains as well as larger work per cycle during actuation.

3.5 Thermo-Mechanical Characterization

Since the actuation of conducting polymers is a diffusion driven process, increasing the diffusion rates can lead to faster actuation. Temperature effects on actuation has been extensively reported [8, 32, 58, 82, 146]. However, effect of temperature on the compliance has not been fully characterized, and SSID procedures can naturally be applied to dynamically measure the compliance as a function of temperature. We conduct the experiments in neat $BMIMPF_6$, since they have been shown to operate in large voltage ranges and the temperature can safely be increased without degrading the solvent. The $PPy-PF_6$ strip was immersed in neat $BMIMPF_6$ in the EDMA. We increased the temperature in steps from $27\,°C$ to $85\,°C$ and then cooled to $27\,°C$. The dynamic compliance was calculated using the stochastic input at different temperatures. For the sake of comparison the compliance at 1 Hz and 10 Hz were also calculated using a sinusoidal signal in order to compare it to dynamic compliance calculated from the stochastic signal.

The compliance of polypyrrole was measured at multiple temperatures using both a stochastic stress input as well as a single sinusoidal input at 1 Hz and 10 Hz. Fig. 3-13 shows the data collected using both techniques at 1 Hz and 10 Hz as the temperature is increased to $85\,°C$ and brought back down to $27\,°C$.

The temperature sweep implies that compliance slowly decreases as the temperature is increased. The data collected from the stochastic input represents more frequencies than those shown in Fig. 3-13, which shows only a small portion of the response. This shows that the stochastic technique can capture the compliance data as well as capture the trends in the changing compliance. In the case of $BMIMPF_6$ the compliance does not significantly as a function of temperature. This indicates that

62
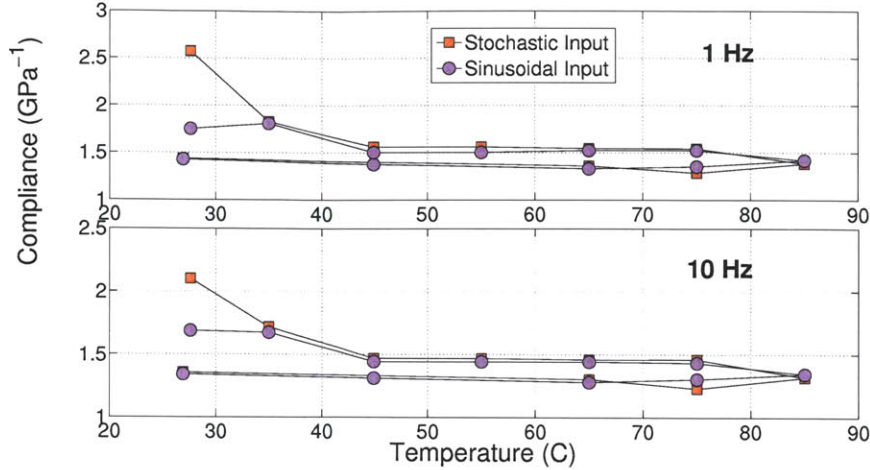
Figure 3-13: Compliance measured at 1 Hz using both stochastic and sinusoidal techniques. (From [104])

actuation in ionic liquid environments are not significantly temperature dependent. This effect will be carefully studies in Chapter 5.

3.6   Conclusions

We have developed a new instrument and a technique that can conduct stochastic mechanical testing on conducting polymers. We have measured the compliance in multiple environments and the differences between cation and anion dominated actuation has been studies. The influence of temperature has also been studied. Shoa et al [124] suggest that the modulus is also a function of the preload applied to the material. We do not see the effect of load on the compliance in ionic liquids due to the lack of solvent incorporation between the polymer chains. However, this technique can also apply if the effect of load on polymer compliance be comes significant. In that case, a stochastic stress signal with a smaller amplitude can be superimposed on a slowly varying load. Alternatively a larger amplitude stochastic signal can be used and the corresponding compliance can be modeled using a nonlinear model structure. These compliance measurements are also made as a function of time and temperature

in different electrochemical environments to understand the influence of different ions and solvents to the compliance. It has been shown that incorporation of small cations cause the largest compliance changes while anions do not cause significant changes. Once the effect of oxidationreduction on the compliance is characterized the strain to charge ratio can be calculated. In this case, the strain caused by the changing compliance can simply be subtracted from the total strain and the strain component due to ion incorporation can be estimated. We have shown that the compliance transfer functions have physical meaning and can provide a fast and efficient means to measure the full frequency response of CPs as a function of the electrochemical charge state. Although we have applied this technique solely to conducting polymers it can also be used to characterize the compliance of other electroactive polymers where the compliance changes significantly. This can help develop better actuators or structural materials with tunable compliances for a variety of devices and applications.

Chapter 4

Electrochemical Characterization

Conducting polymer actuators are driven electrochemically with the polymer forming the working electrode of an electrochemical cell. Hence, understanding the kinetics and thermodynamics of the charge transfer reactions are important [10, 87]. As mentioned in Chapter 3, ion diffusion causes significant changes in compliance of a CP. There are a number of detailed models of diffusion driven using electrochemical potentials. The common type of model used is the porous metal, where the electrode is modeled as highly conductive with electrolyte filled pores. The charging of the double layer can be modeled as a finite transmission line [90, 91, 107]. The solution of these models are solutions to the diffusion equation, which are experimentally difficult to distinguish from each other [87] since they all predict 2 or more governing time constants. Penner et al [101] propose a model where the ion diffusion limits the oxidation of the polymer. The authors described a model that assumed that the electrode is non-conductive and is being doped. They also measure the double layer capacitance and show that it is a function of the oxidation potential. This model has limited utility for studying actuators since the polymer films are required to be electrically conductive. Amemiya et al [5] developed a model for highly conductive films of polypyrrole and determined that diffusion within the polymer pores dominates the overall electochemical performance. Ho et al [62] also propose a model for a porous metal and described the impedance observed during infusion of ions into the pores. They do not account for solution resistance or the charging of the surface of the

material [87]. Another model includes the convection of electrolyte within the pores of polypyrrole [91]. The convection occurs due to the changing stress state within the pores. This can be adapted to measure the admittance of a conducting polymer actuator, however the authors do not explicitly do so. Madden [23, 87] described in detail the DEM of CP actuators and derived an expression for the admittance of an electrochemical cell that included a polymer actuator. When an electrochemical potential is applied to the polymer there is a charging of the electrical double layer. The DEM assumes that the double layer capacitance is independent of the potential applied, and the charge on the surface is proportional to the potential. Due to this, there is migration of ions through the electrolyte to the polymer surface. Then they diffuse through the polymer causing the expansion or contraction of the polymer. In the DEM, the admittance of the polymer is given by Equation 4.1.

$$Y(s) * R = s \frac{\frac{\sqrt{D}}{\delta} \tanh(\frac{a}{2}\sqrt{\frac{s}{D}}) + \sqrt{(s)}}{\frac{\sqrt{s}}{RC} + s^{3/2} + \frac{\sqrt{D}}{\delta} s \tanh(\frac{a}{2}\sqrt{\frac{s}{D}})}. \tag{4.1}$$

Dimensional analysis of Equation 4.1 yields 3 time constants that govern the time response of the polymer actuator.

- $\tau_D = \frac{a^2}{4D}$ where a is the polymer thickness and D is the diffusion constant.

- $\tau_{RC} = RC$ is the double layer charging time.

- $\tau_C = \frac{\delta^2}{D}$ is the diffusion time through the double layer.

Here, Y(s) is the admittance as a function of the Laplace variable s, h is the thickness of the polymer strip, D is the diffusion coefficient of the ion within the polymer, R is the series resistance (which includes any wiring or contact resistance and the resistance of the electrolyte), C is the double layer capacitance, and δ is the thickness of the double layer. These show that the response will be dominated by the largest time constant. Experimentally, this is the time it takes for ions to diffuse into the polymer film (τ_D). These admittance functions are measured using swept sine signals and can related to physical properties of the polymer [87]. However, this model is

generally too complex to model the response and in many cases a simpler model involving a fewer variables can suffice [23].

Stochastic signals were first used to study electrochemical systems by Smith and co workers [34, 134] in 1976. They showed that a pseudorandom white signal could be used to make reliable impedance measurements relative to other periodic signals. Here, frequencies of electrochemical interest were chosen and a corresponding waveform was generated. They then used Fourier analysis to determine the admittance of impedance of the elctrochemical system studied. To the knowledge of this author, these techniques have never been used in the study of conducting polymer actuators. In this chapter, we use stochastic white signals with a Gaussian PDF to measure the impedance of a conducting polymer as it is actuated.

4.0.1 Limitations of the DEM

- **Effects of Finite Conductivity:** The conductivity of a CP begins to influence actuation behavior when the films are long and large currents are required to drive actuation. In these cases, the DEM fails to account for the potential drop across the polymer film. Peter Madden [89] further develops a model to account for the limited conductivity of a polymer film. Making multiple points of contact with a polymer film can increase the speed of the response however, this adds to the complexity of design.

- **Influence of Potential on Volumetric Capacitance:** Penner et al [101] suggest that the bulk volumetric capacitance is a strong function of the oxidation state. The DEM provides few insights into how this evolves as a function of potential or charge.

- **Ability to Predict Polymer Performance:** The expression derived in the DEM cannot be expressed in the time domain and can be difficult to directly compare it to experimental data. In many cases it is too complex and Bowers demonstrated a simpler model can be used [23]. Since there is little direct correlation to the polymer strain or stress, using this model is difficult for engineers

to further CP applications.

4.1 Input Design Considerations

John Madden derived an expression for the admittance in his DEM model. This expression in the denominator of Equation 4.1 is of lower order relative to the numerator. This has also been experimentally verified [23]. Identifying an admittance can become difficult, since inputs with power at high frequencies would need to be generated. Using a potential input and a current output can complicate the SSID procedure since at high frequencies, noise and nonlinearities can become dominant. Therefore it is better to measure impedance rather than admittance. Typical input
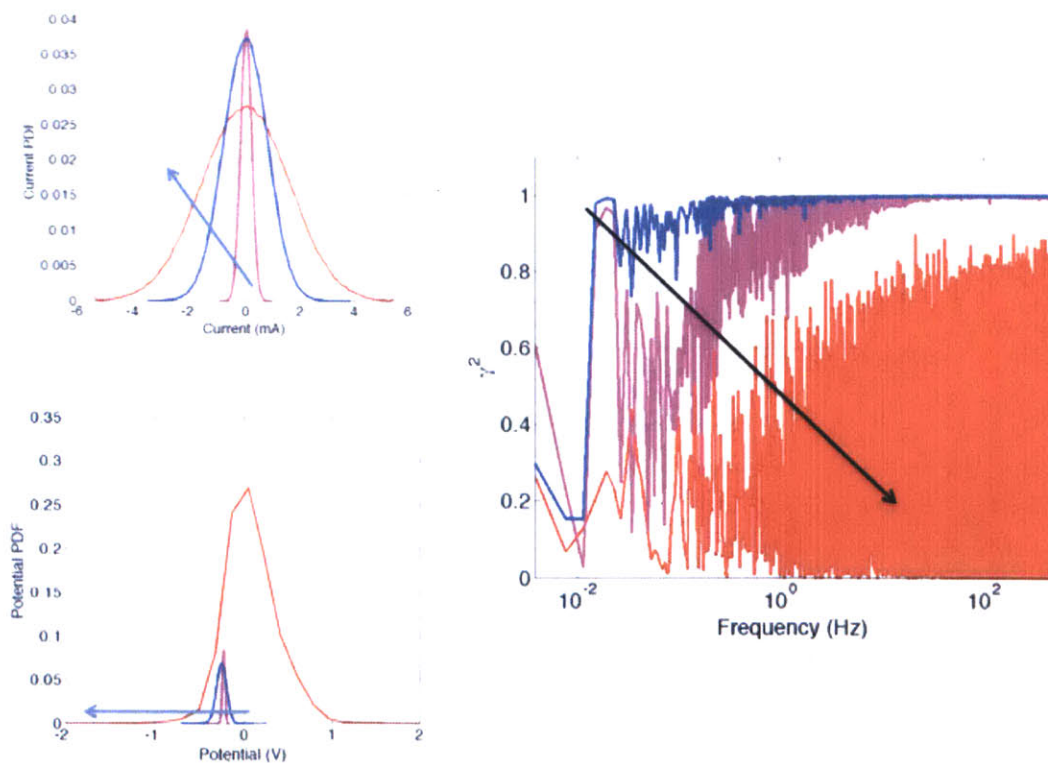
Figure 4-1: Typical PDFs of the input current (top left) and the output potential (bottom right) as the standard deviations of the input is increased. Right: Coherence squared estimate of the impedance transfer function estimated for PPy-PF$_6$ immersed in BMIMPF$_6$.

68

output PDFs are shown in Fig. 4-1. As the amplitude of the current waveforms are increased the response the nonlinearities within the response become significant (Fig. 4-1 right). This occurs due to the oxidation and reduction reactions that occur at potentials at 0.8 V and -0.8V. As the current increases, the oxidation and reduction reactions trigger a large jump in the potential (red curve in Fig. 4-1). These potentials jumps can lead to the electrochemical potential spiking to 10 V at times that can cause degradation of the polymer. These spikes can also be in the predicted potentials relative to the measured potentials (See Fig. 4-2 bottom). The large spikes saturate the potential at $\pm$ 10 V due to the potentiostat. The VAF was calculated using both linear and a wiener system model. The VAF for a linear system model was 15%, so is not sufficient to fully model the system. Fig. 4-2 right could indicate that a wiener system [80] with a static nonlinearity of the form in Equ 4.2 could be a better model for the impedance response.

$$V_{meas} = Ae^{-\frac{V}{V_o}} + Be^{\frac{V}{V_r}} \tag{4.2}$$

Here, V is the predicted potential from a linear block, V_o and V_r are the oxidation and reduction potentials. A and B are parameters to be fitted. Saturation peaks for the predicted potentials occur at $\pm$ 10 V to model the limits of the potentiostat. The resulting VAF using the wiener model is 19%. This is not a significant improvement over the linear system representation, which indicates more complex nonlinear models must be used. For instance, cascaded systems with linear- nonlinear -linear blocks [65, 77] or systems using Volterra [29, 76] basis function can be used. However, these models increase the complexity of the model and do not give any additional insight into the physical phenomenon governing the electrical behavior. Additionally, an advanced model that works in ionic liquid might not necessarily work for other systems. The rest of this chapter describes a simpler approach that can give an alternative view of the impedance of a CP as it is actuated.
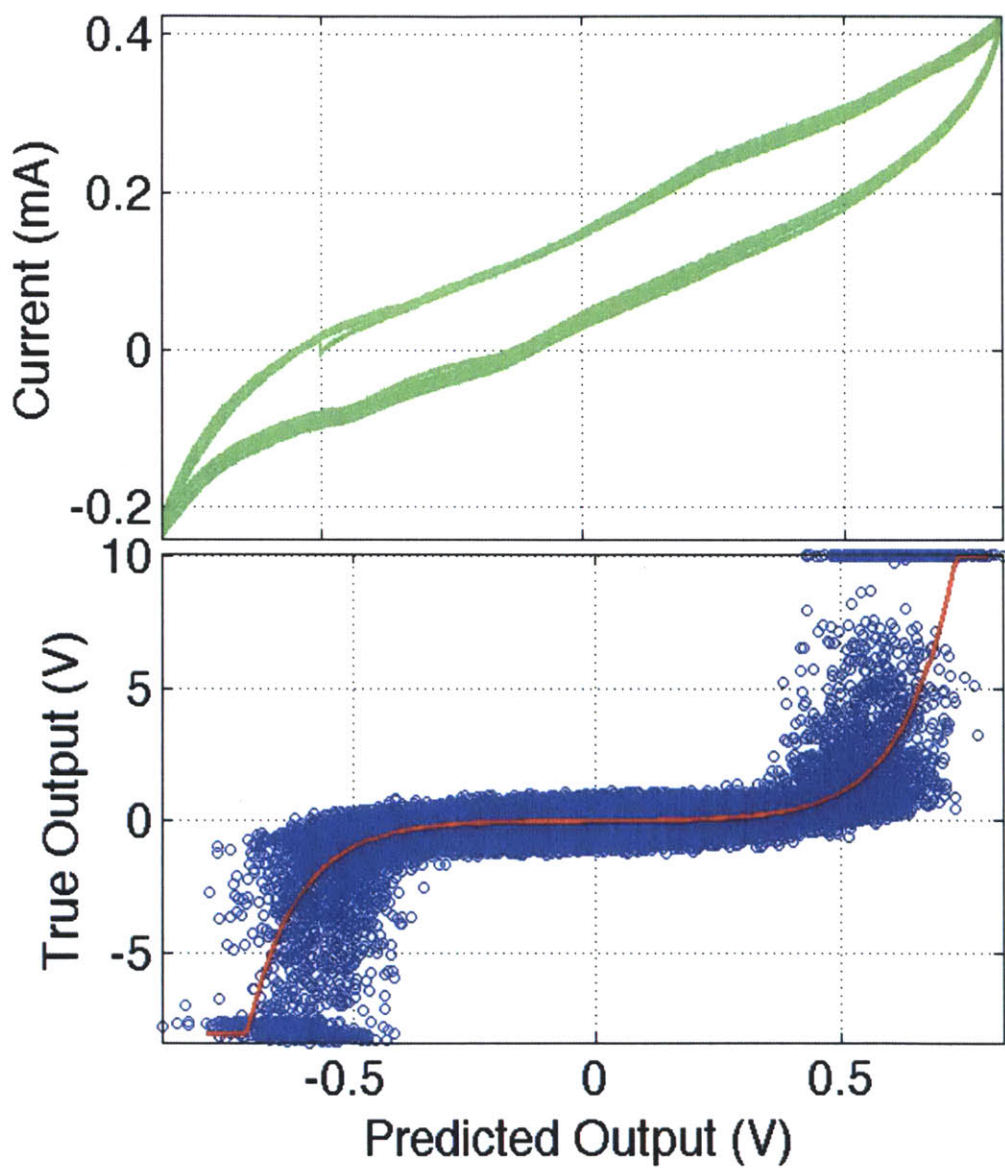
Figure 4-2: Top: Cyclic voltamogram of PPy-PF$_6$ actuated in neat BMIMPF$_6$. The oxidation and reduction reactions happen at 0.75V and -0.7V respectively. Bottom: Predicted potential output and measured output showing nonlinearities at the oxidation and reduction potentials.

4.2 Measurement of Impedance

A linearized impedance can be measured using a stochastic waveform with a gaussian PDF with standard deviation of 2 mA. This input does not oxidize or reduce the polymer and does not cause the film to actuate. This does give a measurement of the impedance that can be related to the DEM model. Fig. 4-3 left shows the impedance impulse response of PPy-PF$_6$ actuated in BMIMPF$_6$ calculated up to 0.06 s with a sampling rate of 100 Hz. Fig. 4-3 right shows the bode response calculated from the same data set. The magnitude plot shows an inflection at 1 Hz, indicating at least a pole and zero in the response. A two exponential model can be used to fit the impulse response function. The impedance impulse response can be represented by
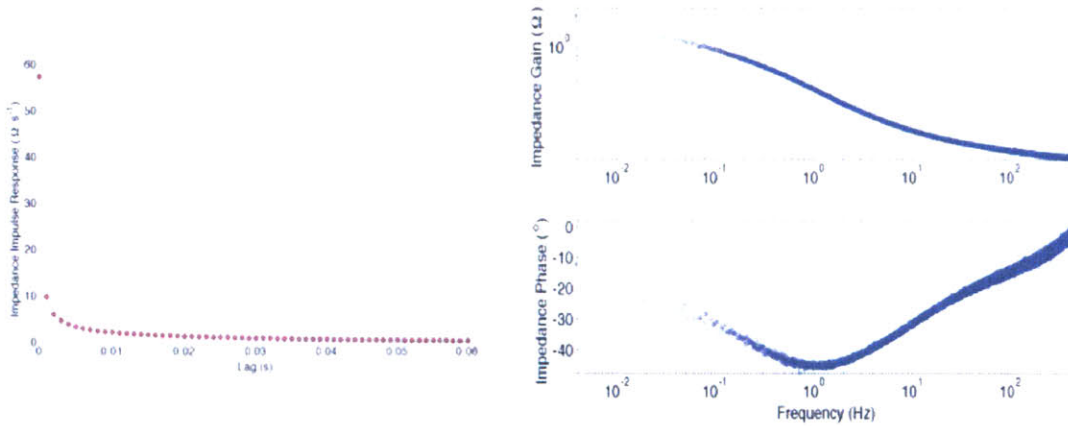
Figure 4-3: Left: Impedance impulse response function calculated using a current input using a gaussian PDF between ±2 mA for PPy-PF$_6$ in BMIMPF$_6$. Right: Bode response of calculated using the same current and potential data.

$$Im(\tau) = ae^{-\frac{t}{b}} + ce^{-\frac{t}{d}} \tag{4.3}$$

Where, a, b, c and d are parameters that can be fitted to the impulse response calculated from the data (Fig. 4-4). The optimal parameters for the coefficients are $a = 48 \pm 4\Omega s^{-1}$, $b=1.2 \times 10^{-3}s$, $c = 4.9 \pm 0.2\Omega s^{-1}$, and $d=0.035s$. These closely resemble the 3 time constant model developed in the DEM model by John Madden. The time constant related to double layer charging (τ_C) is small and does not

71

significantly influence the impedance until much higher frequencies. The sensitivity of the model to the different fitting parameters was calculated and shown in Fig. 4-5. The model shows little sensitivity to parameters a and b, where the VAF does not change significantly by varying them. However, the parameters associated with the larger time constant c and d have a larger influence on the VAF. This time constant is closely associated with the diffusion of ions through the polymer film and with the charging of the polymer capacitance. We can attribute this to the volumetric capacitance of the polypyrrole in the neat $BMIMPF_6$ system.
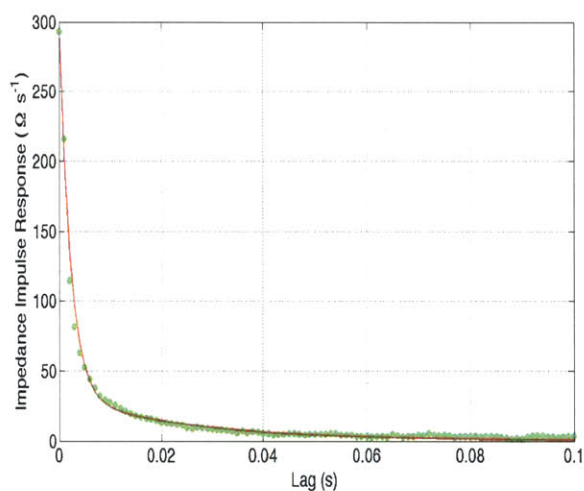
Figure 4-4: Impedance impulse response function calculated for PPy-PF_6 actuated in neat $BMIMPF_6$. A two exponential time constant model can be used to fit the impulse response.

4.3 Changing Impedance

This impedance can be a function of the oxidation state of PPy-PF_6 in neat $BMIMPF_6$. To see the influence of oxidation and reduction on the polymer a triangle wave current was superimposed on the stochastic waveform. The samples were clamped into the SEDMA and preconditioned by applying a triangular wave current input without the stress waveform until the electrochemical response stabilized. This preconditioning is necessary to remove initial transients that occur during electrochemical cycling. In
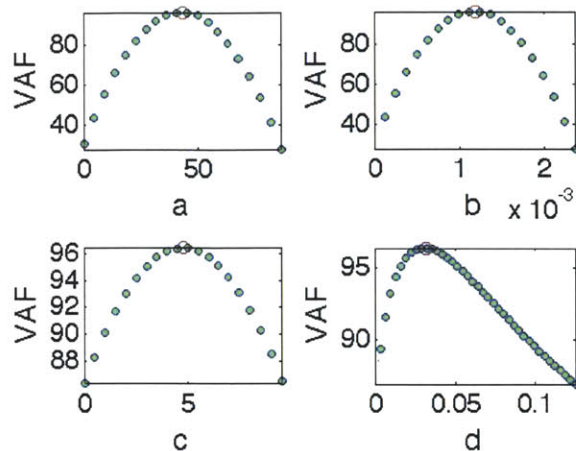
Figure 4-5: Sensitivity analysis of the four parameters fitted to the impedance impulse response. The red circle indicates the optimal parameters calculated using a Toeplitz matrix inversion.

the subsequent test, two separate inputs are used to excite the polymer, an electrochemical current between 2 mA to -2 mA and the stochastic stress. The resulting potential and current data were sectioned into sequences of 10 seconds, and the data were detrended. The impulse response and frequency response functions for each of the sections were calculated. Since the frequency of the applied current is 0.5 mA/s, there was little change to the impedance due to charge injection during the 10 s interval.

The resulting impulse responses are plotted in Fig. 4-7. As the polymer undergoes electrochemical cycling the impulse response evolves as charge is injected and ejected through the polymer. The changes in the impedance closely mimic the changes in the compliance discussed in Chapter 3. By integrating the area under the curve of the impulse response, we calculated the low frequency impedance of the material. This is a strong function of charge with the impedance. The impedance increases as $BMIMPF_6$ ions are injected into the polymer and PF_6^- move out. The low frequency impedance can be calculated by integrating the impulse response function, which would give the impedance at 0.1 Hz. This is plotted in Fig. 4-8 insert. This gives a characteristic "U shaped" curve for the impedance. At low levels of charge (between

73
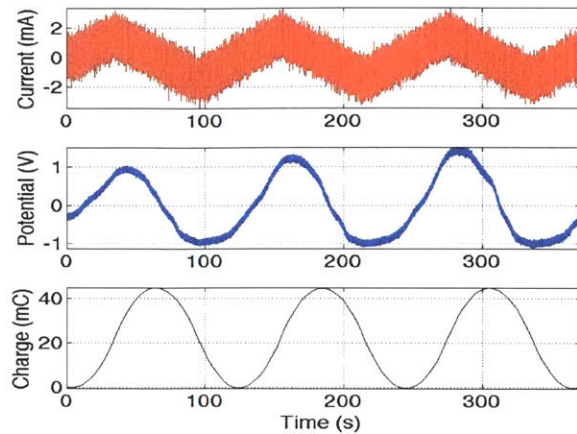
Figure 4-6: The current (top), potential (middle) and charge (bottom) data that were used to calculate the impedance response as a function of charge.

0-10 mC) and at high levels of charge (30-40 mC) there are large concentrations of 1-butyl-3-methylimidazolium ion (BMIM$^+$) ions diffusing into the PPy-PF$_6$ film. This leads to a three times increase in the impedance of the film. The increase in impedance can be attributed to the neutralization of the PF$_6^-$ ion within the film causing the impedance between the polymer chains to increase. However, at very large levels of BMIMPF$_6$ incorporation (greater than 40 mC) the impedance levels off and even decreases slightly. This generally occurs when the polymer is oxidized and is a potential dependent effect.

The two time constant model described in the previous section is fit to the individual impulse responses. The constants a, b and c do not change significantly with charge, however the larger time constant (d) changes significantly (Fig. 4-9). It shows a similar characteristic "U shaped" curve as seen from the low frequency response in Fig. 4-8 insert. To effectively model the data a parametric estimate for the time constant was developed as a function of charge. The form of the parametric function that was fitted to the response is

$$d = Ae^{-Bq} + Ce^{-Dq} \tag{4.4}$$

where A, B, C and D are parameters to be fitted and q is the charge injected into the

74
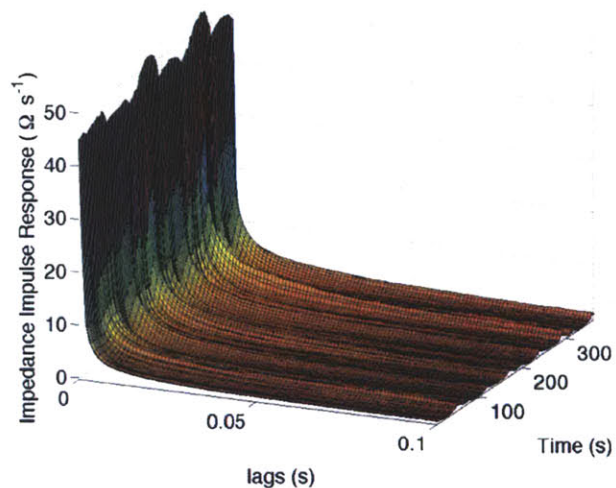
Figure 4-7: The evolving impulse response function as the potential of the polymer is changed.
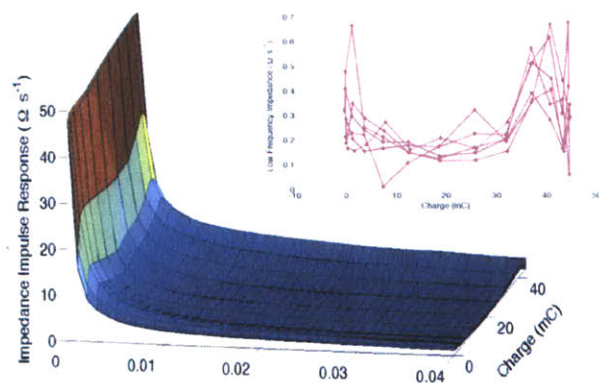
Figure 4-8: The impedance impulse response as a function of charge. Impedance of PPy-PF$_6$ measured in neat ionic liquid BMIMPF$_6$ using a current waveform. Insert: The low frequency impedance (0.1 Hz) changes as a function of charging of the polymer.

polymer. The fitted curve is shown in Fig. 4-9. The error associated with each of this models are calculated and summarized in Table 4.1. Each of the models presented here use various number of parameters to model the data and the VAF is not sufficient to determine if a model is useful. To avoid the negative effects of over fitting, the Akaike information criteria (AIC) criteria [80] described by

$$AIC = 2k + N \left[ln(2\pi \frac{SSE}{N}) + 1 \right] \tag{4.5}$$

$$SSE = \sum_{i=1}^{n} (y(i) - \hat{y}(i))^2 \tag{4.6}$$

was used, where k is the number of parameters in the model, N is the number of sample, SSE is the sum of squared errors (SSE), y is the measured output and $\hat{y}$ is the predicted output. The estimate gets better as the number of samples increases and penalizes a model if it has too many model parameters. For data sets with not enough samples, a AICc can be used.

$$AICc = AIC + \frac{2k(2k+1)}{N-k-1} \tag{4.7}$$

$$\tag{4.8}$$

The MSE, VAF and SSE were calculated for the different models and are summarized in Table 4.1. The non-parametric model with large number of parameters only accounts for a little more VAF relative to using a single average impulse response to describe the impedance. The model with an average impulse response also has the least AICc and is a better model for the impedance. The impedance impulse response measured this way is a strong of charge. However, these do not significantly capture the oxidation and reduction of the polymer.

Fig. 4-10 shows the changing impedance relative to the actuator strain produced. This shows simultaneous measurement of impedance and the strain produced by the polymer. The changing impedance can be used as means to measure the strain of the polymer. This technique can therefore be used to monitor the strain of a polymer

76
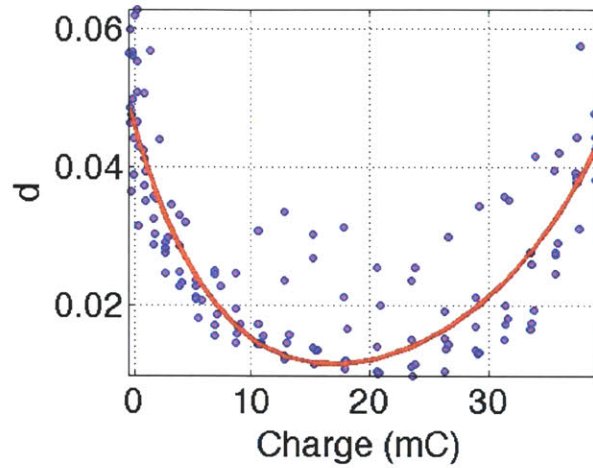
Figure 4-9: Evolving time constant d as a function of charge. Equ. 4.4 shows the fitted curve (red)

Table 4.1: The VAF, MSE and AICc calculated for the different parametric and non-parametric estimates of the impulse responses.

Model	Number of Parameters	VAF (%)	MSE	SSE	AICc
Non-parametric charge varying impulse response	40501	99.1	8.03e-6	119	5.5
Parametric charge varying impulse response	1604	98.7	5.4e-4	181	-3.5
Parametric analytic charge varying impulse response	8	97.13	2.61e-5	337	-3.95
Average impulse response	4	96.7	3.05e-5	365	-3.92

actuator as its being actuated without the need to use an separate strain sensor.
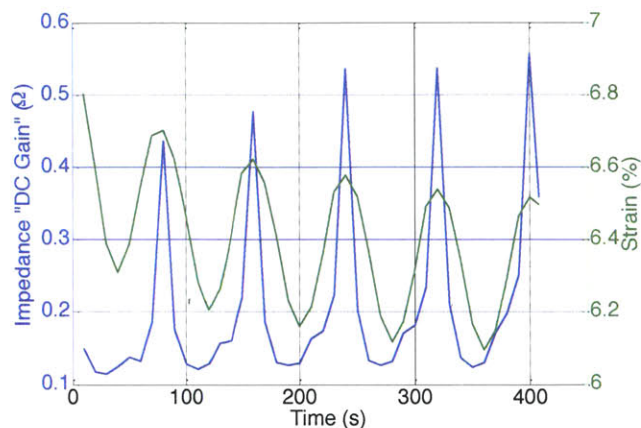
Figure 4-10: The changing impedance and strain of PPy-PF$_6$ actuated in neat BMIMPF$_6$. The changing impedance can be used as method to measure the strain without the need of a strain sensor.

4.4 Conclusions

In this chapter, we have applied stochastic system identification techniques to study the electrochemical impedance of polypyrrole actuators. A pseudo linear model using a slowly evolving FIR model as a function of the input charge is developed. The model is fitted to a two time constant model and the evolution of the parameters of the model is studied. The larger time constant is related to the volumetric capacitance of the polymer and it is measured as a function of charge. The implications of the FIR model structure on the VAF is discussed and it is shown that a single average impulse response is sufficient to model all of the impedance response. Finally the impedance is tracked as function of charge and it is shown how this can be used to simultaneously measure the strain during actuation with the need of an additional strain gauge. This can have advantages when developing multi functional materials where simultaneous measurement and generation of strain are needed from the same material.

Chapter 5

Electrochemical Mechanical Characterization

Linear actuators can be characterized by measuring the active stress, active strain, strain rate and efficiency produced by them. Most typical actuators take in an electrical input and produce a mechanical movement. In conducting polymers, the input electrical signal drives an electrochemical system that in turn causes a mechanical response. The previous chapters described experimental techniques that can measure the evolving properties (mechanical and impedance) as a function of its oxidation state. A variation of this technique can also be used to understand the mechanical response of the polymer directly to an electrical stimulus. The mechanical actuation response can be compared to each other on the basis of the strain that they can generate at a constant preload. Conducting polymers can typically generate up to 10% strain at a 1 MPa preload. However this does not give any information about excitation frequency, any non-linearitys that can be present in the response, or information about the strain to charge ratio or the modulus. These coupled effects make it difficult to truly assess the properties of a conducting polymer actuator and compare improvements in properties objectively. Hence, it has become desirable to be able to easily make dynamic measurements of stress and strain relative to an input current and potential.

There are a number of different input signals that can be used to conduct linear

system analysis and generate a frequency response. These can include impulses, steps, random Gaussian signals, random binary signals and swept sine inputs. Prior work [87, 146] briefly looked at the frequency response of linear conducting polymer actuators using swept sine signals. Furthermore, trilayer actuators have been characterized using swept sine techniques [68]. These techniques however cannot decouple multiple competing effects such as effect of the strain to charge ratio and the modulus. Due to these and other advantages mentioned in Section 1.2, a stochastic signal was used primarily in the various characterization techniques developed in this chapter.

5.1 Isometric Actuation

Isometric actuation occurs when the polymer is held at a constant strain and the corresponding force the polymer can generate is measured. In the case of a conducting polymer, the Equation in Laplace domain (3.1) can be written as

$$\sigma(s) = G\epsilon(s) - \alpha G(s)Q(s) \tag{5.1}$$

$$\sigma(s) = G(s)\epsilon(s) - \alpha G(s)\frac{I(s)}{s} \tag{5.2}$$

$$\Phi_{\sigma I} = -\frac{\alpha G}{s}\Phi_{II} \tag{5.3}$$

The derivation in Equation 5.1 assumes a stochastic waveform for current and that the strain and current signals are orthogonal. The resulting cross-correlation functions are then related by $-\frac{\alpha G}{s}$. This gives a direct measurement of the strain to charge ratio (α) and the modulus (G) in one test. At low frequencies (less than 20 Hz) we can assume G is a constant (Fig. 3-5) as a function of frequency.

The ratio $\frac{\Phi_{\sigma I}}{\Phi_{II}}$ can be calculated and the strain to charge ratio and the modulus can be estimated from the roll off of the frequency response. Thermodynamically, the potential determines the oxidation state of the polymer; hence it is a convenient input to control. This ensures that we can compare the performance of the polymer actuator across multiple samples and conditions. The ratio can be estimated using a

80

Figure 5-1: Typical isometric response for PPy-PF$_6$ in 1M NaPF$_6$, calculated using a random binary input updated at 10 Hz. The roll off at frequencies greater than 0.05 Hz have a slope of αG.

random binary input for potential between -0.7 V to 0.9 V at an update and sampling rate of 10 Hz and a preload of 2 MPa. It is important to pick a potential window where only the anion dominates the actuation. Although multi-ion motion is an interesting phenomenon to understand, any practical actuator application would need to have motion of only one ion species [110]. Since polypyrrole is a cationic system [129], using anions to drive the volumetric expansion tends to be the most desirable. In the case of actuation in aq NaPF$_6$, the potential window of the random binary output is adjusted to ensure only that the PF$_6^-$ ion dominates the actuation (Fig. 5-2).

The potential must be held constant for 0.1 s, which allows the polymer to react and a stress signal to be measured. PPy-PF$_6$ was tested using this technique. The input (current) and the output (stress) are then de-trended to remove the non-zero means. The potential window ensures that only the negatively charged ions move in and out of the polymer. The test lasted for 5000 s, and the first 100 s of the data were disregarded. The calculated response for polypyrrole doped with PF$_6^-$ can be seen in Fig. 5-1. The response rolls off at s^{-1} between 0.05 Hz and 5 Hz. At these frequencies, the coherence squared (Fig. 5-3) is one indicating that the response is linear with little noise or nonlinearities. At lower frequencies, the coherence squared
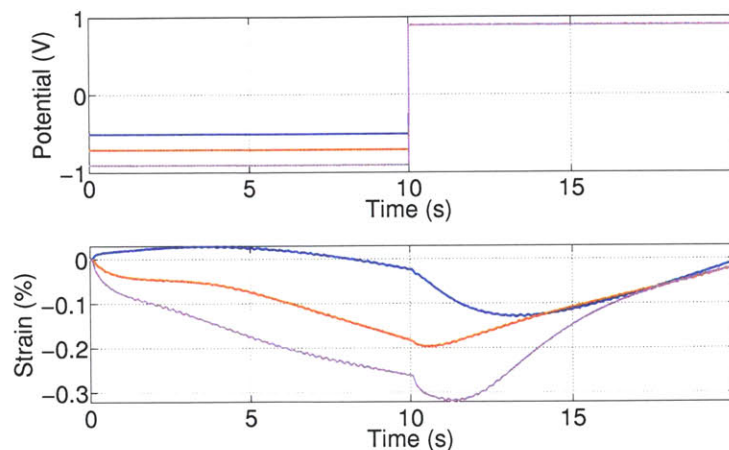
Figure 5-2: PPy-DEHS actuated in aq 0.1 M NaPF$_6$. The potential window was varied until only one ion (PF$_6^-$) moves through the film.

degrades, indicating significant nonlinear behavior possibly due to creep.
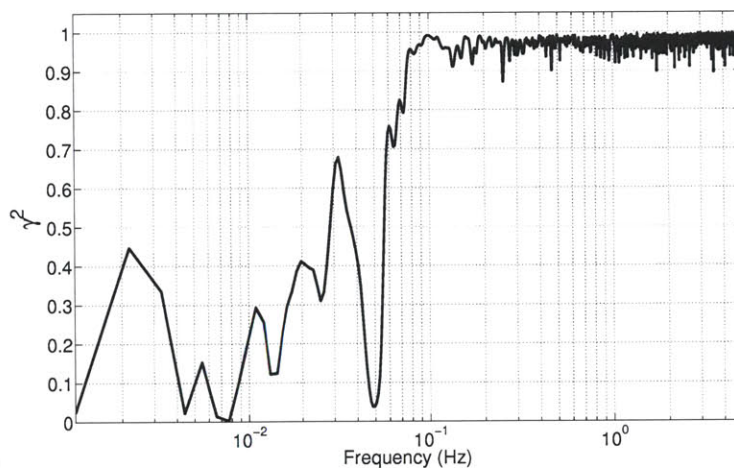
Figure 5-3: Coherence squared estimate of the isometric response using a stochastic signal.

The information in Fig. 5-1 can also be used to estimate the strain to charge ratio (α). We can assume that at lower frequencies (less than 5 Hz), the modulus (G) is a constant relative to the frequency. Furthermore, G changes between 20-40% as a function of charge in the BMIMPF$_6$ system; therefore we can measure α to within that range. In this case, G is 800 MPa; the strain to charge ratio becomes

$1.0 \pm 0.2 \times 10^{-11} m^3 C^{-1}$, which is comparable to results achieved in prior work [87].

5.2 Isotonic Actuation

In isotonic mode, the stress is held at a constant as a potential is applied to the polymer. The Aerotech stage moves to keep the stress constant (as described in Section 2.2). The total strain that a polymer actuator is given by Equation 5.4. Using this as a starting point and assuming stochastic input signals for stress and current Equation 5.6 can be derived.

$$\epsilon_T(s) = J(Q, s)\sigma + \alpha Q(s) \tag{5.4}$$

$$\epsilon_T(s) = J(Q, s)\sigma + \alpha \frac{I}{s} \tag{5.5}$$

$$\Phi_{\epsilon V} = J(Q, s)\Phi_{\sigma V} + \frac{\alpha}{s}\Phi_{IV} \tag{5.6}$$

The feedback loop within the SEDMA during an isotonic test causes the potential and stress signals not to be completely orthogonal, making cross-correlation term $\Phi_{\sigma V}$ non-zero. However, looking at the signals, we can ascertain the overall open loop roll off frequency and the strain at numerous frequencies. Hence, it can be a valuable tool in ascertaining improvements in polymer performance.

The ratio $\frac{\Phi_{\epsilon V}}{\Phi_{VV}}$ represents the amount of strain we can get from a conducting polymer. This can be done by multiplying the magnitude of the frequency response plot with the maximum allowable potential difference. Fig. 5-4 shows the estimated ratio using a random binary input for potential between -0.7 V to 0.9 V at an update and sampling rate of 10 Hz (similar to the signal described in 5.1). The test was conducted for 5000 s and the first 100 s of the data were disregarded. The input (potential) and the output (strain) was then de-trended to remove the non-zero means, and the dataset was usually averaged over 5-10 cycles (500 s-1000 s). In this case, the strain at 0.05 Hz can be calculated to be 1.5%/V with the response rolling off at 0.1 Hz. The coherence squared is close to one between 0.01 Hz and 5 Hz, showing a wider linear region relative to the isometric case (Fig. 5-5). This is not the maximum
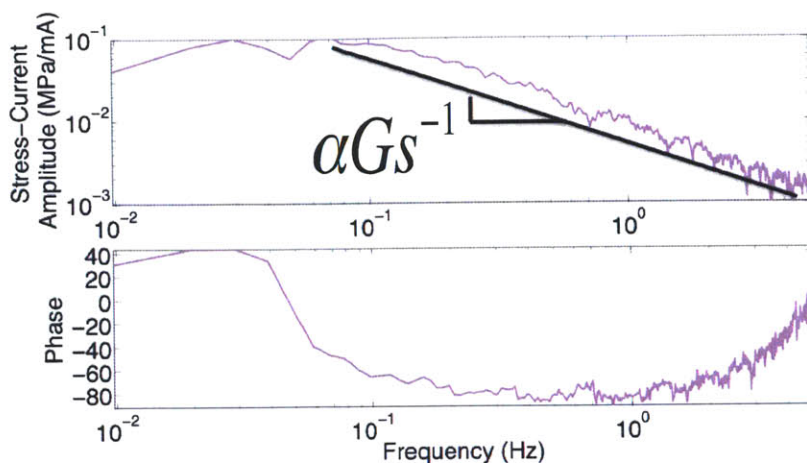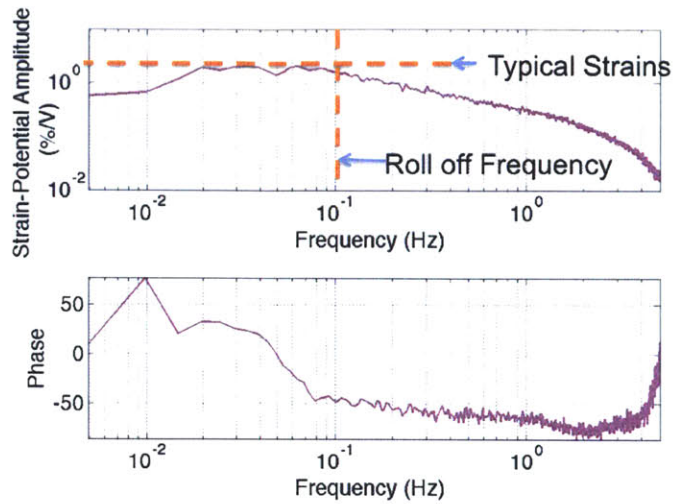
Figure 5-4: Typical isotonic response for PPy-PF$_6$ in 1M NaPF$_6$, calculated using a random binary input updated at 10 Hz at a preload of 2 MPa.
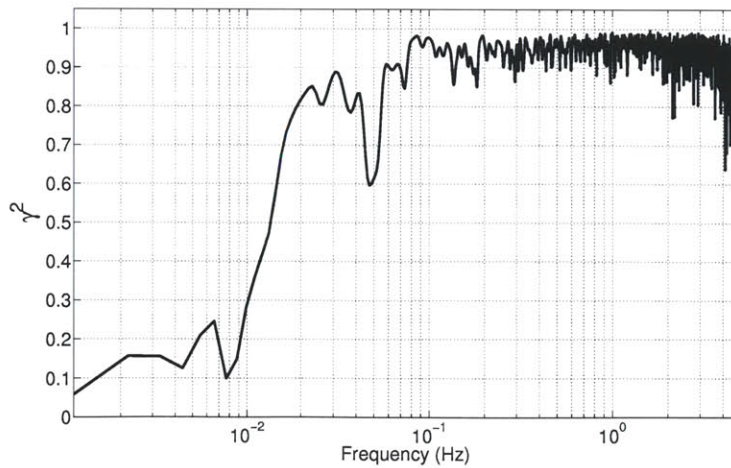
Figure 5-5: Coherence squared estimate of the isotonic response using a stochastic signal.

possible strain at low frequencies but just the typical strains that can be obtained over a large number of cycles. Other authors [87, 146] showed similar results using a swept sine current input and measured the transfer function between strain and current. This also can be used to calculate the strain to charge ratio; however it is difficult to use these curves to compare against other conducting polymer actuators. Since the electrical conductivity of many of these actuators is different, the same current input can cause large fluctuations in potential which can cause damage to the polymer chain. By using a current input, we cannot control which ion species are mobile during actuation.

5.3 Applications of SSID to the Development of Conducting Polymer Actuators

5.3.1 Effect of Solution Resistance and Temperature

It has been widely reported that increasing the temperature significantly enhances the overall strain and performance of PPy actuators [13, 71, 72, 82, 104]. However, the reasons for the enhancement are poorly understood. Various authors conjecture that the increasing temperature enhances diffusion within the polymer resulting in overall improvement in strain. To verify this, numerous stochastic isometric tests were conducted on PPy-PF_6 films in neat $BMIMPF_6$ at various temperatures. The random binary sequence between -0.9 V and 0.9 V was applied and sampled at 10 Hz. This large potential window was used in order to maximize actuation. It has also been established that in neat $BMIMPF_6$, the cation moves over a wide range of potentials [71, 82, 109]. Fig. 5-6 shows the results of the isometric tests. Significant improvements in the overall stress are seen; however, it is not accompanied with any change in roll off frequency. There is no change in the strain to charge ratio or the modulus. This can also be seen when the modulus is measured independently without any actuation (See Fig. 3-13) . Similar tests were conducted with PPy-PF_6 in 0.01 M NaPF_6 at temperatures up to 45 °C (See Fig. 5-7). Higher temperatures could
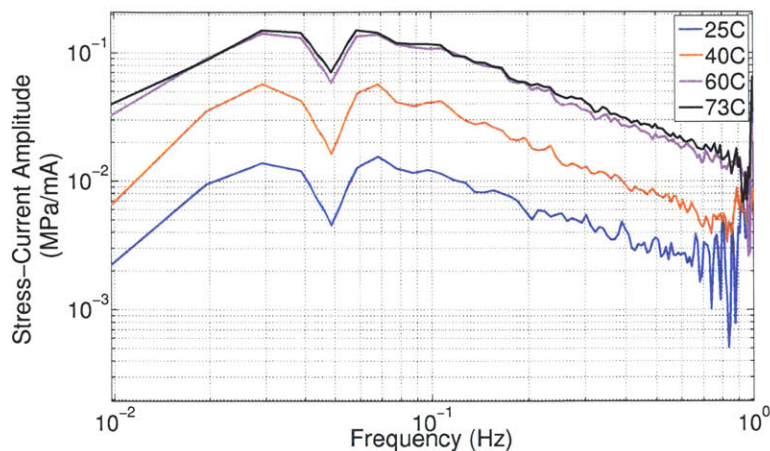
Figure 5-6: PPy-PF$_6$ films actuated at different temperatures in BMIMPF$_6$. The slope of the high frequency represents the product of the modulus and strain to charge ratio.

not be reached without breaking the polymer or rapidly increasing evaporation of the electrolyte. In this case, there was no rapid rise in the stress amplitude as the temperature increased compared to the BMIMPF$_6$ case.

The diffusion within the polymer is relatively unchanged as the temperature rises. However, this can be easily explained by the reduction of electrolyte resistance. The different electrolytes were warmed up as the solution conductivity was measured using a solution conductivity probe. The result can be seen in Fig. 5-8. There is a rapid rise in the conductivity of the BMIMPF$_6$ solution, but the rise in the conductivity of the 0.01 M NaPF$_6$ is not nearly as significant. This implies that the changing solution conductivity is responsible for the increase in stress seen in Fig 5-6. A similar conclusion was drawn in Vandersteeg PhD these [146].

The increase in solution conductivity improves the actuation not only in isometric but also in isotonic mode. To verify this, three solutions were prepared with different solution conductivities by varying the NaPF$_6$ concentration in water. There was a significant increase in overall strain of the PPy-PF$_6$ films, but the roll off frequency stays approximately the same (See Fig. 5-9). Effect of electrolyte concentration on actuation was studied by [61, 24, 20] who did not report any enhanced actuation due to

86
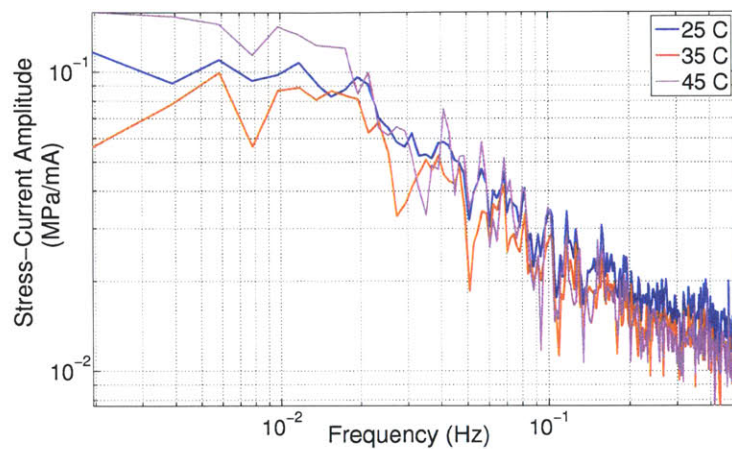
Figure 5-7: PPy-PF$_6$ films actuated at different temperatures in BMIMPF$_6$.
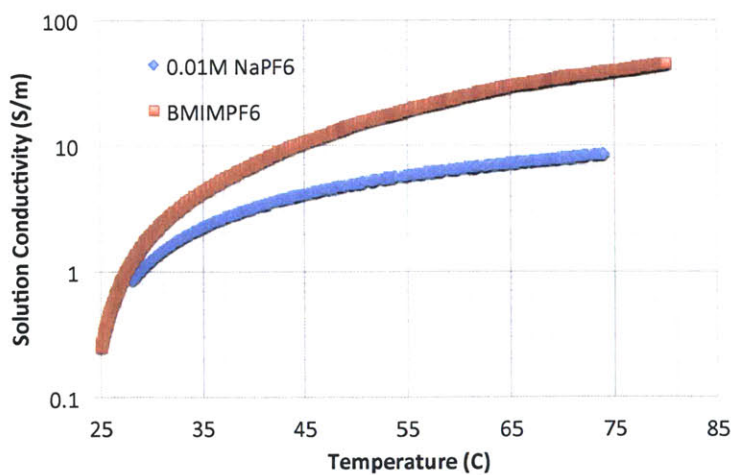
Figure 5-8: The solution conductivity of BMIMPF$_6$ and NaPF$_6$ solutions.

the simple presence of a large number of anions. The increase in solution conductivity effectively reduces the effect of the inherent polymer resistance by minimizing the potential drop across the polymer surface.
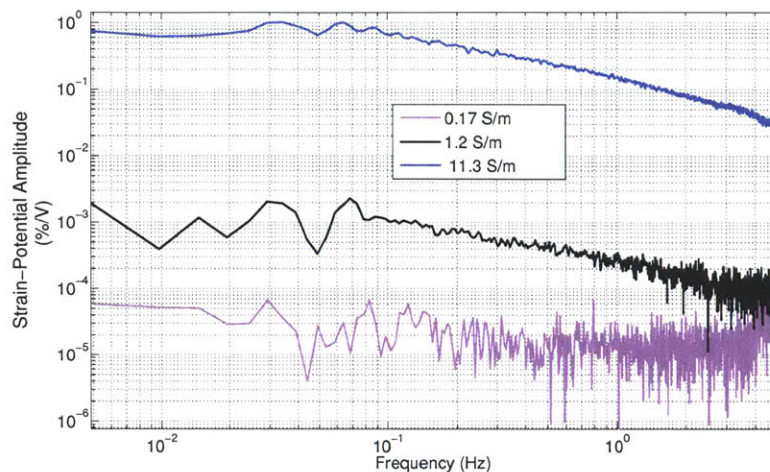
Figure 5-9: Isotonic actuation of PPy-PF$_6$ films in solutions of varying solution conductivity.

The potential of the polymer on the opposite side of the point of application was measured (i.e. the potential drop across the polymer surface) at different solution conductivities. Fig. 5-10 shows that the potential drop is minimized as the solution conductivity decreases. This leads to effectively more of the polymer seeing the same potential, maximizing the strain output. The effect can also be seen when actuating long samples. Two samples, 5 mm and 15 mm were actuated in electrolytes of varying solution conductivities. For solutions with high conductivities, the strain obtained from both the 15 mm and 5 mm films are the same. However, as the conductivity decreases, the strain from the larger film decreases significantly. This is due to the large potential drop across the PPy-PF$_6$ film because of the higher resistance of the larger film (See Fig. 5-11). Minimizing these length effects can be important in developing new conducting polymer actuators with large strokes. Keeping the solution conductivity as large as possible should be an important design for applications that require large strains.
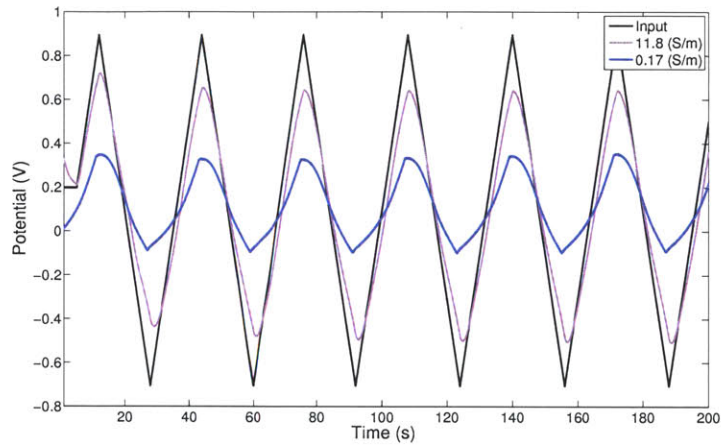
Figure 5-10: A triangle wave waveform (input) is applied to one end of a PPy-PF$_6$ film and the potential at the other end is measured. The potential drop across the polymer is minimized in solutions of high solution conductivity.
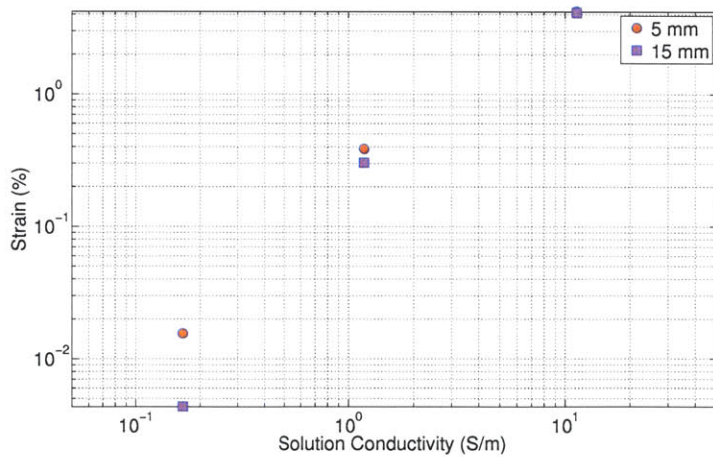
Figure 5-11: Effect of the solution resistance on strain of PPy-PF$_6$ films. The longer 15mm films show lower strains compared to the shorter films.

5.3.2 Effect of Mixtures

Conducting polymer actuators can be developed to generate large strains, large forces, long lifetimes, low creep rate and strain rates. However, achieving multiple useful properties in an actuator simultaneously can be difficult. One way to improve both strains and strain rate can be to actuate the CP in a mixture of highly mobile small ions as well as larger ions that can cause a bigger volumetric expansion. Even though having mobile cations and anions will tend to negate the overall strain an actuator can produce, multiple mobile anions can potentially be used to produce larger strains and strain rates. Most of the studies on multi-ion actuation [19, 51, 127, 129] focus on cation vs anion dominated actuation, where the size, excitation frequency and thermodynamic driving force (potential) determines the permiselectivity of the actuating ion. In addition, conducting polymers might be considered to be used in environments where multiple ions can diffuse into the polymer such as the body [11, 54] or in seawater [138, 144]. Another application of the stochastic techniques is to understand the effects of mixtures of different salts in electrolytes. Fig. 5-12 shows typical strains by PPy actuated in various Group 1 salts in aqueous electrolyte. This data was collected by [20, 32, 48, 58] and this author. The larger strains are due to the diffusion of larger ions such as the DEHS and the trifluorosulfonamide (TFSI). These large strains typically last for fewer than ten cycles due to degradation of the PPy. Smaller, more repeatable strains are produced from smaller ions such as the PF_6^- and chloride ion (Cl). The only exception are the PPy-DEHS films actuated in the dodecyl benzene sulfonate ion (DBSA) molecule where the large molecules cause smaller strains.
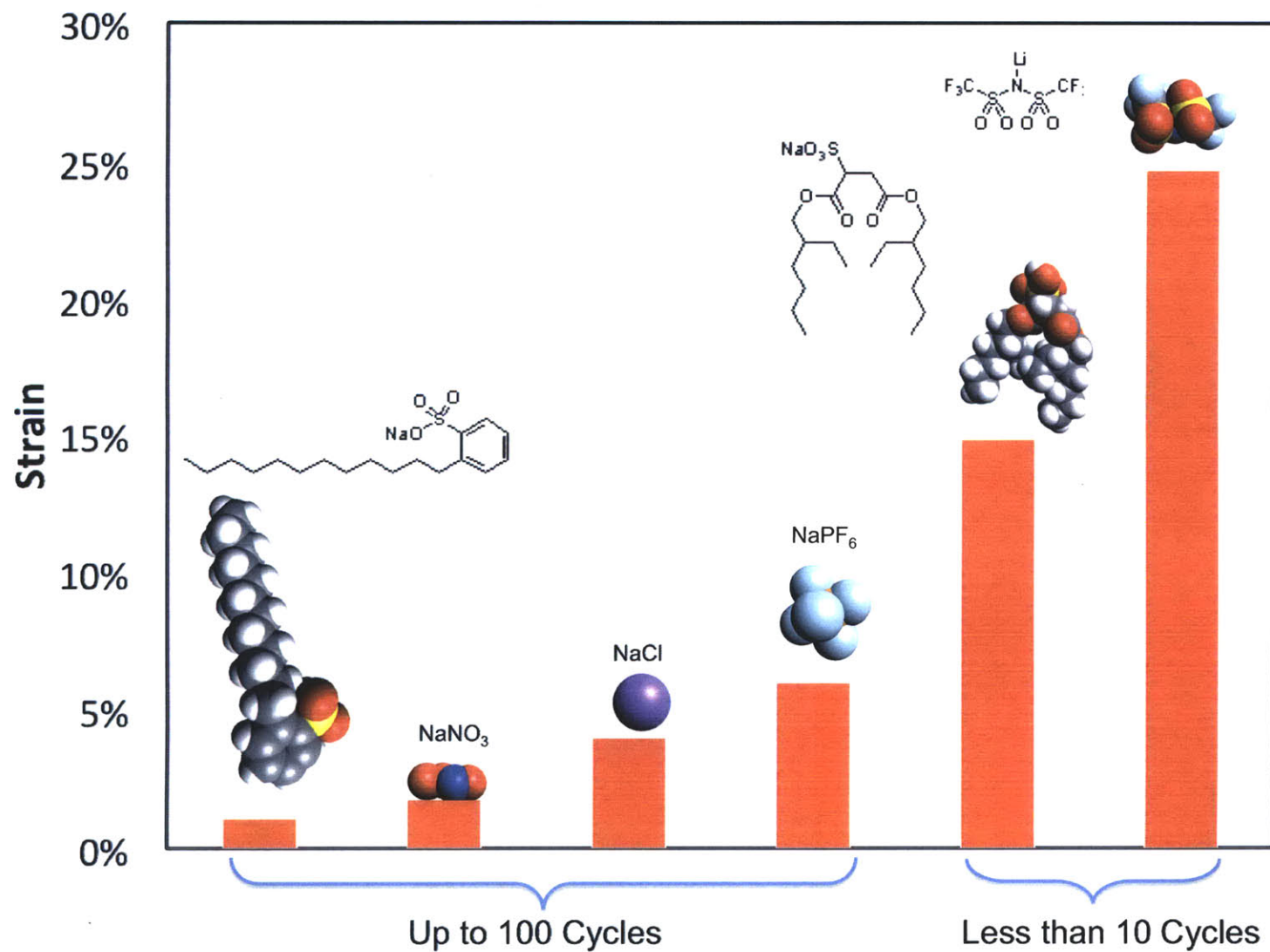
Figure 5-12: Actuation of various PPy films in different Group 1 salts. The larger ions typically cause larger strains, and smaller ions correspond with the smaller strains.

Table 5.1: Actuation of PPy films doped with PF_6^- and DEHS actuated in various salts.

Dopant	Size ($\overset{\circ}{A}$)	Conductivity (S/m)	Actuation Ion	Size ($\overset{\circ}{A}$)	Strain
PF_6^-	3.5	8000	PF_6^-	3.5	6%
			DEHS	12.6	0.8%
DEHS	12.6	891	PF_6^-	3.5	0.5%
			DEHS	12.6	9%
			DBSA	17.9	1%

The PPy-DEHS film is doped with a smaller ion than the DBSA molecule; hence it is difficult to drive the larger DBSA molecule into the polymer matrix. Similar results can be seen in Table 5.1, where PPy doped with smaller ions (such as the PF_6^-) actuated with small strains when actuated in aqueous solutions containing large ions such as the DEHS. On the other hand, the polymer doped with the DEHS ion shows relatively moderate strains when actuated in ions which have equivalent or smaller sizes. This happens in spite of the fact that the electrical conductivity of the PPy-DEHS is lower than the PPy-PF_6 ion. Fig. 5-13 top shows that PPy-DEHS actuated separately in 1 M NaPF$_6$ and in 0.1 M NaDEHS (both solutions are saturated with the highest solution conductivity possible). The larger DEHS ion shows larger strains but a lower roll off frequency compared to the film actuated in the smaller PF_6^- ion. Fig. 5-13 bottom shows an intermediate actuation state, where the overall gain on strain is increased and the roll off frequency is increased as well.

5.3.3   Understanding the Influence of Film Conductivity

It is important to understand the effect of the polymer film's conductivity on the actuation properties. It is generally well known that the larger the conductivity of a film, the larger active strain can be obtained [87, 108, 46]. This can be accomplished by either coating a side of the polymer film with a conducting layer such as gold or by trying to vary the electrodeposition deposition conditions. In this experiment, two PPy-DEHS films were created, one with pyrrole distilled one day before use and one
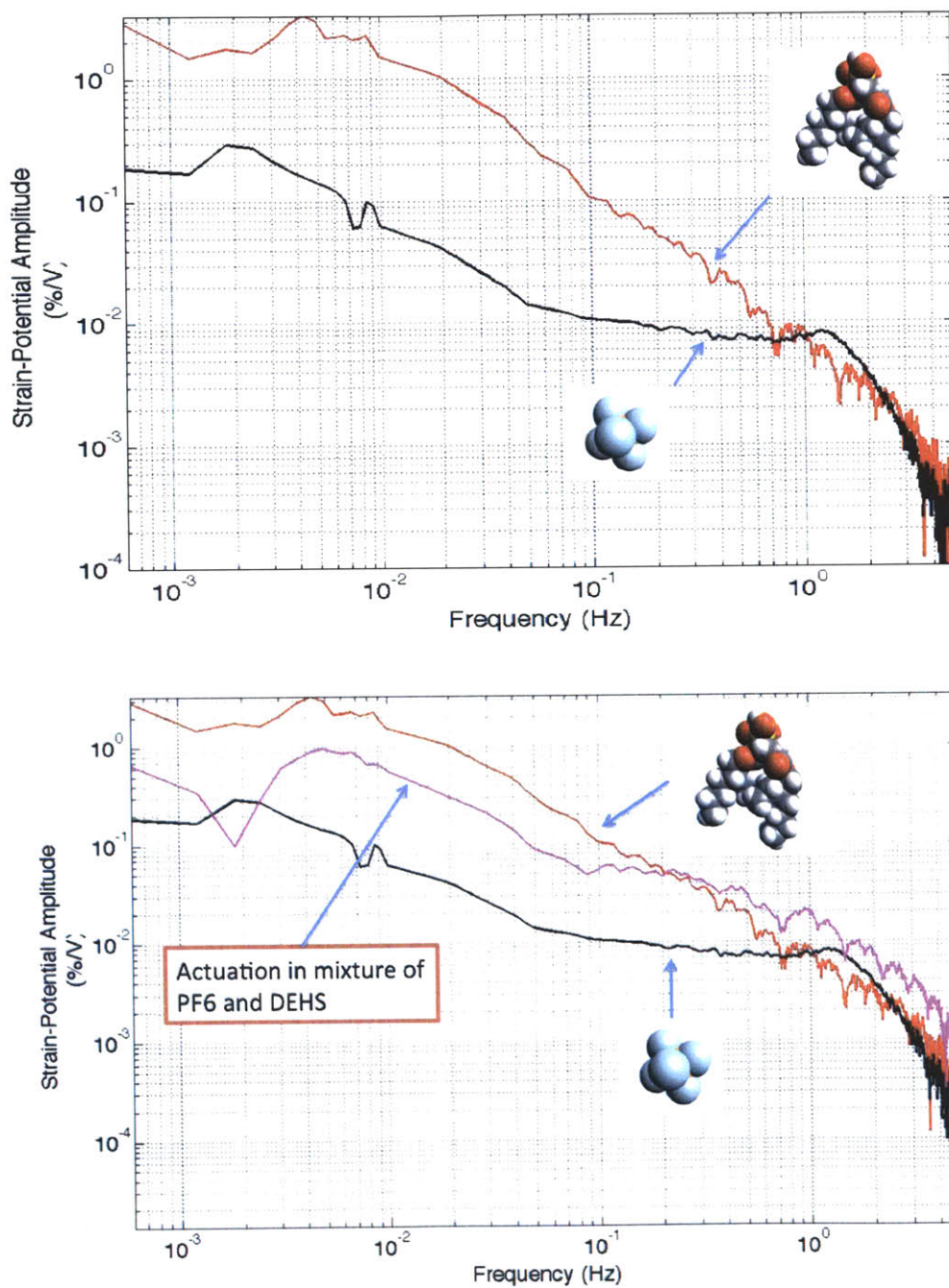
Figure 5-13: Top: PPy-DEHS actuated separately in 1 M NaPF$_6$ and in 0.1 M NaDEHS in water and ACN in 3:1 ratio. Bottom: PPy-DEHS actuated simultaneously in 1 M NaPF$_6$ and in 0.1 M NaDEHS

with pyrrole distilled four months before use. The conductivity of the film with freshly distilled pyrrole was 4500 S/m, while the PPy-DEHS film with the older pyrrole had a lower conductivity of 1680 S/m. The film with a larger conductivity showed not only larger strains but also a higher roll off frequency.
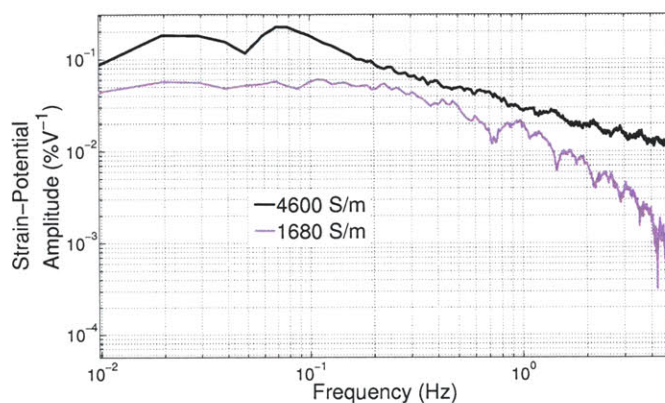
Figure 5-14: Increase in actuation strain due to increase in the conductivity of the PPy-DEHS film. Films were actuated in mixture of 0.1 M NaPF6 and 0.1 M NaDEHS solution.

5.4   Conclusions

In this chapter, we have developed a technique that helps us visualize the influence of various dopants, actuation environments, film conductivity and solution conductivity on the actuation of a conducting polymer. It has been demonstrated that increasing the solution conductivity can significantly improve actuation strain and strain rates by minimizing resistive losses. The random binary signals can be developed for the CP that ensures that either the cation or the anion is dominant and the influence of that ion on actuation can be studied. The effects of the active ion species on the strain and strain rates can also be studied. The slope of the high frequency section of the frequency response in isometric configuration gives information about the modulus and strain to charge ratio. In isotonic mode, the overall strain and the strain rate can be efficiently determined.

Chapter 6

Application of Soluble Carbon Nanotubes to Polymer Actuators

The previous chapters describe novel methods that can be used to understand and improve CP actuator properties. However, they do not describe any efficient method to eliminate the effect of creep from these actuators. These effects can lead to highly undesirable performance during any practical actuator performance [87, 4, 86]. In addition, limited electrical conductivities and poor mechanical properties can hinder the development of these actuators. Many of these properties can be improved by incorporating various fillers such as carbon black, metals and CNTs having desirable properties into the polymer matrix [149, 39, 146, 141]. Carbon nanotube-polymer composites have drawn significant attention lately [121, 2, 1, 111, 147]. These composites are created to increase conductivity, robustness and improve stiffness of the underlying polymer matrix. In many cases, it is difficult to control the concentration of the carbon nanotubes into the polymer matrix and therefore difficult to characterize their influence on actuation. This chapter discusses various techniques studied to incorporate CNTs into CPs and their effects on actuation properties.

6.1 Incorporation of CNTs in Conducting Polymers

Conducting polymer CNTs composites have been studied as muscle like actuators [63, 141, 122, 137]. In most cases, the actuation properties vary significantly based on the techniques used to create the composite material. Various approaches exist to create these composites that include mechanical mixing [14], in situ polymerization [45, 56, 64, 154], layer by layer approaches [146] and simple drop casting [36, 141, 146]. When blended in a certain (layered) configuration, these composites offer greater actuation than its pristine components. Some authors have suggested that incorporation of CNTs into CP actuator films could lead to an actuator that benefits from the high stress and strain usually observed in CP actuators. The larger stiffnesses of the CNTs lead to a more reversible actuation behavior [137, 141]. For example, polyaniline-carbon nanotube composite (PA-CNT) fibers and composite sheets had actuation strain higher than pure CNTs.

This work investigated several techniques for incorporating CNTs and CPs, including direct deposition of CNTs during electrochemical polymer synthesis, soaking and sonicating the polymer film in a CNT suspension, electrostatic self-assembly of CNTs, and fabrication of a multilayer polymer- CNTs film by alternating drop-casting of a CNTs suspension and electrodeposition of the polymer. These techniques required the CNTs to be easily processible and soluble in polar and even ionic solvents. Pristine CNTs are insoluble in most solvents due to the strong van der Waals interactions between them. However, multiwalled covalently functionalized carbon nanotubes have larger solubilities in organic and aqueous solutions [139, 117, 153, 152]. These functionalized carbon nanotubes (fCNTs) are ideal candidates for incorporation into the CP fabrication process.

6.1.1 Direct Incorporation of CNTs

The simplest method to incorporate CNTs into a CP is to directly dissolve the fCNTs into an electrolyte during the deposition process. However, doing so invariably leads to samples with poor mechanical stability. Depositions were tried in aqueous solutions, propylene carbonate and ionic liquid $BMIMPF_6$, all of which generated films with poor mechanical properties, and their effectiveness as actuators could not be accessed. A better method would be to directly grow PPy films on a CNT substrate. We cast fCNTs on a glass slide and electrodeposited PPy-PF_6 on top of the film. The film was deposited in 0.05 M pyrrole in propylene carbonate and 0.05 M tetrabutylammonium hexafluorophosphate (TBAP). Two samples were prepared; one where the fCNT film was dissolved (PPy) to get a free standing film, and one where the fCNT film was left on the film PPy-CNT. (This work was done in conjunction with Dr. Jei Ding and Dr. Wei Zhang who prepared the samples for testing).
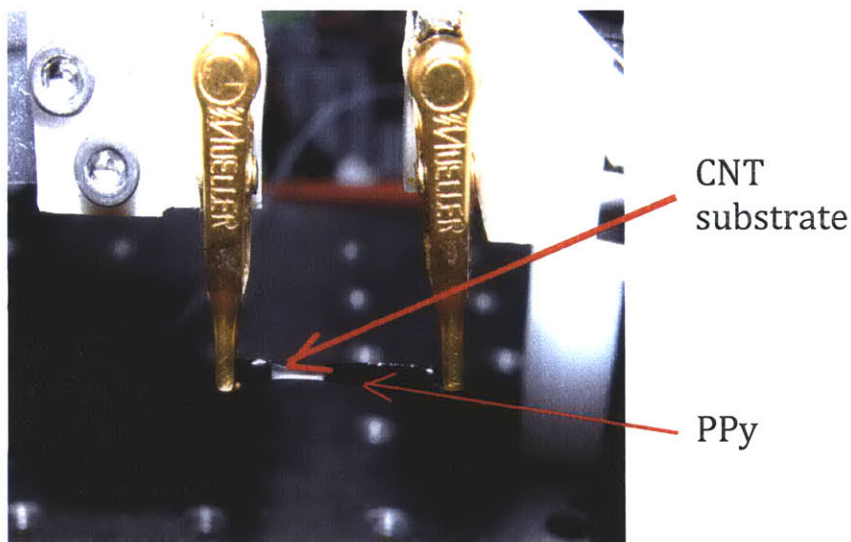
Figure 6-1: The PPy film grown on the surface of a dry fCNT film. The fCNT is much more compliant than the PPy layer, causing it to break under large pre-loads.

We measured the conductivities, densities and modulus of the films and are shown in Table 6.1. The fCNTs are generally more compliant and less conductive than PPy; therefore, the measured modulus of the composite and the conductivity are lower

than pristine PPy yet higher than the pristine fCNTs. When actuating these films, we have to account for the difference in compliance, since at large loads PPy can break (Fig. 6-1) and delaminate from the substrate.

Table 6.1: The measured properties of PPy and PPy-CNT composite films. The modulus was measured at 1 Hz.

Polymer	Thickness (μm)	Conductivity (S/m)	Density (kg/m^3)	Modulus (MPa)
PPy	40	3.529×10^3	2.064×10^3	215
PPy-CNT	310	4.484×10^2(PPy side)	4.081×10^2	17.5

We actuated the films in neat BMIMPF$_6$ in order to access any improvement in actuator performance (Fig. 6-2). There is no significant change in the performance of the composite as compared to the PPy film. Both showed the same creep rates and actuation strains. This deposition technique leads to very little direct incorporation of the fCNTs into the polymer matrix; hence, it simply acts as a passive mechanical layer with little influence on overall strain or strain rates. Therefore, it is desirable to use other techniques to directly incorporate fCNTs into the PPy matrix.
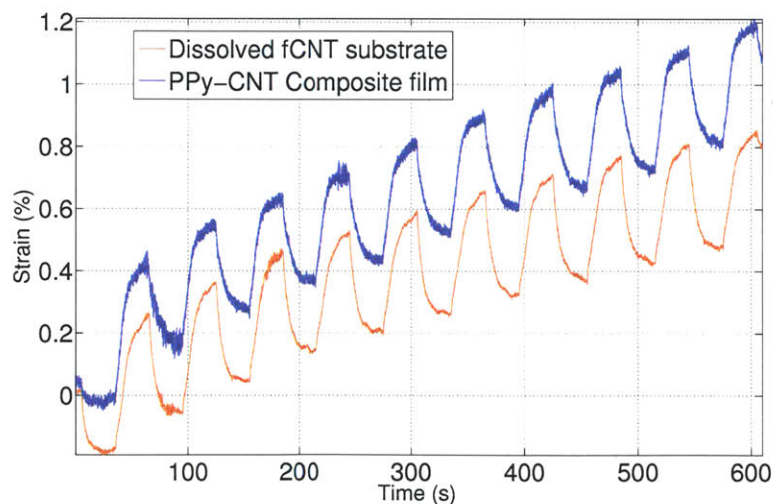
Figure 6-2: The strain and creep rates in PPy-CNT and PPy films actuated in neat BMIMPF$_6$ between 0.8V and -0.8V at 1 MPa preload.

98

6.1.2 Incorporation using Electrostatic Assembly

Another approach to prepare the PPy-CNT composite involved incorporating functionalized fCNTs into PPy-PF$_6$ film via physical absorption. The fCNT forms a crust on a substrate when the solvent the fCNT is dispersed in evaporates [40]. We grew the PPy-PF$_6$ thin film in a propylene carbonate solution containing 0.05 M pyrrole monomer and 0.05 M TBAP, with 1% (v/v) water. PPy-PF$_6$ films were deposited onto polished glassy carbon substrates at a current density of 2.5 A/m^2. A piece of polished copper was used as the counter electrode, and an Ag wire was used as the reference electrode. The cell deposition temperature was controlled at -40 °C and the solution was nitrogen saturated. The film was grown at a constant current for 16 hours. The PPy-PF$_6$ film was washed with propylene carbonate and peeled from the glassy carbon electrode. The film thickness was 22 μm. Subsequently, the free standing film was placed in a well dispersed solution of fCNTs (1.0 mg/ml) in propylene carbonate for 30 minutes, then dried with nitrogen gas (PPy-fCNT physical adsorption). The measured film thickness was still 22 μm. However, SEM (Fig. 6-4) indicates that only a small amount of fCNTs were deposited on PPy surface(this work was done in conjunction with Dr. Jei Ding and Dr. Wei Zhang who provided the samples and conducted the passive characterization experiments). Another approach to prepare the PPy-CNT composite involved depositing fCNTs onto PPy-PF$_6$ films via electrostatic-driven self-assembly under an applied electric field. The PPy-PF$_6$ film was prepared by following the same procedure as in the previous approach. The PPy-PF$_6$ thin film deposited on the glassy carbon electrode was placed into fCNT solutions with different concentrations (0.1 mg/ml and 0.01 mg/ml in propylene carbonate). The electrostatic assembly of fCNTs was conducted by applying a 0.65 V potential on the PPy-PF$_6$ film for 30 minutes. Here, the electric field attracted the negatively charged fCNT to the surface of the PPy-PF$_6$ film. The composite film was then washed with propylene carbonate and peeled off from the glassy carbon electrode. The film thickness was 32 μm (PPy-fCNT electrostatic assembly). Based on the thermogravimetric analysis (TGA), the PPy-PF$_6$ polymer showed a 37% weight
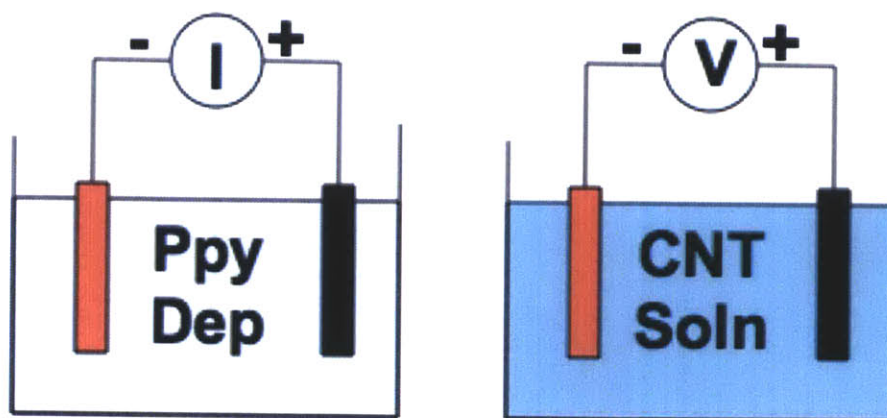
Figure 6-3: Schematic of creating the composite films using electrostatic assembly. The PPy film is grown under standard deposition conditions. The film is then switched to another container with well dispersed fCNTs, where the film is either soaked or exposed to an electric field.

loss, while TGA of fCNT showed a 44% weight loss. Since the higher weight loss corresponds to the higher ratio of the fCNT to PPy-PF$_6$ in the composite, this TGA result showed the highest CNT content in the composite prepared via this approach. Also from Fig. 6-4, we can see the presence of a higher density of fCNTs on the surface of the PPy-PF$_6$ (data courtesy of Dr. Jie Ding).

Actuation of Electrostatically Assembled Films

Fig. 6-5 shows the strain response of control and composite films to a potential square wave at 0.05 Hz between -1.0 V and 1.0 V vs. Ag wire. The composite materials not only exhibited improved conductivity over the control sample but also showed greatly minimized creep behavior during actuation tests. The PPy-fCNT physical adsorption and the electrostatic discharge films show smaller creep rates than the control PPy-PF$_6$ films. They also have on average smaller strain amplitude (3%) than the control films (5%). The modulus is calculated at 1 Hz and is 1000 MPa, the electrical conductivity for the control film is 2500 S/m, and the films exposed to fCNTs are 2800 S/m. However, the differences in these properties are not sufficient to explain the large variation in active mechanical properties seen in Fig. 6-5. We characterized

100
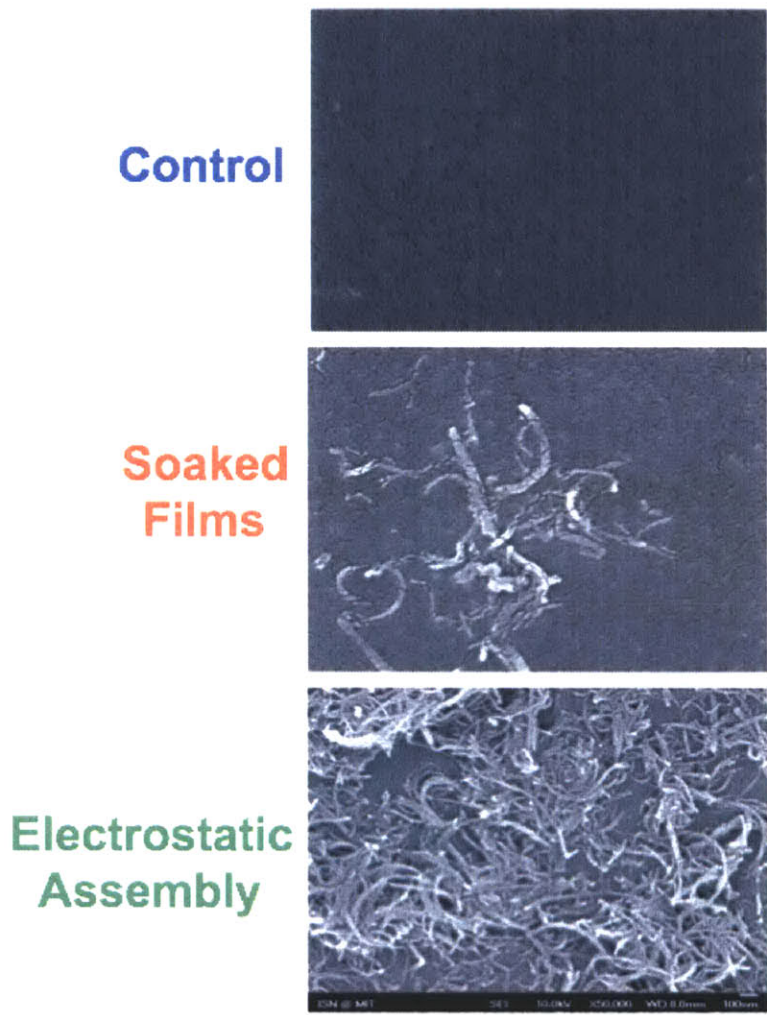
Figure 6-4: SEM images of the PPy-PF$_6$ and fCNT film composites. Blue: Control PPy-PF$_6$ film without fCNTs. Red: PPy-PF$_6$ film with fCNTs included using physical adsorption. Green: PPy-PF$_6$ film with fCNTs included using electrostatic assembly (Picture courtesy Dr. J. Ding).
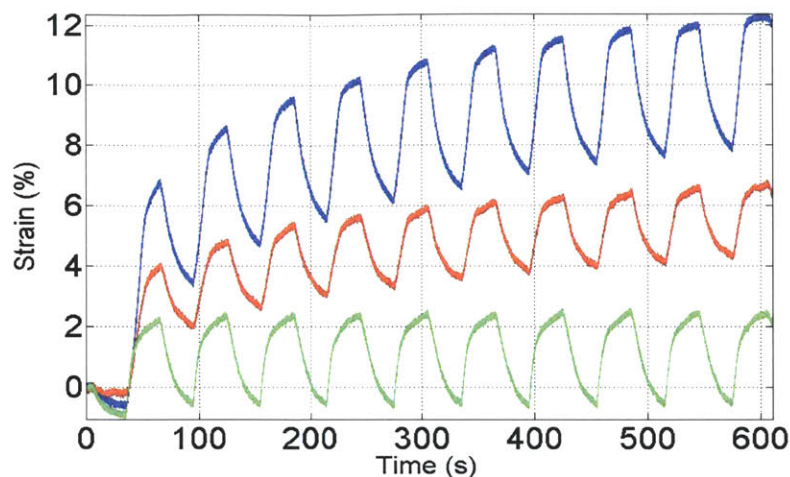
Figure 6-5: Active strain in the PPy-fCNT physical adsorption (Red) and the electrostatic discharge (Green) films relative to a control PPy-PF$_6$ (Blue) film. The films exposed to CNTs showed significantly lower creep rates relative to the control films.

the creep response of composite using a step change in stress and measuring the corresponding strain (Fig. 6-6). The mechanical creep rates are the same in all of the films: this shows that actuation of the films directly causes the decrease in actuation.

6.1.3   Incorporation using Layer by Layer Drop Casting

Although the electrostatically assembled films show improvement in creep responses of a polymer actuator, it is difficult to incorporate a controlled amount of CNTs into the polymer. To actively control the weight of the CNTs a layer by layer approach was used. Similar approaches have been used in the development of batteries [79, 38, 78]. In these experiments, we used multi-walled sCNTs, which provided the desired solubility and ionic properties while maintaining conductivity. The sCNTs polymer composites were obtained by alternating drop-casting of sCNT with electrodeposition of the polymer 6-7. Using this method, the ratio of sCNTs to polymer in the composite could be easily controlled by the amount of suspension added, and therefore, allowed us to investigate how increasing amounts of sCNTs affected the
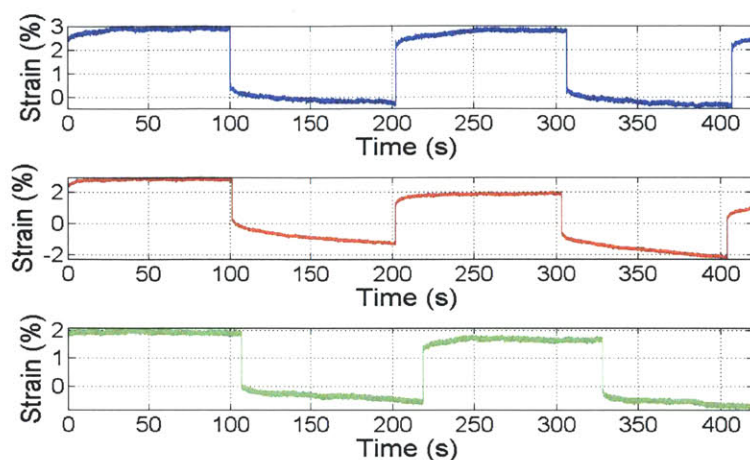
Figure 6-6: The creep response of the mechanical component was measured using a step change in stress and measuring the corresponding strain.

composites properties: creep rate, conductivity, stiffness, thickness, and active strain. In this study, PEDOT and PPy were used as the CP materials to fabricate Poly(3,4-ethylenedioxythiophene)-carbon nanotube composite (PEDOT-CNT) and PPy-CNT composites, due to the fact that free-standing PEDOT and PPy films could be easily synthesized electrochemically using similar procedures. It was observed that the sCNTs significantly reduced the creep rate of both PEDOT and PPy but also reduced the overall strain and active stress. However, actuating the polymer at larger preloads can eliminate these effects (this work was done in conjunction with Yenmei Keng, Prof Ali Sheikh and Jan Schnorr).

PPy-CNT composites were fabricated into multilayer structures. Nine-layer PPy-CNT composites were brittle, and the layers tend to separate when the sCNT content was higher than 20%. The PPy-CNT composites were fabricated with three layers of PPy sandwiching two layers of sCNTs, forming five layers. The deposition setup for PPy layers were the same as the setup used for PPy layers, except that the monomer added was 0.13 M of distilled pyrrole. We repeated the drop-casting and weighing steps for PPy-CNTs. The PPy-CNT composites were made for approximately 10%, 30% of sCNTs by weight.

103
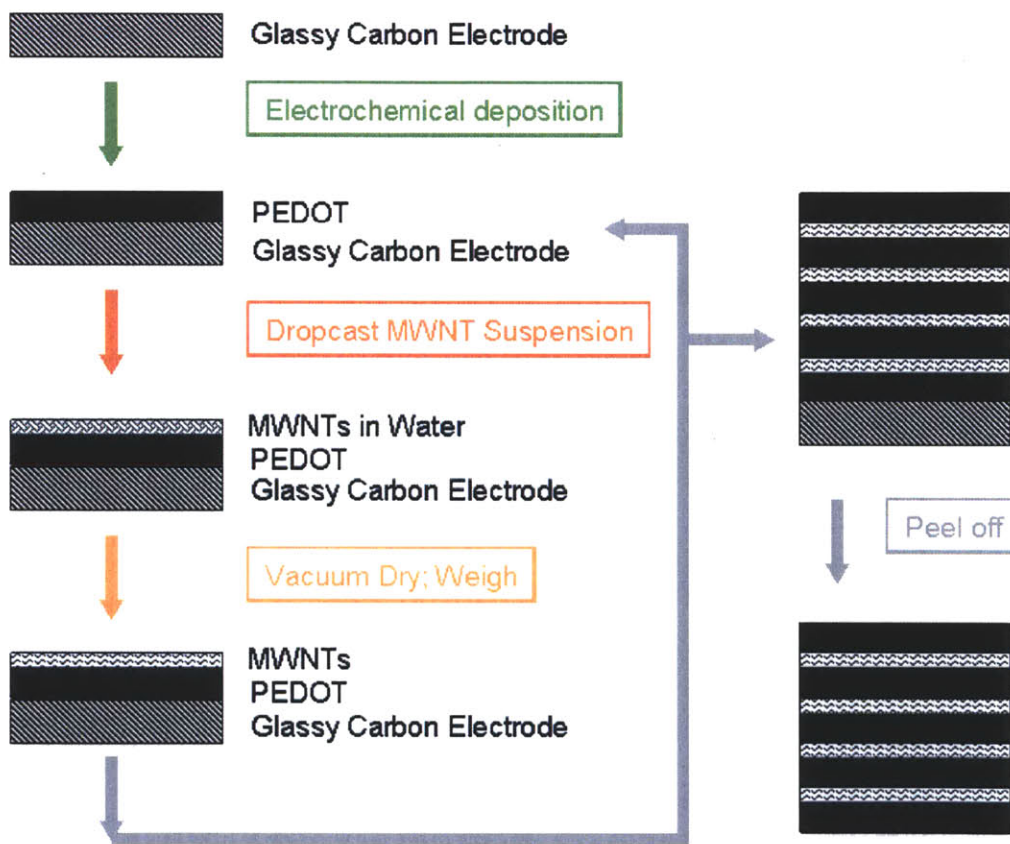
Figure 6-7: The procedure for fabricating layer-by-layer PEDOT-sCNT composite films included electrochemical deposition of PEDOT layers and drop-casting sCNT water suspension (image courtesy of Y. Keng).

Actuation of Layer By Layer Drop Cast Films

Isotonic results showed that increasing the amount of sCNTs decreased the creep rate in PPy-CNT composites. Fig. 6-8 left shows that the creep rate decreased significantly when the sCNTs content increased from 0% to 10%, and it decreased further when another 10% sCNT (total 20% sCNTs) was deposited. The charge motion through the composite films was more reversible than the PPy control; i.e. the same number of ions diffused into the polymer bulk as moved out (Fig. 6-8 right). In contrast, in the PPy films with no sCNTs, the average charge decreased with time, implying that some cations remained in the polymer bulk as the film was being actuated. Although increasing the sCNT content also reduces the total strain, this can be mitigated using larger preloads [73].
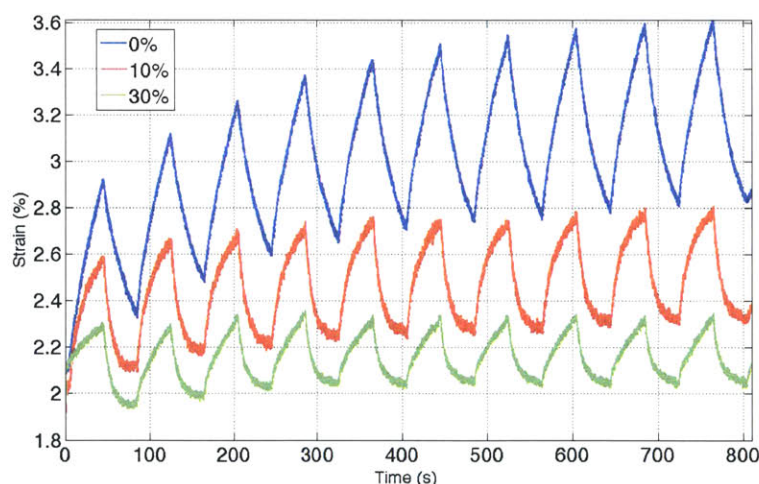
Figure 6-8: Increasing the amount of sCNTs reduced the creep and strain of the PPy composite. The 20% sCNT composite had no creep, while the PPy control crept more than the 10% and the 20% sCNT composites.

6.1.4   Effect of sCNTs on Actuation

Fig. 6-9 displays a proposed mechanism that shows the influence of carbon nanotubes during the actuation cycle. The carbon nanotubes cross link with the CP chains, reinforcing the polymer matrix. The top row in Fig. 6-9 shows the actuation cycle

in CP films. As ions diffuse in and out of the film, the CP films do not go back to their original configuration, which leads to a permanent deformation. However, in the sCNT blended films seen in the bottom row of Fig. 6-9, the strong bonding between CNTs and the CP chains act as internal springs and is able to restore the polymer matrix back to its original configuration. This also results in the reduction of strain amplitude in the blended film compared to the control CP films. Similar results can
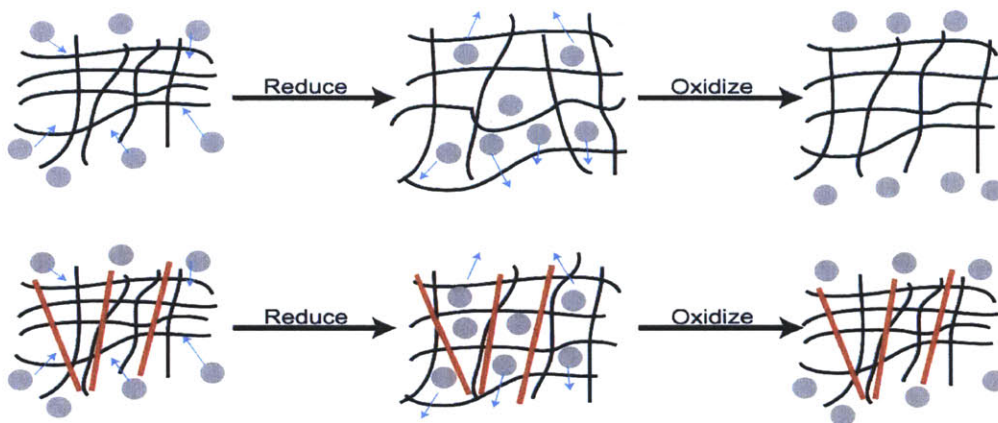
Figure 6-9: A speculated mechanism on how the sCNT influence polymer actuator behavior. The PEDOT control could expand evenly while ions diffused into the polymer, but the composite could only actuate fully at the areas where the sCNTs were absent. The dots are used for position reference. The grey dots represent the areas affected by sCNTs, the red dots represent the unaffected areas, and the blue curve represents a sCNT.

also be seen when studying Li ion batteries [41, 42, 52]. Here, the incorporation of CNTs into the battery electrodes increases the reversibility of charge-discharge cycles of these batteries. The incorporation of CNTs, improves the stiffness and electrical conductivities, thereby improving overall battery performance.

The addition of CNTs significantly reduces the creep rates in both PPy and PE-DOT composite films (Fig. 6-10). The optimal CNT content to eliminate creep in both cases is between 10-20% when the films are synthesized using a layer by layer approach. Adding additional CNTs does not improve creep performance but reduces the strain.
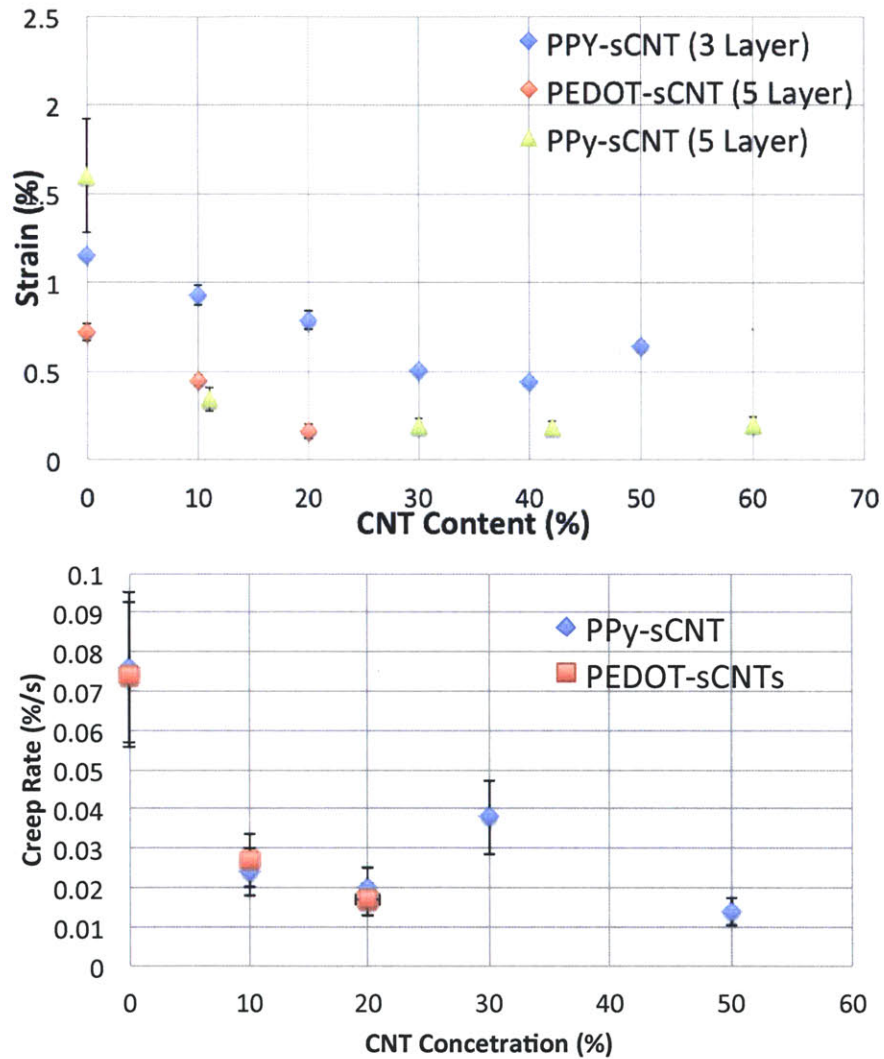
Figure 6-10: The strains (top) and creep rates (bottom) for different polypyrrole and PEDOT and carbon nanotube composites. There is a reduction of strain and corresponding creep rates in both materials as the CNT content is increased. (Parts of the data was collected by Y. Keng)

6.2 Effect of Rolling on PPy-sCNT composites

Pytel et al [108] showed that rolling of PPy samples significantly increased the polymer actuator conductivity as well as active strain. These improvements can be attributed to the improved conductivity as the polymer chains align in the direction perpendicular to the rolling direction. Keng [73] showed that some of the films developed using a layer by layer process showed visible gaps (in an SEM) between layers, indicating poor bonding. Actuation properties of the films developed using the layer by layer approach might be further improved by rolling the films. Rolling might compress the films to improve the bonding between layers as well as improve conductivities between layers and across the thickness of the films. Rolling might also result in alignment of the CNTs within the films which could improve actuation properties as well (Fig. 6-11) (work done in conjunction with Juan Lozada and Dr. Ali Sheikh, who prepared samples).

We grew one layer of PPy from 0.05 M TEAP in PC. The glassy carbon electrode was removed from the deposition environment and dried. A second layer of sCNTs was drop cast from a 5 mg/ml solution. The new layer of polypyrrole was grown on top of the film to create a three layer structure. Films of varying sCNT concentrations by weight were made. The films were rolled using the dunston rolling machine shown in Fig. 6-11. The films typically showed a 30% increase in strain in the length direction, 10% increase in strain in the width direction and a 20% decrease in strain in the thickness direction. The electrical conductivity of the films were measured in all the directions. Generally, electrical conductivities were highest perpendicular to the rolling direction and lower parallel to the rolling direction (Fig. 6-12). The films were actuated in neat BMIMPF$_6$ between 0.8 V and -0.8 V using a square wave potential waveform with a 0.025 Hz frequency. There is a significant increase in strain in the direction perpendicular to the rolling direction, which is consistent with previous results [108]. These is a seven fold increase strain for all films regardless of the CNT content (Fig. 6-13). This implies that the CNTs are not aligned using the rolling process within the PPy or that it does not influence actuation.
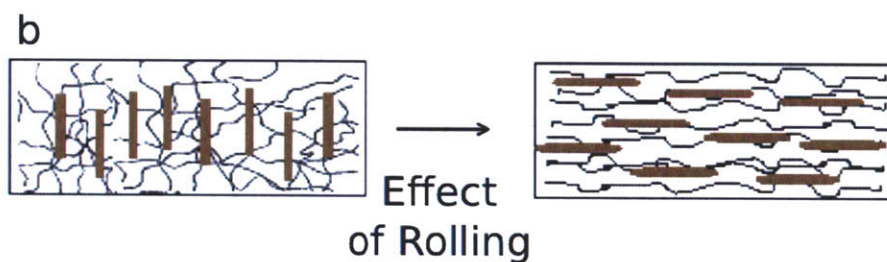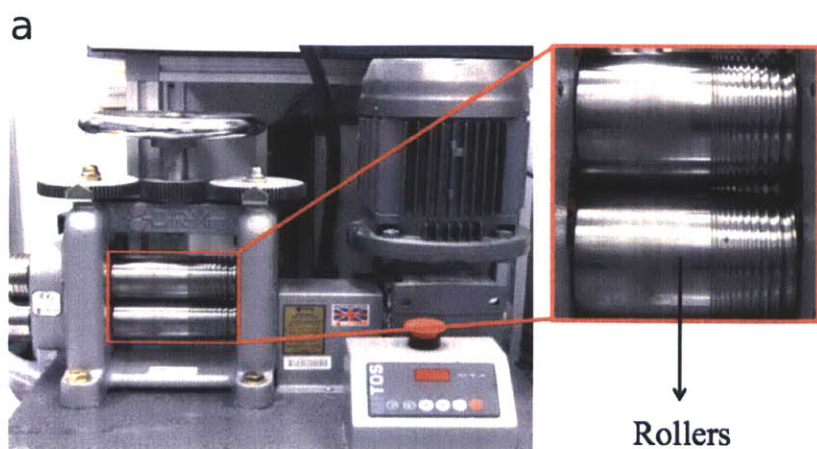
Figure 6-11: Top: Dunston rolling machine: The polymer films are rolled between the rollers at a constant load and velocity. Bottom: Effect of the rolling on CNT alignment.
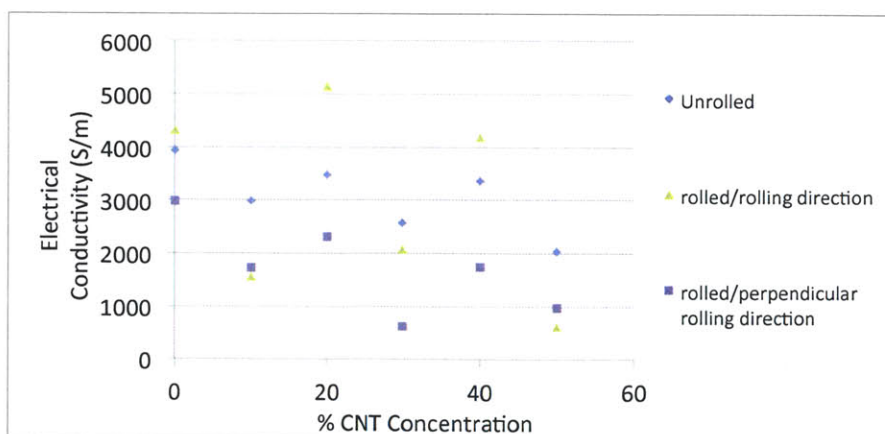
Figure 6-12: Conductivities of the rolled films in the different directions relative to the unrolled films.
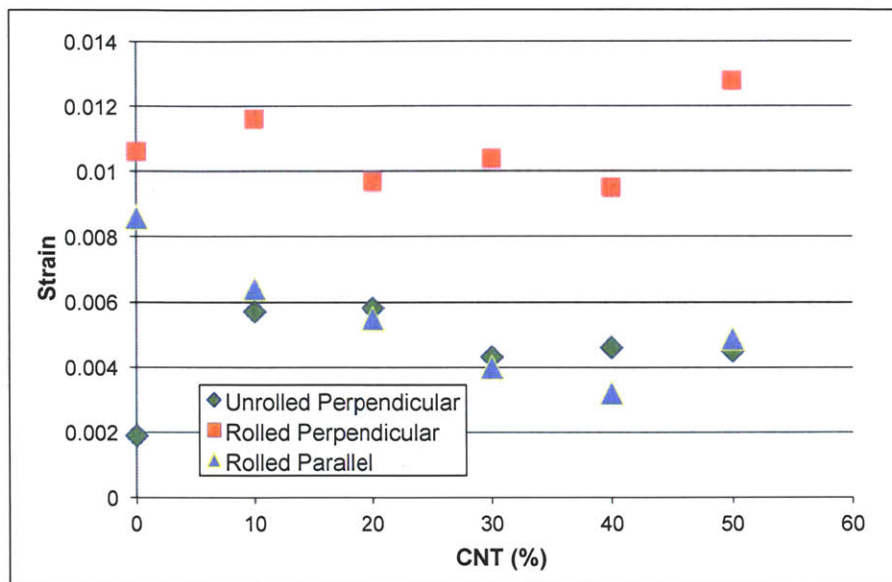
Figure 6-13: Effect of rolling on the actuation strain relative to the different rolling directions. Strain in the direction perpendicular to rolling direction is the largest.

6.3   Conclusions

In this chapter, we have discussed different techniques to incorporate CNTs into CPs. The electrostatic assembly approach involves alternate growing of a polymer and then assembling CNTs on the surface by applying a negative potential on the surface of the grown film. Another approach would be to use alternate electrodeposition and drop casting steps to incorporate the CNTs. Using this method we are able to precisely control the carbon nanotube content within the polymer and study the effects of increasing the CNT concentration on actuation properties. One of the drawbacks of using a multi layer approach of assembling these films is the separation that occurs between layers. This can be rectified by post processing the films. We rolled the films and show that rolling increases the conductivity and actuation strain that can be obtained in the direction perpendicular to the rolling direction. However, increasing the CNT content does not improve the overall strain that one can generate from the polymer.

Chapter 7

Conclusions

Conducting polymer actuators are currently studied using traditional triangle wave, square wave or sinusoidal excitation potentials. These signals are useful in studying actuators, but many different experiments are necessary to fully characterize one polymer system in a single actuation environment. Since the combinations of polymer, dopant, electrolyte, and active ion are numerous, this can significantly slow the development of these materials. The stochastic techniques developed in this thesis can be used to quickly generate frequency response plots which are far more informative. It can also be used to track compliance and impedance transfer functions relative to a oxidation state. Beyond that, the same techniques can be used to measure the compliance, impedance and actuation properties as a function of load, temperature and even humidity. These new techniques promise to speed up the development of electrochemical actuators to a point where they can be incorporated into engineering systems. In Chapter 3, we have shown that incorporation of small cations causes the largest compliance changes, while anions do not cause significant changes. Once the effect of oxidation reduction on the compliance is characterized, we can also show how the strain to charge ratio can be estimated from the same graph. In this case, the strain caused by the changing compliance can simply be subtracted from the total strain, and the strain component due to ion incorporation can be measured. Similarly we have shown how the impedance transfer functions can be measured and how they can be used to make simultaneous measurements of strain while actuating a polymer

without the need of a separate strain sensor. We have tied the parameters of the impulse response to physical parameters and have associated physical meaning to these parameters. These techniques were then applied to study actuation in conducting polymers. One can use correlation analysis to measure the modulus and the strain to charge ratio in stochastic isometric tests. In stochastic isotonic tests one can quickly measure the actuator open loop bandwidth as well as the strain a typical actuator can produce in this configuration. These were then used to show the effects of various dopant ions and actuation ions on the overall strain and speed of actuation. It was also used to show the effects of temperature and solution conductivity on strain and a means to improve the overall strain was also described. These techniques can be further used to characterize the effects of various solvents, porosity and even geometry on polymer actuator behavior.

Finally, the influence of carbon nanotubes on actuation has been studied. Multiple methods of incorporating functionalized carbon nanotubes into conducting polymers have been studied. The functionalized carbon nanotubes are readily soluble in various solvents which lend them to be easily incorporable into CPs. Our layer by layer approach allows us to easily control the amount of CNTs in the polymer film. Increasing the amount of CNTs significantly reduces the creep and improves performance. However, adding more carbon nanotubes also reduces the electrical conductivity of the composite and then lowering the overall strain that can be achieved. This can be overcome by actuating the polymer at larger pre-loads. This is not always the ideal approach since actuation at larger preloads can cause the polymer to break. The conductivity of CNTmaterials must be improved to where they are comparable to CPs. This will ensure that there is no loss of electrical conductivity between in the composite.

7.1 Suggestions for Future Work

We engineers develop new and varied applications of conducting polymers that go beyond actuators, new tools and techniques are required that can measure and improve

their properties. This thesis for the first time applies stochastic system identification techniques to conducting polymers and has shown how these methods can be used to improve CP properties. Beyond that, these techniques are uniquely capable of making in-situ measurements of conducting polymer compliance and impedance that were not possible with any traditional techniques. Not only can these methods be applied to study of actuators but also can be used to study sensors, electronics and even polymer based super capacitors. Many of these systems have multiple competing effects that can hinder the properties of these materials. The stochastic techniques developed in this thesis can be used to study these materials and enhance their properties. In addition, applications can be developed where a combined actuator, sensor and power storage are required. Here, stochastic techniques can be used to discriminate between the functions of the different components.

The deposition growth of conducting polymers is still not very well understood. The creation of highly conductive free standing thin films of conducting polymers is still done be trial and error. Stochastic techniques can be used to study the electro deposition process itself. This process is a strong function of solvent, dopant, chemical potentials and currents and temperatures. A stochastic signal can be superimposed on the traditional waveforms and be used to measure the impedance during the electrodeposition process. This can lead to a better understanding of the deposition process as well as improve conductivity and mechanical properties of the resultant polymer films.

These techniques can be used to characterize other types of artificial muscle actuators. For example, they can be used to study the compliance changes in dielectric elastomers as these are subjected to large voltages. The polymer breaks down, and this degradation can be measured using a stochastic force input coupled with the potential input. We can envision using these signals to develop new experiments that couple mechanical, electrical, thermal and magnetically driven actuators to study the coupling across domains.

The stochastic methods used to in this thesis can be applied individually or in novel combinations, in traditional or new conducting polymer systems. It is our hope

that the stochastic techniques presented here will help remind conducting polymer researchers as of the value that can be added by these experimental techniques.

Bibliography

[1] SV Ahir, YY Huang, and EM Terentjev. Polymers with aligned carbon nanotubes: Active composite materials. *Polymer*, 49(18):3841–3854, 2008.

[2] PM Ajayan, O. Stephan, C. Colliex, and D. Trauth. Aligned carbon nanotube arrays formed by cutting a polymer resin—nanotube composite. *Science*, 265(5176):1212, 1994.

[3] K. J. Albert, N. S. Lewis, C. L. Schauer, G. A. Sotzing, S. E. Stitzel, T. P. Vaid, and D. R. Walt. Cross-reactive chemical sensor arrays. *Chem. Rev.*, 100(7):2595–2626, 2000.

[4] G. Alici and N.N. Huynh. Performance quantification of conducting polymer actuators for real applications: a microgripping system. *Mechatronics, IEEE/ASME Transactions on*, 12(1):73–84, 2007.

[5] T. Amemiya, K. Hashimoto, and A. Fujishima. Frequency-resolved faradaic processes in polypyrrole films observed by electromodulation techniques: electrochemical impedance and color impedance spectroscopies. *The Journal of Physical Chemistry*, 97(16):4187–4191, 1993.

[6] MR Anderson, BR Mattes, H. Reiss, and RB Kaner. Gas separation membranes: a novel application for conducting polymers. *Synthetic Metals*, 41(3):1151–1154, 1991.

[7] P. Anquetil. *Large Contraction Conducting Polymer Molecular Actuators*. PhD thesis, Massachusetts Institute of Technology, 2004.

[8] R. Ansari Khalkhali, WE Price, and GG Wallace. Quartz crystal microbalance studies of the effect of solution temperature on the ion-exchange properties of polypyrrole conducting electroactive polymers. *Reactive and Functional polymers*, 56(3):141–146, 2003.

[9] C. Arbizzani, M. Mastragostino, and F. Soavi. New trends in electrochemical supercapacitors. *J. Power Sources*, 100(1-2):164–170, 2001.

[10] P. W. Atkins. *Physical Chemistry*. Oxford University Press, 1990.

[11] W.J. Bae. Cortical recording with conducting polymer electrodes. Master's thesis, Massachusetts Institute of Technology, 2008.

[12] M. Bahrami-Samani, D. C. Cook, J. D. Madden, G. Spinks, and P. G. Whitten. Quartz crystal microbalance study of volume changes and modulus shift in electrochemically switched polypyrrole. *Thin Solid Films*, 516:2800–2807, 2008.

[13] M. B. Bahrami-Samani, P. G. Whitten, G. Spinks, and C. D. Cook. Modelling of polypyrrole actuators. In *Materials Research Society Fall Meeting*, pages –, Boston, MA, 2006.

[14] M. Baibarac and P. Gomez-Romero. Nanocomposites based on conducting polymers and carbon nanotubes: from fancy materials to functional applications. *Journal of nanoscience and nanotechnology*, 6(2):289–302, 2006.

[15] P. Bandyopadhyay. Trends in biorobotic autonomous undersea vehicles. *IEEE Journal of Oceanic Engineering*, 30:109 – 139, 2005.

[16] Y. Bar-Cohen. *Electroactive polymer (EAP) actuators as artificial muscles: reality, potential, and challenges*. SPIE Press, Bellingham, WA, 2nd edition, 2004.

[17] R. Baughman, R. Shacklette, and R. Elsenbaumer. Microelectromechanical actuators based on conducting polymers. *Molecular Electronics*, pages 267–89, 1991.

[18] R. H. Baughman. Conducting polymer artificial muscles. *Synth.Met.*, 78(3):339–354, 1996.

[19] L. Bay, T. Jacobsen, S. Skaarup, and K. West. Mechanism of actuation in conducting polymers: osmotic expansion. *The Journal of Physical Chemistry B*, 105(36):8492–8497, 2001.

[20] L. Bay, N. Mogensen, S. Skaarup, P. Sommer-Larsen, M. Jorgensen, and K. West. Polypyrrole doped with alkyl benzenesulfonates. *Macromolecules*, 35(25):9345–9351, 2002.

[21] C. Bellan. Field dependence of viscoelastic properties of mr elastomers. *International Journal of Modern Physics B (IJMPB)*, 17(18):2447–2453, 2002.

[22] T. Berzina, A. Smerieri, M. Bernabò, A. Pucci, G. Ruggeri, V. Erokhin, and MP Fontana. Optimization of an organic memristor as an adaptive memory element. *Journal of Applied Physics*, 105(12):124515–124515, 2009.

[23] T.A. Bowers. Modeling, simulation, and control of a polypyrrole-based conducting polymer actuator. Master's thesis, Massachusetts Institute of Technology, 2004.

[24] S. Bruckenstein, K. Brzezinska, and A.R. Hillman. EQCM studies of polypyrrole films. 1. Exposure to aqueous sodium tosylate solutions under thermodynamically permselective conditions. *Electrochimica acta*, 45(22-23):3801–3811, 2000.

[25] L. H. Carney, M. J. McDuffy, and I. Shekhter. Frequency glides in the impulse responses of auditory-nerve fibers. *The Journal of the Acoustical Society of America*, 105, 1999.

[26] F. Carpi, D. De Rossi, R. Kornbluh, R. Pelrine, and P. Sommer-Larsen. *Dielectric elastomers as electromechanical transducers*. Elsevier Amsterdam, 2008.

[27] Angela Chen. Large displacement fast conducting polymer actuators. Master's thesis, Massachusettes Institute of Technology, 2006.

[28] X. Chen and O. Inganäs. Doping-induced volume changes in poly (3-octylthiophene) solids and gels. *Synth.Met.*, 74(2):159–164, 1995.

[29] Y. Chen and I. W. Hunter. In vivo characterization of skin using a weiner nonlinear stochastic system identification method. In *Conf.Proc.IEEE Eng.Med.Biol.Soc.*, volume 1, pages 6010–6013, United States, 2009.

[30] CK Chiang, CR Fincher Jr, YW Park, AJ Heeger, H. Shirakawa, EJ Louis, SC Gau, and A.G. MacDiarmid. Electrical conductivity in doped polyacetylene. *Physical Review Letters*, 39(17):1098–1101, 1977.

[31] S. Cichos, J. Haberland, and H. Reichl. Performance analysis of polymer based antenna-coils for RFID. In *Polymers and Adhesives in Microelectronics and Photonics, 2002. POLYTRONIC 2002. 2nd International IEEE Conference on*, pages 120–124. IEEE, 2002.

[32] M. Cole and J.D. Madden. The effect of temperature exposure on polypyrrole actuation. In *Materials Research Society Symposium Proceedings*, volume 889, page 105. Warrendale, Pa.; Materials Research Society; 1999, 2006.

[33] S. Coyle, W.U. Yanzhe, K.T. Lau, D. De Rossi, G. Wallace, and D. Diamond. Smart nanotextiles: A review of materials and applications. *MRS bulletin*, 32(5):434–442, 2007.

[34] Sam. C. Creason, John W. Hayes, and Donald E. Smith. Fourier transform faradaic admittance measurements iii. comparison of measurement efficiency for various test signal waveforms. *Journal of Electroanalytical Chemistry and Interfacial Electrochemistry*, 47(1):9 – 46, 1973.

[35] X. Cui, J. Wiler, M. Dzaman, R.A. Altschuler, and D.C. Martin. In vivo studies of polypyrrole/peptide coated neural probes. *Biomaterials*, 24(5):777–787, 2003.

[36] L. Dai and A.W.H. Mau. Controlled synthesis and modification of carbon nanotubes and C 60: carbon nanostructures for advanced polymeric composite materials. *Advanced Materials*, 13(12-13):899–913, 2001.

[37] S.N. Davidson. Development of conducting polymer based biomimetic muscles and fabrication techniques for an artificial pectoral fish fin. Master's thesis, Massachusetts Institute of Technology, 2005.

[38] G. Decher. Fuzzy nanoassemblies: toward layered polymeric multicomposites. *Science*, 277(5330):1232, 1997.

[39] J. Ding, L. Liu, G.M. Spinks, D. Zhou, G.G. Wallace, and J. Gillespie. High performance conducting polymer actuators utilising a tubular geometry and helical wire interconnects. *Synthetic metals*, 138(3):391–398, 2003.

[40] R. Duggal, F. Hussain, and M. Pasquali. Self-Assembly of Single-Walled Carbon Nanotubes into a Sheet by Drop Drying. *Advanced Materials*, 18(1):29–34, 2006.

[41] M. Endo, YA Kim, T. Hayashi, K. Nishimura, T. Matusita, K. Miyashita, and MS Dresselhaus. Vapor-grown carbon fibers (VGCFs):: Basic properties and their battery applications. *Carbon*, 39(9):1287–1297, 2001.

[42] M. Endo, M. Strano, and P. Ajayan. Potential applications of carbon nanotubes. *Carbon Nanotubes*, pages 13–61, 2008.

[43] M. Farshad and A. Benine. Magnetoactive elastomer composites. *Polymer Testing*, 23(3):347–353, 2004.

[44] M. Farshad and M. Le Roux. Compression properties of magnetostrictive polymer composite gels. *Polymer Testing*, 24(2):163–168, 2005.

[45] W. Feng, XD Bai, YQ Lian, J. Liang, XG Wang, and K. Yoshino. Well-aligned polyaniline/carbon-nanotube composite films grown by in-situ aniline polymerization. *Carbon*, 41(8):1551–1557, 2003.

[46] T.A. Fofonoff. *Fabrication and use of conducting polymer linear actuators*. PhD thesis, Massachusetts Institute of Technology, 2008.

[47] J. Foroughi. *Development of novel nanostructured conducting polypyrrole fibres*. PhD thesis, Faculty of Engineering, University of Wollongong, 2009.

[48] J. Foroughi, G.M. Spinks, and G.G. Wallace. High strain electromechanical actuators based on electrodeposited polypyrrole doped with di-(2-ethylhexyl) sulfosuccinate. *Sensors and Actuators B: Chemical*, 2010.

[49] M. Fuchiwaki, W. Takashima, and K. Kaneto. Comparative study of electrochemomechanical deformations of poly(3-alkylthiophene)s, polyanilines and polypyrrole films. *Japanese Journal of Applied Physics Part 1-Regular Papers Short Notes & Review Papers*, 40(12):7110–7116, December 2001.

[50] H. L. Galiana, H. L. H. Smith, and A. Katsarkas. Modeling non-linearities in the vestibulo-ocular reflex (vor) after unilateral or bilateral loss of peripheral vestibular function. *Experimental Brain Research*, 137(3):369–386, 2001.

[51] MR Gandhi, P. Murray, GM Spinks, and GG Wallace. Mechanism of electromechanical actuation in polypyrrole. *Synthetic metals*, 73(3):247–256, 1995.

[52] B. Gao, A. Kleinhammes, XP Tang, C. Bower, L. Fleming, Y. Wu, and O. Zhou. Electrochemical intercalation of single-walled carbon nanotubes with lithium. *Chemical physics letters*, 307(3-4):153–157, 1999.

[53] M. G. Garcia-Webb, A. J. Taberner, N. C. Hogan, and I. W. Hunter. A modular instrument for exploring the mechanics of cardiac myocytes. *American journal of physiology.Heart and circulatory physiology*, 293(1):H866–74, Jul 2007.

[54] P.M. George, A.W. Lyckman, D.A. LaVan, A. Hegde, Y. Leung, R. Avasare, C. Testa, P.M. Alexander, R. Langer, and M. Sur. Fabrication and biocompatibility of polypyrrole implants suitable for neural prosthetics. *Biomaterials*, 26(17):3511–3519, 2005.

[55] M. Gerard, A. Chaubey, and B. D. Malhotra. Application of conducting polymers to biosensors. *Biosensors and Bioelectronics*, 17(5):345–359, 2002.

[56] M. Guo, J. Chen, J. Li, B. Tao, and S. Yao. Fabrication of polyaniline/carbon nanotube composite modified electrode and its electrocatalytic property to the reduction of nitrite. *Analytica chimica acta*, 532(1):71–77, 2005.

[57] S. Hara, T. Zama, S. Sewa, W. Takashima, and K. Kaneto. Highly stretchable and powerful polypyrrole linear actuators. *Chemistry Letters*, 32(7):576–577, 2003.

[58] S. Hara, T. Zama, W. Takashima, and K. Kaneto. Artificial muscles based on polypyrrole actuators with large strain and stress induced electrically. *Polymer Journal*, 36(2):151–161, 2004.

[59] S. Hara, T. Zama, W. Takashima, and K. Kaneto. Tfsi-doped polypyrrole actuator with 26% strain. *Journal of Materials Chemistry*, 14:1516–1517, 2004.

[60] S. Hara, T. Zama, W. Takashima, and K. Kaneto. Free-standing polypyrrole actuators with response rate of 10.8% s-1. *Synthetic Metals*, 149(2-3):199–201, 2005.

[61] A.R. Hillman, D.C. Loveday, M.J. Swann, S. Bruckenstein, and C.P. Wilde. Transport of neutral species in electroactive polymer films. *J. Chem. Soc., Faraday Trans.*, 87(13):2047–2053, 1991.

[62] C. Ho, ID Raistrick, and RA Huggins. Application of A-C Techniques to the Study of Lithium Diffusion in Tungsten Trioxide Thin Films. *Journal of the Electrochemical Society*, 127:343, 1980.

[63] W.K. Hsu, H.Y. Chu, T.H. Chen, T.W. Cheng, and W. Fang. An exceptional bimorph effect and a low quality factor from carbon nanotube–polymer composites. *Nanotechnology*, 19:135304, 2008.

[64] J.E. Huang, X.H. Li, J.C. Xu, and H.L. Li. Well-dispersed single-walled carbon nanotube/polyaniline composite films. *Carbon*, 41(14):2731–2736, 2003.

[65] IW Hunter and MJ Korenberg. The identification of nonlinear biological systems: Wiener and Hammerstein cascade models. *Biological Cybernetics*, 55(2):135–144, 1986.

[66] IW Hunter and S. Lafontaine. A comparison of muscle with artificial actuators. *Solid-State Sensor and Actuator Workshop, 1992. 5th Technical Digest., IEEE*, pages 178–185, 1992.

[67] E.W.H. Jager, E. Smela, and O. Ingans. Microfabricating conjugated polymer actuators. *Science*, 290(5496):1540, 2000.

[68] S.W. John, G. Alici, and C.D. Cook. Validation of a resonant frequency model for polypyrrole trilayer actuators. *IEEE/ASME Trans. Mechatronics*, 13(4):401–409, 2008.

[69] Jer-Nan Juang. *Applied System Identification*. PTR Prentice Hall Englewood Cliffs, 1994.

[70] R. E. Kearney and I. W. Hunter. System identification of human joint dynamics. *Critical Reviews in Biomedical Engineering*, 18(1):55–87, 1990.

[71] Y. Keng, P. V. Pillai, and I. W. Hunter. Characterizing the effect of temperature increase on polypyrrole active strength and stress rate. In *ASME Conference on Smart Materials, Adaptive Structures & Intelligent Systems*, Active Materials, Mechanics and Behavior, page 1258, Oxnard, CA, 2009.

[72] Y. Keng, P. V. Pillai, and I. W. Hunter. The effect of ion delivery on polypyrrole strain and strain rate under elevated temperature. In *Microelectromechanical Systems —Materials and Devices III*, volume 1222, Boston, MA, 2009.

[73] Yenmei Keng. The effects of temperature and carbon nanotubes on conducting polymer actuator performance. Master's thesis, Massachusetts Institute of Technology, 2010.

[74] JG Killian, BM Coffey, F. Gao, TO Poehler, and PC Searson. Polypyrrole Composite Electrodes in an All-Polymer Battery System. *Journal of the Electrochemical Society*, 143:936, 1996.

[75] D. Kincal, A. Kumar, A.D. Child, and J.R. Reynolds. Conductivity switching in polypyrrole-coated textile fabrics as gas sensors. *Synthetic metals*, 92(1):53–56, 1998.

[76] M. J. Korenberg and I. W. Hunter. The identification of nonlinear biological systems: Volterra kernel approaches. *Annals of Biomedical Engineering*, 24(2):250–268, 1996.

[77] M.J. Korenberg and IW Hunter. The identification of nonlinear biological systems: LNL cascade models. *Biological Cybernetics*, 55(2):125–134, 1986.

[78] S.W. Lee, B.S. Kim, S. Chen, Y. Shao-Horn, and P.T. Hammond. Layer-by-layer assembly of all carbon nanotube ultrathin films for electrochemical applications. *Journal of the American Chemical Society*, 131(2):671–679, 2008.

[79] S.W. Lee, N. Yabuuchi, B.M. Gallant, S. Chen, B.S. Kim, P.T. Hammond, and Y. Shao-Horn. High-power lithium batteries from functionalized carbon-nanotube electrodes. *Nature Nanotechnology*, 5(7):531–537, 2010.

[80] L. Ljung. *System identification: theory for the user*, volume 280. Prentice-Hall NJ, 2nd edition, 1987.

[81] R.R. Llinas, K.D. Walton, M. Nakao, I. Hunter, and P.A. Anquetil. Neuro-vascular central nervous recording/stimulating system: Using nanotechnology probes. *Journal of Nanoparticle Research*, 7(2):111–127, 2005.

[82] W. Lu, A. G. Fadeev, B. H. Qi, E. Smela, B. R. Mattes, J. Ding, G. M. Spinks, J. Mazurkiewicz, D. Z. Zhou, G. G. Wallace, D. R. MacFarlane, S. A. Forsyth, and M. Forsyth. Use of ionic liquids for pi-conjugated polymer electrochemical devices. *Science*, 297(5583):983–987, 2002.

[83] C. Luo and A. Chakraborty. Effects of dimensions on the sensitivity of a conducting polymer microwire sensor. *Microelectronics Journal*, 40(6):912–920, 2009.

[84] J. Madden, P. Madden, and I Hunter. Conducting polymer actuators as engineering materials. In *Proceedings of SPIE*, volume 4695, 2002.

[85] J. D. Madden, P. G. Madden, P. A. Anquetil, and I. W. Hunter. Load and time dependence of displacement in a conducting polymer actuator. In *Materials Research Society Symposium Proceedings*, volume 698, pages 137–144. Warrendale, Pa.; Materials Research Society; 1999, 2002.

[86] J. D. W. Madden, N. A. Vandesteeg, P. A. Anquetil, P. G. A. Madden, A. Takshi, R. Z. Pytel, S. R. Lafontaine, P. A. Wieringa, and I. W. Hunter. Artificial muscle technology: Physical principles and naval prospects. *IEEE J.Ocean.Eng.*, 29(3):706—728, 2004.

[87] J.D.W. Madden. *Conducting polymer actuators*. PhD thesis, Massachusetts Institute of Technology, 2000.

[88] John D. Madden. Actuation selection tool, 2010.

[89] Peter Madden. *Development and Modeling of Conducting Polymer Actuators and the Fabrication of a Conducting Polymer Based Feedback Loop*. PhD thesis, Massachusetts Institute of Technology, 2003.

[90] Huanyu Mao, Jolanta Ochmanska, Chris D. Paulse, and Peter G. Pickup. Ion transport in pyrrole-based polymer films. *Faraday Discuss. Chem. Soc.*, 88:165–176, 1989.

[91] A. Mazzoldi, A. Della Santa, and D. De Rossi. *Conducting polymer actuators: Properties and modeling.* Springer Verlag, Heidelberg, 1999.

[92] A. Mirmohseni and R. Solhjo. Preparation and characterization of aqueous polyaniline battery using a modified polyaniline electrode. *European polymer journal*, 39(2):219–223, 2003.

[93] L Montemayor, P.V. Pillai, and I.W Hunter. In-situ measurement of actuation in thin films of conducting polymers. In J Bagdahn, N. Sheppard, K. Turner, and S. Vengallatore, editors, *Mater. Res. Soc. Symp. Proc*, volume 1222-DD03-02 of *Microelectromechanical Systems — Materials and Devices III.* MRS, 2010.

[94] M. Munih, K. Hunt, and N. Donaldson. Variation of recruitment nonlinearity and dynamic response of ankle plantarflexors. *Medical engineering & physics*, 22(2):97–107, 2000.

[95] B.J. Munro, J.R. Steele, T.E. Campbell, and G.G. Wallace. Wearable textile biofeedback systems: are they too intelligent for the wearer. *Stud Health Technol Inform*, 108:271–7, 2004.

[96] B. Muthulakshmi, D. Kalpana, S. Pitchumani, and N. G. Renganathan. Electrochemical deposition of polypyrrole for symmetric supercapacitors. *J.Power Sources*, 158(2):1533–1537, 2006.

[97] T. Nakashima, D. Kumar, W. Takashima, T. Zama, S. Hara, S. Sewa, and K. Kaneto. Enhanced electrochemical strain in polypyrrole films. *Current Applied Physics*, 5(2):202–208, 2005.

[98] T. Otero, C. Lopez, and A. Vazquez. Mechanical characterization of freestanding polypyrrole film. *Materials Science and Engineering: C*, 27(1):18–22, 2007.

[99] E. Paster, B.P. Ruddy, P.V. Pillai, and I.W. Hunter. Conducting polymer-based multifunctional materials. In *ASME Conference on Smart Materials, Adaptive Structures and Intelligent Systems.* ASME, 2010.

[100] Q. B. Pei and O. Inganas. Electrochemical musclesbending strips built from conjugated polymers. *Synthetic Metals*, 57(1):3718–3723, April 1993.

[101] R.M. Penner, L.S. Van Dyke, and C.R. Martin. Electrochemical evaluation of charge-transport rates in polypyrrole. *The Journal of Physical Chemistry*, 92(18):5274–5282, 1988.

[102] P Pillai, E. Paster, L. Montemayor, C. Benson, and I. Hunter. Development of soldier conformable antennae using conducting polymers. In *Advanced Materials and Manufacturing Technology in Army Science Conference*, number GP-08 in Army Science Conference Proceedings. US Army, Devember 2010 2010.

[103] P. V. Pillai and I. W. Hunter. Stochastic system identification of the compliance of conducting polymers. In Z. Cheng, Q. Zhang, S. Bauer, and D. A. Wrobleski, editors, *Materials Research Society Symposium Proceedings*, number BB in BB07-03, pages BB07–03, Warrendale, PA, 2008.

[104] P. V. Pillai and I. W. Hunter. Thermo-mechanical characterization of polypyrrole compliance using stochastic system identification. In C. Laschi and A. Barrera, editors, *Hybrid Organic Synthetic Biomaterials for Sensing and Actuation*, volume Minneapolis, MN, page 6834, 2009.

[105] P.V. Pillai. Conducting polymer actuator enhancement through microstructuring. Master's thesis, Massachusetts Institute of Technology, 2007.

[106] PV Pillai, IW Hunter, and E. Hernandez. Application of stochastic system identification to the study of the compliance of electroactive polymers. *The Review of scientific instruments*, 82(2):025103, 2011.

[107] FA Posey and T. Morozumi. Theory of potentiostatic and galvanostatic charging of the double layer in porous electrodes. *Journal of the Electrochemical Society*, 113:176, 1966.

[108] R. Pytel, E. Thomas, and I. Hunter. Anisotropy of electroactive strain in highly stretched polypyrrole actuators. *Chemistry of Materials*, 18(4):861—863, 2006.

[109] R. Pytel, E. Thomas, and I. Hunter. In-situ observation of dynamic elastic modulus in polypyrrole actuators. *Polymer*, 49:2008–2013, 2008.

[110] Rachel Pytel. *Artificial Muscle Morphology: Structure/Property relationships in Polypyrrole Actuators*. PhD thesis, Massachusetts Institute of Technology, 2007.

[111] L. Qu, Q. Peng, L. Dai, et al. Carbon nanotube electroactive polymer materials: Opportunities and challenges. *MRS bulletin*, 33(3):215–224, 2008.

[112] Derek G Rinderknecht. Design of a dynamic mechanical analyzer for the active characterization of conducting polymer actuators. Master's thesis, Massachusetts Institute of Technology, 2002.

[113] S Roth. *One-dimensional Metals*. Springer-Verlag, 1995.

[114] A. Rudge, I. Raistrick, S. Gottesfeld, and J.P. Ferraris. A study of the electrochemical properties of conducting polymers for application in electrochemical capacitors. *Electrochimica acta*, 39(2):273–287, 1994.

[115] M.A. Saez. Fabrication and characterization of conducting polymer microwires. Master's thesis, Massachusetts Institute of Technology, 2009.

[116] M.A. Saez. Fabrication and characterization of conducting polymer microwires. In *Mater. Res. Soc. Symp. Proc*, volume 1240E-WW04-05 of *Polymer Nanofibers–Fundamental Studies and Emerging Applications*. MRS, Massachusetts Institute of Technology, 2009.

[117] J.M. Schnorr and T.M. Swager. Wiring-up catalytically active metals in solution with sulfonated carbon nanotubes. *J. Mater. Chem.*, 2011.

[118] H.L. Schreuder-Gibson, Q. Truong, J.E. Walker, J.R. Owens, J.D. Wander, and W.E. JONES. Chemical and biological protection and detection in fabrics for protective clothing. *MRS bulletin*, 28(8):574–578, 2003.

[119] Aurora Scientific. Comercial muscle testing apparatus, 2011.

[120] J.C. Scott and L.D. Bozano. Nonvolatile memory elements based on organic materials. *Advanced Materials*, 19(11):1452–1463, 2007.

[121] M.S.P. Shaffer and A.H. Windle. Fabrication and characterization of carbon nanotube/poly (vinyl alcohol) composites. *Advanced Materials*, 11(11):937–941, 1999.

[122] S.R. Shin, C.K. Lee, IS So, J.H. Jeon, T.M. Kang, CW Kee, S.I. Kim, G.M. Spinks, G.G. Wallace, and S.J. Kim. DNA-Wrapped Single-Walled Carbon Nanotube Hybrid Fibers for supercapacitors and Artificial Muscles. *Advanced Materials*, 20(3):466–470, 2008.

[123] T. Shoa, M. Cole, N. R. Munce, V. Yang, and J. D. Madden. Polypyrrole operating voltage limits in aqueous sodium hexafluorophosphate. In *Proc. of SPIE Vol*, volume 6524, pages 652421–652421, 2007.

[124] T. Shoa, T. Mirfakhrai, and J. D. W. Madden. Electro-stiffening in polypyrrole films: Dependence of young's modulus on oxidation state, load and frequency. *Synthetic Metals*, 2010.

[125] H. Sirringhaus, T. Kawase, RH Friend, T. Shimoda, M. Inbasekaran, W. Wu, and EP Woo. High-resolution inkjet printing of all-polymer transistor circuits. *Science*, 290(5499):2123, 2000.

[126] S.P. Sitaram, J.O. Stoffer, and T.J. O'Keefe. Application of conducting polymers in corrosion protection. *Journal of Coatings Technology*, 69(866):65–69, 1997.

[127] S. Skaarup, L. Bay, K. Vidanapathirana, S. Thybo, P. Tofte, and K. West. Simultaneous anion and cation mobility in polypyrrole. *Solid state ionics*, 159(1-2):143–147, 2003.

[128] E. Smela. Conjugated polymer actuators for biomedical applications. *Adv. Mater.*, 15(6):481–494, 2003.

[129] E. Smela and N. Gadegaard. Surprising volume change in PPy (DBS): an atomic force microscopy study. *Advanced Materials*, 11(11):953–957, 1999.

[130] E. Smela and N. Gadegaard. Volume change in polypyrrole studied by atomic force microscopy. *The Journal of Physical Chemistry B*, 105(39):9395–9405, 2001.

[131] E. Smela, O. Inganas, and I. Lundstrom. Controlled folding of micrometer-size structures. *SCIENCE*, 268(5218):1735–1738, June 1995.

[132] E. Smela, M. Kallenbach, and J. Holdenried. Electrochemically driven polypyrrole bilayers for moving and positioning bulk micromachined silicon plates. *Journal of Microelectrochemical Systems*, 8(4):373–383, December 1999.

[133] E. Smela, W. Lu, and B.R. Mattes. Polyaniline actuators:: Part 1. PANI (AMPS) in HCl. *Synthetic metals*, 151(1):25–42, 2005.

[134] Donald E. Smith. The enhancement of electroanalytical data by on-line fast fourier transform data processing in electrochemistry. *Analytical Chemistry*, 48(6):517A–526a, 1976.

[135] G. M. Spinks and V. T. Truong. Work-per-cycle analysis for electromechanical actuators. *Sensors and Actuators A*, 119(2):455–461, 2005.

[136] G.M. Spinks, L. Liu, G.G. Wallace, and D. Zhou. Strain response from polypyrrole actuators under load. *Advanced Functional Materials*, 12(6-7):437–440, 2002.

[137] G.M. Spinks, V. Mottaghitalab, M. Bahrami-Samani, P.G. Whitten, and G.G. Wallace. Carbon-nanotube-reinforced polyaniline fibers for high-strength artificial muscles. *Advanced Materials*, 18(5):637–640, 2006.

[138] K. Sugiyama, K. Ishii, K. Yamato, and K. Kaneto. Development of a Biomimetic Fin Actuator using Electroconductive Polymer. In *OCEANS 2007*, pages 1–6. IEEE, 2007.

[139] Y.P. Sun, K. Fu, Y. Lin, and W. Huang. Functionalized carbon nanotubes: properties and applications. *Accounts of Chemical Research*, 35(12):1096–1104, 2002.

[140] A. J. Taberner and I. W. Hunter. Calibration of a horizontally acting force transducer with the use of a simple pendulum. *Rev.Sci.Instrum.*, 77:125103–, 2006.

[141] M. Tahhan, V.T. Truong, G.M. Spinks, and G.G. Wallace. Carbon nanotube and polyaniline composite actuators*. *Smart materials and structures*, 12:626, 2003.

125

[142] W. Takashima, M. Fukui, M. Kaneko, and K. Kaneto. Electrochemomechanical deformation of polyaniline films. *Japanes Journal of Applied Physics Part 1-Regular Papers Short Notes & Review Papers*, 34(7B):3786–3789, July 1995.

[143] W. Takashima, S.S. Pandey, M. Fuchiwaki, and K. Kaneto. Cyclic step-voltammetric analysis of cation-driven and anion-driven actuation in polypyrrole films. *Jpn. J. Appl. Phys*, 41:7532–7536, 2002.

[144] J. Tangorra, P. Anquetil, T. Fofonoff, A. Chen, M. Del Zio, and I. Hunter. The application of conducting polymers to a biorobotic fin propulsor. *Bioinspiration & Biomimetics*, 2:S6, 2007.

[145] S. W. Thomas III, G. D. Joly, and T. M. Swager. Chemical sensors based on amplifying fluorescent conjugated polymers. *Chem.Rev.*, 107(4):1339–1386, 2007.

[146] Nate Vandersteeg. *Synthesis and Characterization of Conducting Polymer Actuators*. PhD thesis, Massachusetts Institute of Technology, 2006.

[147] J. Wang, J. Dai, and T. Yarlagadda. Carbon nanotube-conducting-polymer composite nanowires. *Langmuir*, 21(1):9–12, 2005.

[148] Y. Wu, G. Alici, J. D. W. Madden, G. M. Spinks, and G. G. Wallace. Soft mechanical sensors through reverse actuation in polypyrrole. *Advanced Functional Materials*, 17(16):3216–3222, 2007.

[149] Y. Wu, D. Zhou, GM Spinks, PC Innis, WM Megill, and GG Wallace. TITAN: a conducting polymer based microfluidic pump. *Smart materials and structures*, 14:1511, 2005.

[150] B.B. Xi, VT. Truong, P. Whitten, J. Ding, GM. Spinks, and GG. Wallace. Poly(3-methylthiophene) electrochemical actuators showing increased strain and work per cycle at higher operating stresses. *Polymer*, 47:7720–7725, 2006.

[151] H. Yuan, D. T. Westwick, E. P. Ingenito, K. R. Lutchen, and B. Suki. Parametric and nonparametric nonlinear system identification of lung tissue strip mechanics. *Annals of Biomedical Engineering*, 27(4):548–562, 1999.

[152] W. Zhang, J.K. Sprafke, M. Ma, E.Y. Tsui, S.A. Sydlik, G.C. Rutledge, and T.M. Swager. Modular Functionalization of Carbon Nanotubes and Fullerenes. *Journal of the American Chemical Society*, 131(24):8446–8454, 2009.

[153] W. Zhang and T.M. Swager. Functionalization of single-walled carbon nanotubes and fullerenes via a dimethyl acetylenedicarboxylate-4-dimethylaminopyridine zwitterion approach. *Journal of the American Chemical Society*, 129(25):7714–7715, 2007.

[154] X. Zhang, J. Zhang, and Z. Liu. Conducting polymer/carbon nanotube composite films made by in situ electropolymerization using an ionic surfactant as the supporting electrolyte. *Carbon*, 43(10):2186–2191, 2005.